5-2008

RANDOM ROAD ANALYSIS AND IMPROVED GEAR RATIO SELECTION OF A FRONT WHEEL DRIVE DRAG RACING CAR

Thomas New
Clemson University, tnew222@hotmail.com

RANDOM ROAD ANALYSIS AND IMPROVED GEAR RATIO SELECTION
OF A FRONT WHEEL DRIVE DRAG RACING CAR

A Thesis
Presented to
the Graduate School of
Clemson University

In Partial Fulfillment
of the Requirements for the Degree
Master of Science
Mechanical Engineering

by
T. Michael New
May 2008

Accepted by:
Dr. E. Harry Law, Committee Chair
Dr. Imtiaz Haque
Dr. John Wagner

ABSTRACT

Drag racing has been around since the 1950's and has become a very popular and very competitive sport. The difference between winning and losing can be hundredths and even thousandths of a second. Drag racing teams need every advantage they can get in order to excel in their field. On-track testing is very expensive and can consume large amounts of time and resources that a race team may not be able to afford.

One way to address this potential problem of high cost is by using computer simulation to show how your drag race car may perform at different tracks and how changes to your car may affect the performance at those tracks. A simulation could allow you to "run" a test at different tracks without actually having to go to those tracks. While computer simulation can not completely replace real testing, it could save money and increase productivity at testing sessions. Additionally, the ability to generate vehicle dynamic responses specific to different tracks could be helpful in selecting vehicle parameters specifically for those tracks.

This thesis describes the development of a tool to study the vehicle dynamics of a front wheel drive drag racing car. A 5 degrees-of-freedom (DOF) model of the dynamic response of the vehicle on different track surfaces is developed and simulated in MATLAB and Simulink. The input to the simulation is a user-specified power spectral density (PSD) of the vertical road profile, tire-to-road adhesion level, and specific vehicle parameters. Outputs of the model include drag times, normal forces, longitudinal accelerations, heave, pitch angle, wheel slip, traction force, vehicle and wheel speeds, and engine RPM. Simulations are run comparing the effects of different road surfaces on the

vehicle dynamic response and drag performance. Also, a gear ratio improvement loop is used to evaluate different gear sets on drag performance in an effort to improve the quarter mile time and trap speed.

The vehicle simulation shows that differing road surfaces have a large effect on vehicle dynamics and affect the overall performance of the vehicle on the drag run. The gear ratio improvement loop shows that quarter mile time improvements of 2% and trap speed improvements of over 4% could be achieved simply by using gear ratios that are chosen for a particular track surface. This simulation could produce beneficial and significant improvements in the drag racing world for teams looking for that extra edge on the competition. An overall improvement of 4% could be the difference between winning and losing.

ACKNOWLEDGMENTS

I would like to express my sincerest gratitude to my advisor, Dr. E. Harry Law, for his guidance and assistance throughout my college career. I am grateful for his persistence in the planning of my thesis research and his encouragement as the research was being performed.

I would like to thank Prof. Frank Paul, Prof. John Wagner and Prof. Imtiaz Haque for the education they have provided and for being part of my thesis committee.

I would also like to give thanks to my parents, Thom and Pat New, for encouraging and supporting my decision to continue my education. Their constant support through the entire process has been invaluable.

Finally, I would like to especially thank my wife, Amy New, for her constant support. She was an integral part in the completion of this thesis and her constant love and support were vital to my success.

TABLE OF CONTENTS

Table of Contents (Continued)

LIST OF TABLES

LIST OF FIGURES

List of Figures (Continued)

Figure   Page

List of Figures (Continued)

Figure   Page

List of Figures (Continued)

Figure   Page

NOMENCLATURE

Variable	Definition	Units
A	Vehicle Frontal Area	ft²
C	Tire Damping Element Per Unit Length of Contact Patch	lb/ ft²/s
C_d	Drag Coefficient	-
$C_{f,r}$	Front/Rear Damping Constant	lb/ft/sec
$C_{tf,tr}$	Front/Rear Tire Damping Constant	lb/ft/sec
D_a	Drag Force	lb
f	Friction Coefficient	-
F	Traction Force	lb
$F_{cf,cr}$	Front/Rear Damper Force on Sprung Mass	lb
$F_{kf,kr}$	Front/Rear Spring Force on Sprung Mass	lb
$F_{x1,x2}$	Front/Rear Axle Longitudinal Force on Sprung Mass	lb
$F_{z1,z2}$	Front/Rear Axle Vertical Force on Sprung Mass	lb
G	Gravitational Constant	lb*ft/s²
H	Vehicle CG height from Road	ft
h_a	Vertical Distance from Road to Drag Force Application	ft
$I_{f,r}$	Front/Rear Axle Rotational Moment of Inertia	slugs*ft²
I_s	Sprung Mass Rotational Moment of Inertia	slugs*ft²
$K_{f,r}$	Front/Rear Spring Constant	lb/ft
$K_{tf,tr}$	Front/Rear Tire Spring Constant	lb/ft
K	Tire Stiffness Element Per Unit Length of Contact Patch	lb/ft²
L	Vehicle Wheelbase	ft
l_1	Distance From Front Axle to Vehicle CG	ft
l_2	Distance from Vehicle CG to Rear Axle	ft
L_t	Tire Contact Patch Length	ft
L_w	Distance from Rear Axle to Wheelie Bar Pin Joint	ft
m_s	Vehicle Sprung Mass	lbm
$m_{tf,tr}$	Front/Rear Axle Mass	lbm
N	Number of Points used for Tire Contact Patch	-
$N_{f,r}$	Front/Rear Normal Force	lb
P_w	Normal Force at Wheelie Bar to Road Contact	lb
R	Tire Radius	In
$R_{f,r}$	Rolling Resistance of Front/Rear Axle	lb
T	Torque Applied by Motor	ft*lb
V	Vehicle Longitudinal Velocity	ft/s
W	Vehicle Weight	lb
W_{sm}	Sprung Mass Weight	lb
X	Vehicle Longitudinal Position on Track	ft
Y	Vertical Displacement of Vehicle CG	ft

Nomenclature (continued)

Variable	Definition	Units
$y_{tf,tr}$	Vertical Displacement of Front/Rear Axle	ft
$y_{rf,rr}$	Vertical Displacement of Front/Rear Tire to Road Contact	ft
y_{rw}	Vertical Displacement of Wheelie Bar to Road Contact	ft
$y_o(x)$	Leading Edge of Tire Contact Patch	ft
$y_i(x)$	i^{th} point of Tire Contact Patch	ft
$y_n(x)$	n^{th} point of Tire Contact Patch	ft
$\omega_{f,r}$	Rotational Velocity of Front/Rear Axle	rad/s
ρ	Density of Air	lb/ft³
θ	Vehicle Pitch Angle	deg
$\hat{x}$	Distance Between Elements of Tire Model	ft

CHAPTER ONE

INTRODUCTION

<u>Introduction</u>

Drag racing front wheel drive cars has become a growing sport on the amateur as well as professional level. This thesis dives into the sport of front wheel drive drag racing to try to shed some insight on the complex dynamics these machines exhibit. A five degrees-of-freedom (DOF) vehicle model is used to represent the drag car. The vehicle model incorporates a wheelie bar, random road input, nonlinear shocks, and wheel slip, along with other effects, to attempt to recreate the actual dynamics of the vehicle in a relatively simple model.

The model used in this research was identical to that derived by Knauff [1]. However, the governing equations were derived independently in this project and then checked against Knauff's equations. The work described in this thesis and Knauff's work were two parts of a combined project. This thesis focuses on different, but related, issues to those addressed by Knauff. Knauff's research investigated anti-squat chassis configurations and flexible chassis components.

<u>Outline of Thesis</u>

The first objective of this thesis research is to implement a random road, similar to a real road surface, into the simulation and to examine the effects of different road surfaces on the predicted performances. The second objective is to develop a methodology for selecting a set of gear ratios that will produce improved quarter-mile

performance. Also, the robustness of the improved gear ratios will be established by performing a sensitivity study on the gear ratios with respect to the track surface coefficient of friction.

This thesis will be presented in five main sections. The first section will explain the vehicle model that is used for this simulation. This will include the model of the front wheel drive drag racing vehicle, equations of motion, and a short explanation of the vehicle's nonlinear dampers.

The second section will describe the road model of the vehicle simulation. This will mainly focus on the generation of the random road profiles and the method used for ensuring their validity.

The third section will focus on the methodology for the improved gear ratio selection.

The fourth section will give the results of the studies conducted in this project. These include case studies of the vehicle traversing different road surfaces and the determination of the gear ratios for improved drag racing performance. The differences in performance and dynamics for the different case studies will be explained in detail. Also, the sensitivity of the gear ratio selection to the tire-to-road adhesion level will be evaluated.

The last major section of this thesis will involve a summary of the results. Also included will be recommendations for future work that may lead to potential for performance improvements.

CHAPTER TWO

VEHICLE MODEL

Introduction

In this chapter, the description of the five DOF front wheel drive drag racing car model is given and the equations of motion of the system are derived. These equations of motion are ultimately implemented in Simulink in a block diagram format. MATLAB is used first to generate the random road profile and then used to input all of the physical data of the front wheel drive drag racing car. MATLAB then calls Simulink to run the drag racing simulation. A more detailed derivation of the equations of motion is given in Appendix A.

This thesis presents the second part of a larger project. Knauff [1] has described the first part. His work describes the development of a dynamic model and simulation for a front wheel drive drag racing car. He investigates suspension kinematic properties (anti-squat) and chassis flexibility effects.

In this part of the project, the same physical model was used as described in [1]. However, the equations of motion were derived independently and compared with those of [1]. The simulation developed and described in [1] was used as a basis for the simulation for the work described in this report. However, significant additions were made to incorporate the random road and the improved gear ratio selection methodology.

Model Description

The five DOFs of this model are longitudinal velocity, pitch displacement, front and rear axle vertical displacements, and rotational or angular velocity of the front axle. The drag racing car is modeled as having a wheelie bar. The purpose of the wheelie bar is to mitigate the adverse effects of longitudinal weight shift on front normal load, thus increasing available tractive force on the front wheels. The contact of the wheelie bar with the road is modeled as a pin joint that is free to roll in the longitudinal direction, along the road surface, but restrained to follow the road profile in the vertical direction. The bar is assumed rigid and is cantilevered from the rear of the vehicle.

Free body diagrams were drawn and used to derive the equations of motion. The diagram of the front wheel drive drag racing car is given in Figure 2.1. Refer to the Nomenclature for definitions of variables used throughout this thesis. Also, the actual vehicle parameters that are used in the simulation are given in detail in Appendix B.

The vehicle is modeled as a rigid body. The wheelie bar is rigidly connected to the rear of the vehicle and is not allowed to flex at the mounting point. The road contact of the wheelie bar is free to roll in the longitudinal direction but is confined to follow the vertical road profile. The upper spring and damper elements, shown in Figure 2.1, represent the springs and shocks of the vehicle suspension while the lower spring and damper elements represent the spring and damping characteristics of the tires. The masses in between the two spring and damper models symbolize the unsprung masses of the front and rear axles. Inputs to the system include the vertical irregularities of the road at the front and rear axles and at the wheelie bar, as well as the torque generated at the

drive axle of the vehicle. The force generated by aerodynamic drag of the vehicle is applied to the front of the vehicle, aligned with the vehicle center of gravity (CG). The free body diagram of the sprung mass is shown in Figure 2.2.

The longitudinal equation of motion can be derived by summing the forces in the x-direction. The traction force, F, creates the forward motion. The aerodynamic drag of the vehicle, D_a, is represented by half of the density of air times the drag coefficient and the frontal area of the vehicle finally multiplied by the squared velocity of the car. The other two drag forces are the rolling resistance of the tires at the front and rear axles, R_f and R_r respectively. These forces are calculated by multiplying the rolling resistance coefficient, f, by the normal forces, N_f and N_r, of the contact between the respective axle and the road surface. The normal load, P_w, at the point contact between the wheelie bar and track surface is determined by the longitudinal weight shift of the vehicle. Rolling resistance at this point contact is assumed negligible. By summing these forces (Figure 2.1) and setting them equal to the mass of the vehicle multiplied by the longitudinal acceleration of the vehicle, we compile the longitudinal equation of motion for the front wheel drive drag racing car.

$$F - \frac{1}{2}\rho v^2 C_D A - fN_f - fN_r = \frac{W}{g}\dot{v} \tag{1}$$
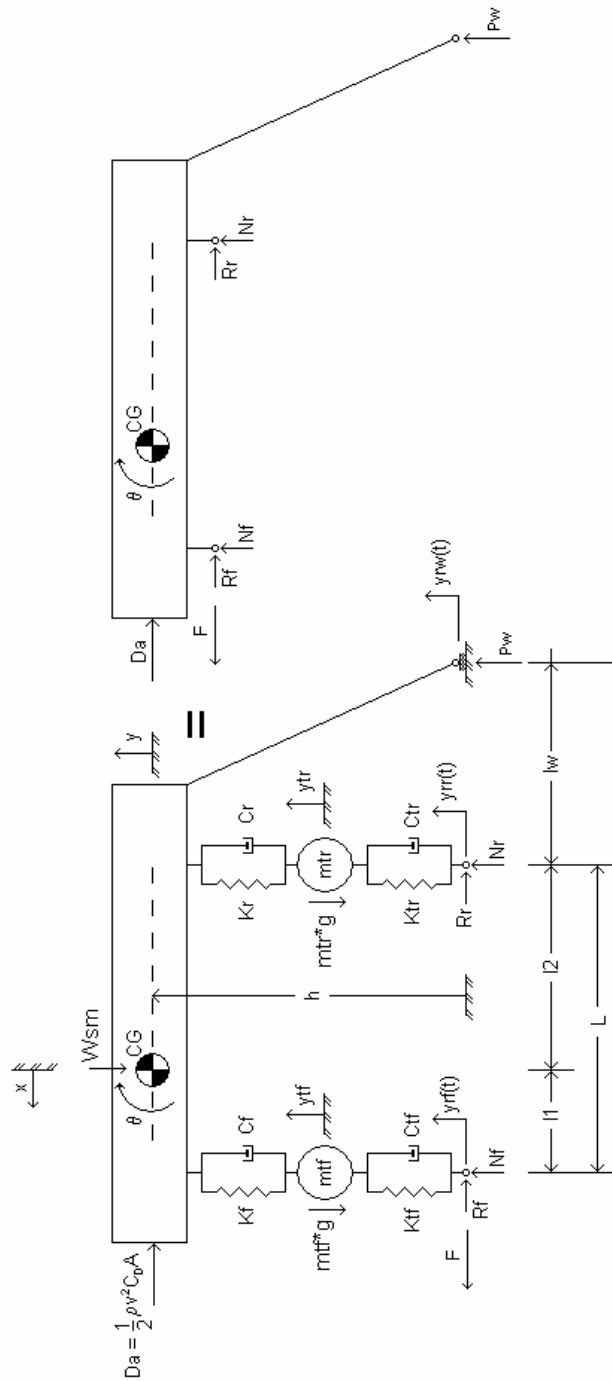
Figure 2.1: Front Wheel Drive Drag Racing Car 5 DOF Model

Modeling of Sprung Mass

The sprung mass of the front wheel drive drag racing car is modeled as a rigid body having pitch inertia and mass. The vehicle is assumed to be a laterally symmetric body. This assumption is based on the fact that drag racing cars should see very little lateral dynamics since they race in a straight line on relatively flat tracks. The wheelie bar is modeled as a rigid extension of the sprung mass to the point contact with the road. The contact is modeled as a pin joint that is free to move without friction along the x-axis (longitudinally) but is restricted to follow the road profile in the vertical direction. The free body diagram of the sprung mass, including the body accelerations, is shown in Figure 2.2.

Since all coordinates are measured from static equilibrium, only dynamic forces are considered. Therefore, the equations of motion are written from an equilibrium position and the weight of the car can be neglected.

The forces acting on the bottom of the sprung mass are the forces exerted on the sprung mass through the vehicle suspension. The vertical forces (F_{kf}, F_{cf}, F_{kr}, and F_{cr}) are transmitted by the vehicle springs and shocks, while the longitudinal forces (F_{x1} and F_{x2}) are applied through the rigid suspension components such as the upper and lower A-arms. The vehicle aerodynamic drag force (D_a) is applied on the front of the vehicle at the vertical height of the CG. Torque due to the traction force on the drive tire (T) is applied at the front suspension mount. The wheelie bar force (P_w) is only in the vertical direction since the road point contact is modeled as a pin and is free to roll in the longitudinal direction. The vehicle pitches (θ) around the point contact of the wheelie bar with the
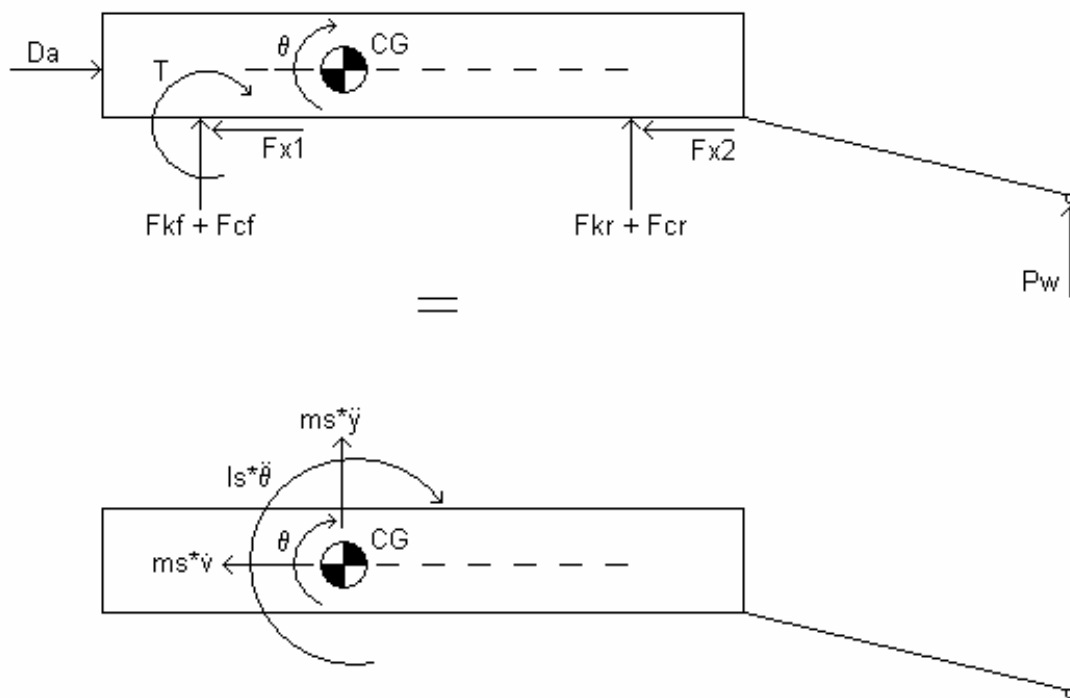
Figure 2.2: Free Body Diagram of Sprung Mass

road surface. The longitudinal, heave, and angular accelerations are shown on the right-hand side of the diagram.

By summing moments about the point where the wheelie bar attaches to the road surface, the equation of motion for the pitch of the vehicle can be derived. This equation, simplified by collecting like terms, is shown in Equation (2).

$$
\begin{aligned}
\ddot{\theta} = \frac{1}{I_s + m_s(l_2 + l_w)^2} & \Big(T + (L + l_w)\big[K_f\{y_{tf} - (L + l_w)\theta - y_{rw}(t)\} + C_f\{\dot{y}_{tf} - (L + l_w)\dot{\theta} - \dot{y}_{rw}(t)\}\big] \\
& + l_w\big[K_r\{y_{tr} - l_w\theta - y_{rw}(t)\} + C_f\{\dot{y}_{tr} - l_w\dot{\theta} - \dot{y}_{rw}(t)\}\big] \\
& - D_a(h - h_a) + (F_{x1} + F_{x2})\{h - r + (l_2 + l_w)\theta + y_{rw}(t)\}
\end{aligned}
\tag{2}
$$

The vertical force on the wheelie bar can be calculated by summing the forces in the vertical direction. The weight of the sprung mass is ignored due to the equations being written from an equilibrium position as described earlier.

$$
\begin{aligned}
P_w = m_s\{(l_2 + l_w)\ddot{\theta} + \ddot{y}_{rw}(t)\} & - K_f\{y_{tf} - (L + l_w)\theta - y_{rw}(t)\} + C_f\{\dot{y}_{tf} - (L + l_w)\dot{\theta} - \dot{y}_{rw}(t)\} \\
& - K_r\{y_{tr} - l_w\theta - y_{rw}(t)\} - C_f\{\dot{y}_{tr} - l_w\dot{\theta} - \dot{y}_{rw}(t)\}
\end{aligned}
\tag{3}
$$

Modeling of Unsprung Masses

The unsprung masses of the front wheel drive drag racing car are modeled as laterally symmetric solid axles. Forces acting on the front and rear axles are the rolling resistances (R_f, R_r), traction force (F, front axle only), torque from the transmission (T, front axle only), reaction forces from the tire-to-road interfaces ($F_{ktf, ktr}$ and $F_{ctf, ctr}$), and reaction forces from the shocks and dampers ($F_{kf, kr}$ and $F_{cf, cr}$). These forces are shown on the front and rear axle free body diagrams in Figures 2.3 and 2.4, respectively. The vertical forces applied to the axles come from the shocks and springs of the vehicle and compression and rebound of the tires. The forces from the springs and shocks (F_{kf}, F_{cf}, F_{kr}, and F_{cr}) originate from the differences in vertical displacement and velocities of the sprung mass and unsprung mass. The forces from the spring and damping characteristics of the tires (F_{ktf}, F_{ctf}, F_{ktr} and F_{ctr}) result from the differences in vertical displacements and velocities of the unsprung masses and the road profile. The rotational inertia of the front axle (I) is accounted for in the equations for wheel slip. F_{x1}, F_{z1} and F_{x2}, F_{z2} are the reaction forces exerted by the sprung mass on the front and rear unsprung masses respectively. Figure 2.5 shows these reaction forces exerted on the sprung mass by the front unsprung mass. By summing the forces in the x and z directions, we get Equations (4) and (5) respectively.

$$F_{x1} = F - R_f - m_{tf} * \dot{v} \tag{4}$$

$$F_{z1} = Nf - m_{tf} * g - m_{tf} * \ddot{y}_{tf} \tag{5}$$

The same equations can be used on the rear axle by omitting the Traction Force (F) and replacing the front axle parameters with the rear axle parameters.
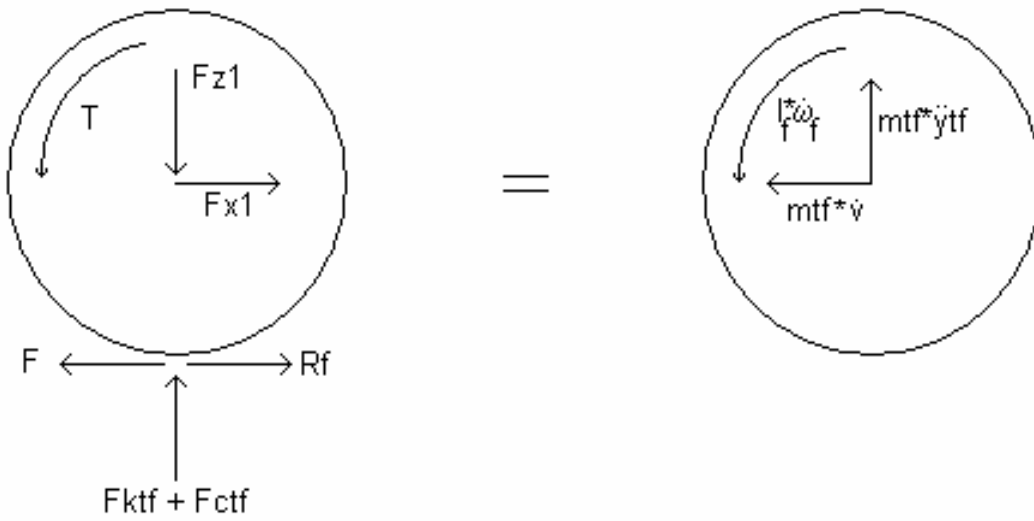
Figure 2.3: Front Unsprung Mass Free Body Diagram
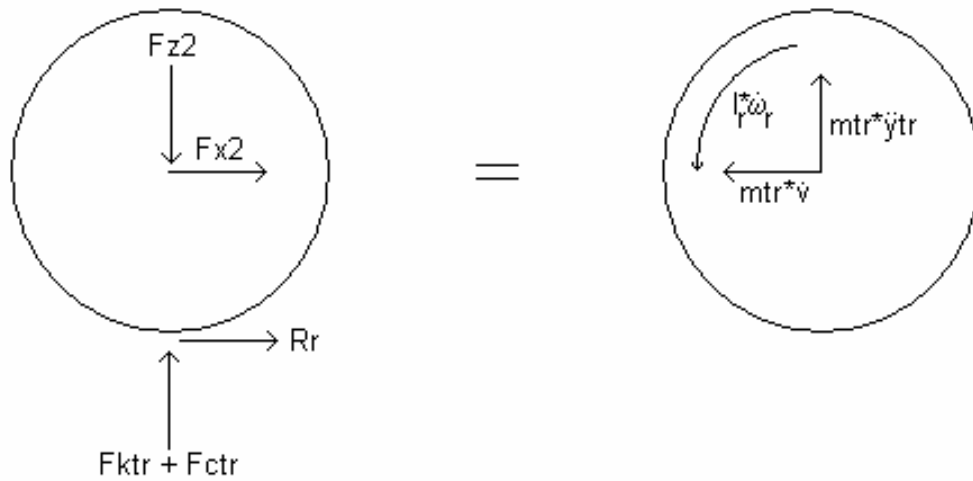
Figure 2.4: Rear Unsprung Mass Free Body Diagram
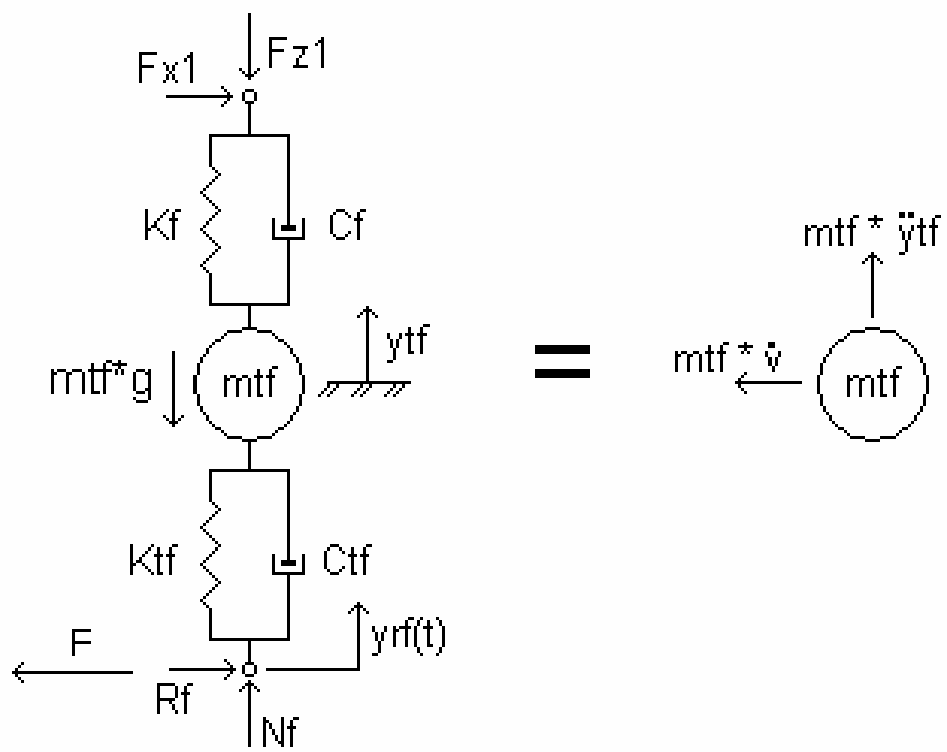
Figure 2.5: Unsprung / Sprung Mass Reaction Forces

The vertical equations of motion for the front and rear axles can be found by summing the forces in the vertical direction. The front and rear vertical force equations are given in Equations (6) and (7), respectively.

$$\ddot{y}_{tf} = \frac{1}{m_{tf}}\left[K_f\left\{(L+l_w)\theta + y_{rw}(t) - y_{tf}\right\} + C_f\left\{(L+l_w)\dot{\theta} + \dot{y}_{rw}(t) - \dot{y}_{tf}\right\}\right]$$
$$+ K_{tf}\left\{y_{rf}(t) - y_{tf}\right\} + C_{tf}\left\{\dot{y}_{rf}(t) - \dot{y}_{tf}\right\} \tag{6}$$

$$\ddot{y}_{tr} = \frac{1}{m_{tr}}\left[K_r\left\{l_w\theta + y_{rw}(t) - y_{tr}\right\} + C_r\left\{l_w\dot{\theta} + \dot{y}_{rw}(t) - \dot{y}_{tr}\right\}\right]$$
$$+ K_{tr}\left\{y_{rr}(t) - y_{tr}\right\} + C_{tr}\left\{\dot{y}_{rr}(t) - \dot{y}_{tr}\right\} \tag{7}$$

By summing the moments about the center of the front axle, the equation of motion for front wheel rotation can be found. This is shown in Equation (8).

$$\dot{\omega}_f = \frac{1}{I}\left(T - F_r - fN_f r\right) \tag{8}$$

The angular velocity of the wheel, when related to the actual longitudinal velocity of the car, can be used to calculate the amount of wheel slip generated during the drag run. This dynamic is very important in drag racing because the more slip that occurs, the more power that is not used in accelerating the vehicle.

Fixed Footprint Tire Model

The fixed footprint tire model was developed by Captain et al [2]. This model assumes the tire is comprised of evenly distributed stiffness and damping elements that conform to the profile of the road surface. The tire model thus uses an average height of the road profile that is underneath the footprint of the tire to determine the force transmitted to the axle through the tire itself. The model of the fixed footprint tire model is shown in Figure 2.6.
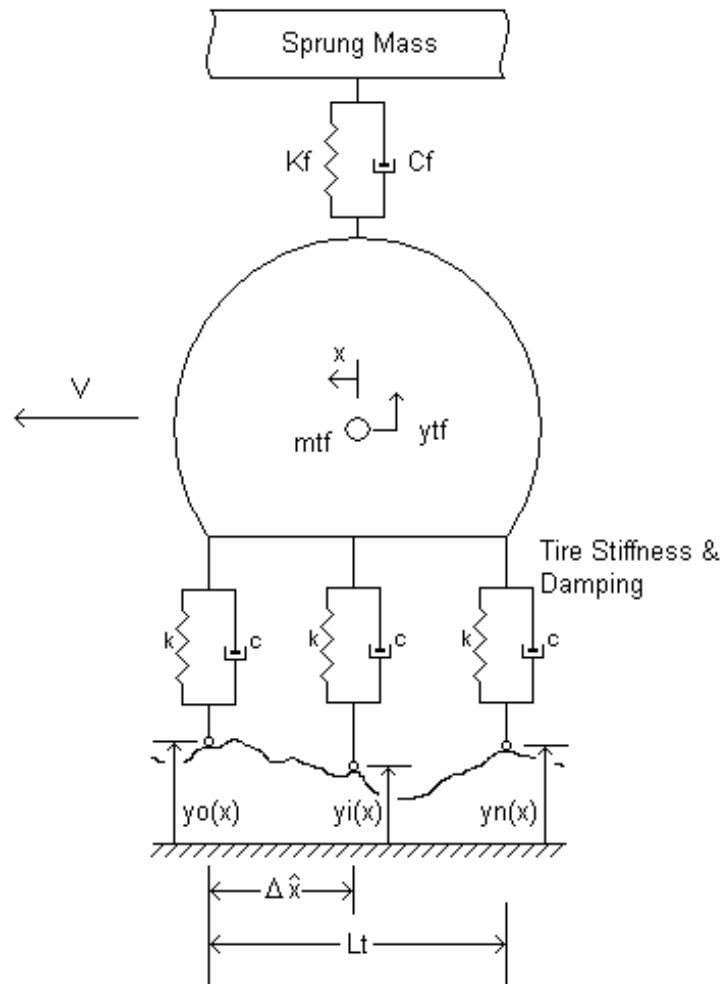
Figure 2.6: Fixed Footprint Tire Model

The fixed footprint tire model, in effect, acts as a filter to reduce the harshness that would be generated by the road profile if there were a point contact tire model. By integrating the road profile over the contact patch surface, the displacement of each element within the tire can be found and a force transmitted through the tire can be derived. From the free body diagram, we can derive the equation for the force transmitted through the tire. The total force, exerted by the footprint, acting on the tire mass is given in Equation (9), where k' and c' are the spring and damper constants per unit length of the tire contact patch.

$$F(x) = \sum_{i=0}^{n} k' y_i(x)\Delta\hat{x} + \sum_{i=0}^{n} c' \dot{y}_i(x)\Delta\hat{x} - k' y_{tf} L_t - c' \dot{y}_{tf} L_t \tag{9}$$

where, $y_i(x) = y_o(x - i\Delta\hat{x})$ (10)

By substituting Equation (10) into Equation (9), and replacing the summations with integrals across the length of the contact patch, we can derive Equation (11).

$$F(x) = \int_0^{Lt} k' y_o(x - \hat{x})d\hat{x} - \int_0^{Lt} c' \dot{y}_o(x - \hat{x})d\hat{x} - k' y_{tf} L_t - c' \dot{y}_{tf} L_t \tag{11}$$

where, $\hat{x}$ is the distance between each spring element of the tire.

Defining the averages, $y_{avg}(x)_{0 \to Lt}$ and $\dot{y}_{avg}(x)_{0 \to Lt}$ as

$$y_{avg}(x)_{0 \to Lt} = \frac{1}{Lt} \int_0^{Lt} y_o(x - \hat{x})d\hat{x} \tag{12}$$

$$\dot{y}_{avg}(x)_{0 \to Lt} = \frac{1}{Lt} \int_0^{Lt} \dot{y}_o(x - \hat{x})d\hat{x} \tag{13}$$

we have

$$F(x) = k_t y_{avg}(x)_{0 \to Lt} + c_t \dot{y}_{avg}(x)_{0 \to Lt} - k_t y_{tf} - c_t \dot{y}_{tf} \tag{14}$$

where k_t is the spring constant of the front (k_{tf}) or rear (k_{tr}) tire, and c_t is the damping constant of the front (c_{tf}) or rear (c_{tr}) tire. F(x) is the force transmitted to the axle, either front or rear, through the tire as a function of position on the track at the center of the tire.

It is assumed that the footprint area is rectangular. Therefore, the length of the static footprint is

$$L_t = \frac{N}{W_t \cdot P_t} \tag{15}$$

where, N is the tire normal force, W_t is the width of the tire contact patch, and P_t is the air pressure inside the tire.

Equation (15) assumes that the normal force is equal to the tire pressure multiplied by the footprint area and ignores the assumed negligible contribution of the tire carcass to N. It also neglects dynamic changes to the footprint area as the tire normal force changes. The contact patch size during the simulation is calculated using the static loading of the vehicle to ensure a reasonable contact patch size is used throughout the entire simulated drag run.

Equations of Motion

The five equations of motion for the front wheel drive drag racing car have been derived and are summarized below.

$$F - \frac{1}{2}\rho\dot{x}^2 C_D A - fN_f - fN_r = \frac{W}{g}\dot{v} \tag{16}$$

$$\dot{\omega}_f = \frac{1}{I}\left(T - F_r - fN_f r\right) \tag{17}$$

$$\ddot{y}_{tf} = \frac{1}{m_{tf}}\left[K_f\left\{(L+l_w)\theta + y_{rw}(t) - y_{tf}\right\} + C_f\left\{(L+l_w)\dot{\theta} + \dot{y}_{rw}(t) - \dot{y}_{tf}\right\}\right]$$
$$+ K_{tf}\left\{y_{rf}(t) - y_{tf}\right\} + C_{tf}\left\{\dot{y}_{rf}(t) - \dot{y}_{tf}\right\} \tag{18}$$

$$\ddot{y}_{tr} = \frac{1}{m_{tr}}\left[K_r\left\{l_w\theta + y_{rw}(t) - y_{tr}\right\} + C_r\left\{l_w\dot{\theta} + \dot{y}_{rw}(t) - \dot{y}_{tr}\right\}\right]$$
$$+ K_{tr}\left\{y_{rr}(t) - y_{tr}\right\} + C_{tr}\left\{\dot{y}_{rr}(t) - \dot{y}_{tr}\right\} \tag{19}$$

$$\ddot{\theta} = \frac{1}{I_s + m_s(l_2 + l_w)^2}\left(T + (L+l_w)\left[K_f\left\{y_{tf} - (L+l_w)\theta - y_{rw}(t)\right\} + C_f\left\{\dot{y}_{tf} - (L+l_w)\dot{\theta} - \dot{y}_{rw}(t)\right\}\right]\right)$$
$$+ l_w\left[K_r\left\{y_{tr} - l_w\theta - y_{rw}(t)\right\} + C_f\left\{\dot{y}_{tr} - l_w\dot{\theta} - \dot{y}_{rw}(t)\right\}\right]$$
$$- D_a(h - h_a) + (F_{x1} + F_{x2})\left\{h - r + (l_2 + l_w)\theta + y_{rw}(t)\right\} \tag{20}$$

The variable definitions are given in the Nomenclature.

Nonlinear Dampers

The shocks located on the front and rear axles are modeled as nonlinear dampers (Figure 2.7). These shocks have nonlinear relationships between the velocity across the dampers and damper forces created. The shock data shown in Figure 2.7 was obtained from [1].
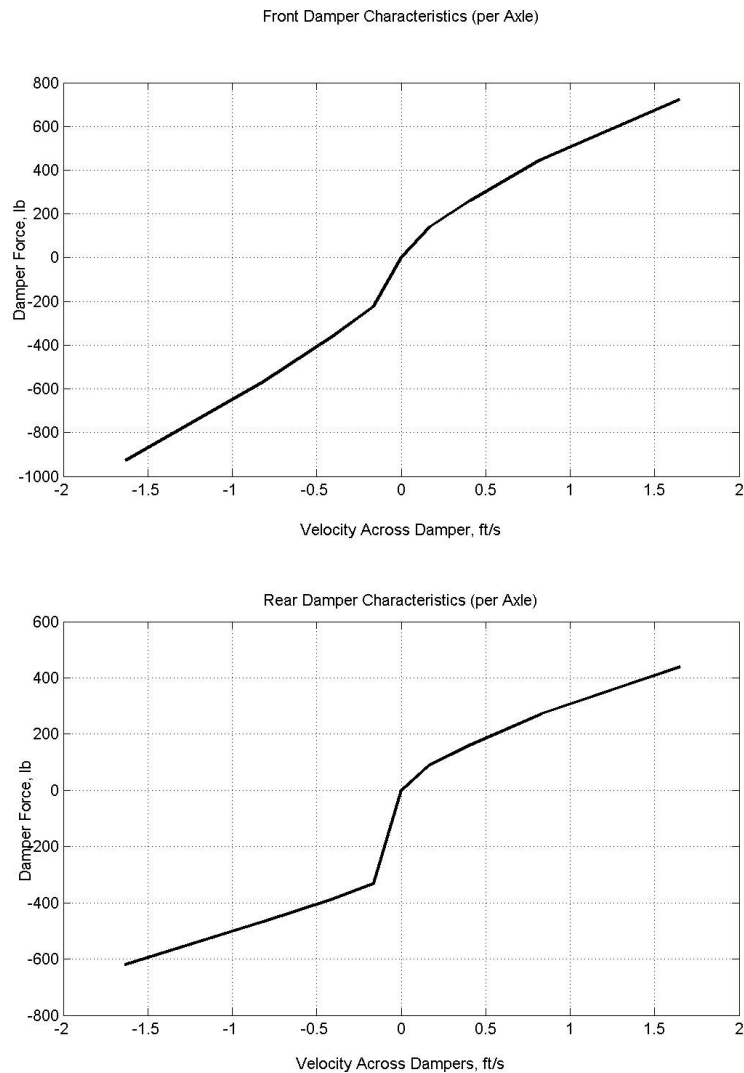
Figure 2.7: Front and Rear Damper Characteristics

CHAPTER THREE

METHOD FOR IMPROVED GEAR RATIO SELECTION

The main goal of developing a new gear ratio selection procedure is to find the gear ratios, from first to sixth gear, that reduce the simulated quarter mile time of the front wheel drive drag racing vehicle. Drive tires need to operate at a certain longitudinal slip percentage to provide the maximum amount of traction that is available. If the tires are slipping below or above this optimal percentage, the traction provided is less than the maximum. The understanding and employment of this concept is critical to attaining the fastest quarter mile time. If a gear ratio is selected that delivers more torque to the drive tires than there is traction available, the tires will slip at a higher percentage which will yield a lower tractive force. The same phenomenon occurs for a gear ratio that produces too little drive torque. With tire slippage below the optimal level, the tractive force yielded will be lower than the maximum.

The original gear ratios have an inherent problem that causes the quarter mile time to be slower than the vehicles potential. Large differences in consecutive gear ratios cause significant drops in available tractive force when up-shifting. If gear ratios are too far apart, the torque provided by the engine in the next gear will be too low to utilize the available traction. If the gear ratios are too closely spaced, the tractive force available for each gear can overlap, wasting some of the torque available from the engine. Figure 3.1 shows the available traction force for two sets of gear ratios. The gear set portrayed on the left plot is similar to the original gears and has the problems discussed earlier. The gear set shown on the right utilizes a more linear progression to operate more efficiently.

Available Tractive Force (Assuming No Slip)

Available Tractive Force (Assuming No Slip)
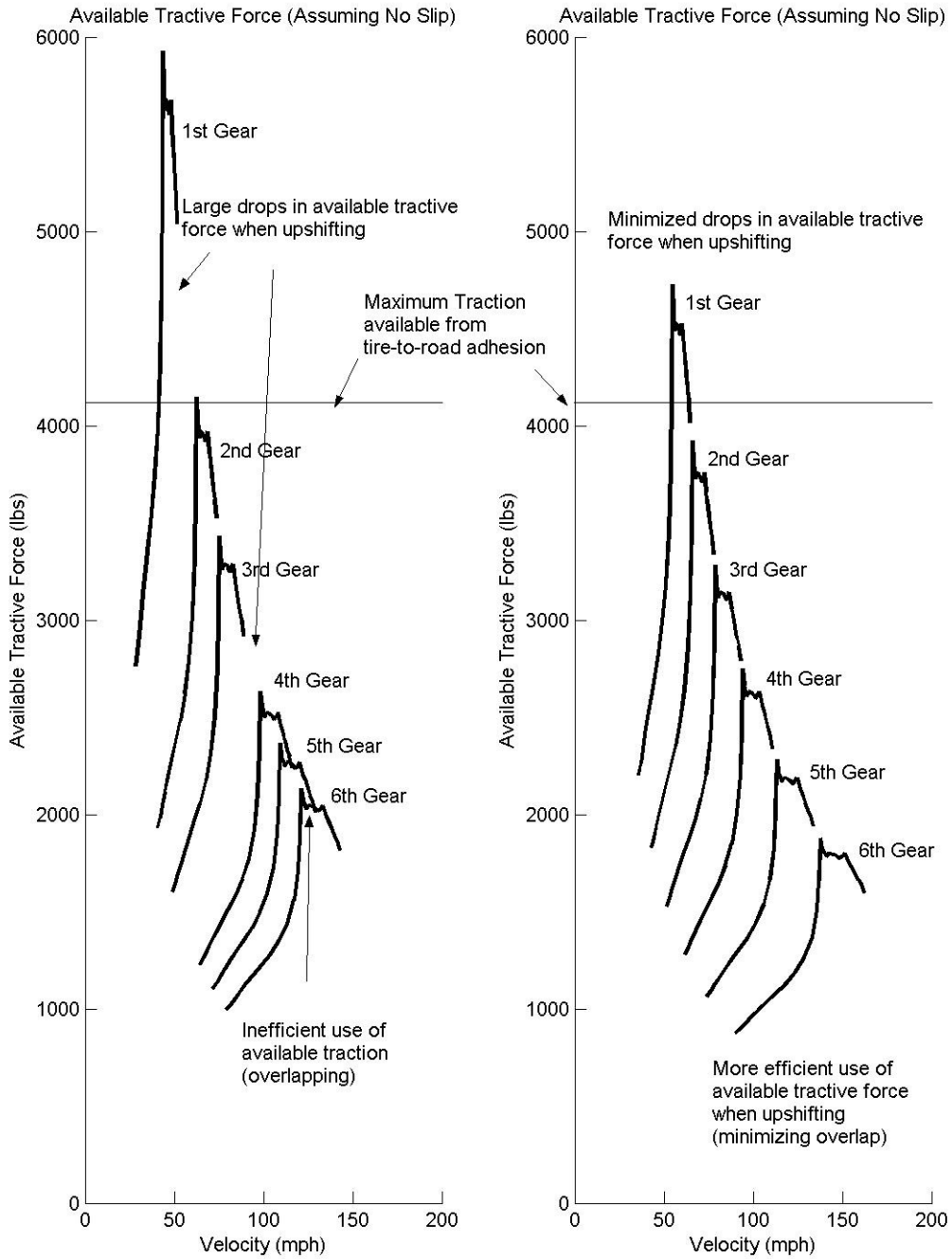
Figure 3.1: Gear Ratio Effect on Available Tractive Force

Figure 3.1 also contains the theoretical maximum traction force available from tire to road adhesion on the drive axle. This number was estimated by multiplying the static load on the drive axle with the estimated mu value at the tire to road contact. The gear set shown on the left in Figure 3.1 creates a high amount of tractive force that far exceeds the capability of the tire. This high amount of tractive force will cause excessive wheel spin and slower quarter mile times.

With the original gear ratios, the drag car experiences a significant amount of wheel slippage early in the drag run. The gear ratio improvement will try to eliminate this excess wheel slippage to better utilize the available traction. By simulating a quarter mile run, while incorporating wheel slip, the gear ratio improvement program will iterate the first gear ratio to find the gear that will produce the lowest simulated quarter mile time. Once a first gear ratio has been selected, the same iteration process will be performed on the remaining gears until all have been selected.

Figure 3.2 shows wheel slip and velocity for a vehicle using two different gear sets, A and B. Gear Set A (dotted lines) causes excessive wheel spin while Gear Set B (solid lines) does not. It can be seen that reducing the amount of wheel slip, assuming it is excessive, will increase the forward velocity that the drag car will attain during the beginning of a quarter mile run. The most efficient gear ratios will use as much of the available traction as possible, while minimizing large drops in torque when up-shifting. The gear ratio improvement program inherently covers both of these shortfalls that the original gear ratio setup exhibits. As the gear ratios are improved, the available traction will be more efficiently used which should, in turn, provide faster quarter mile times.
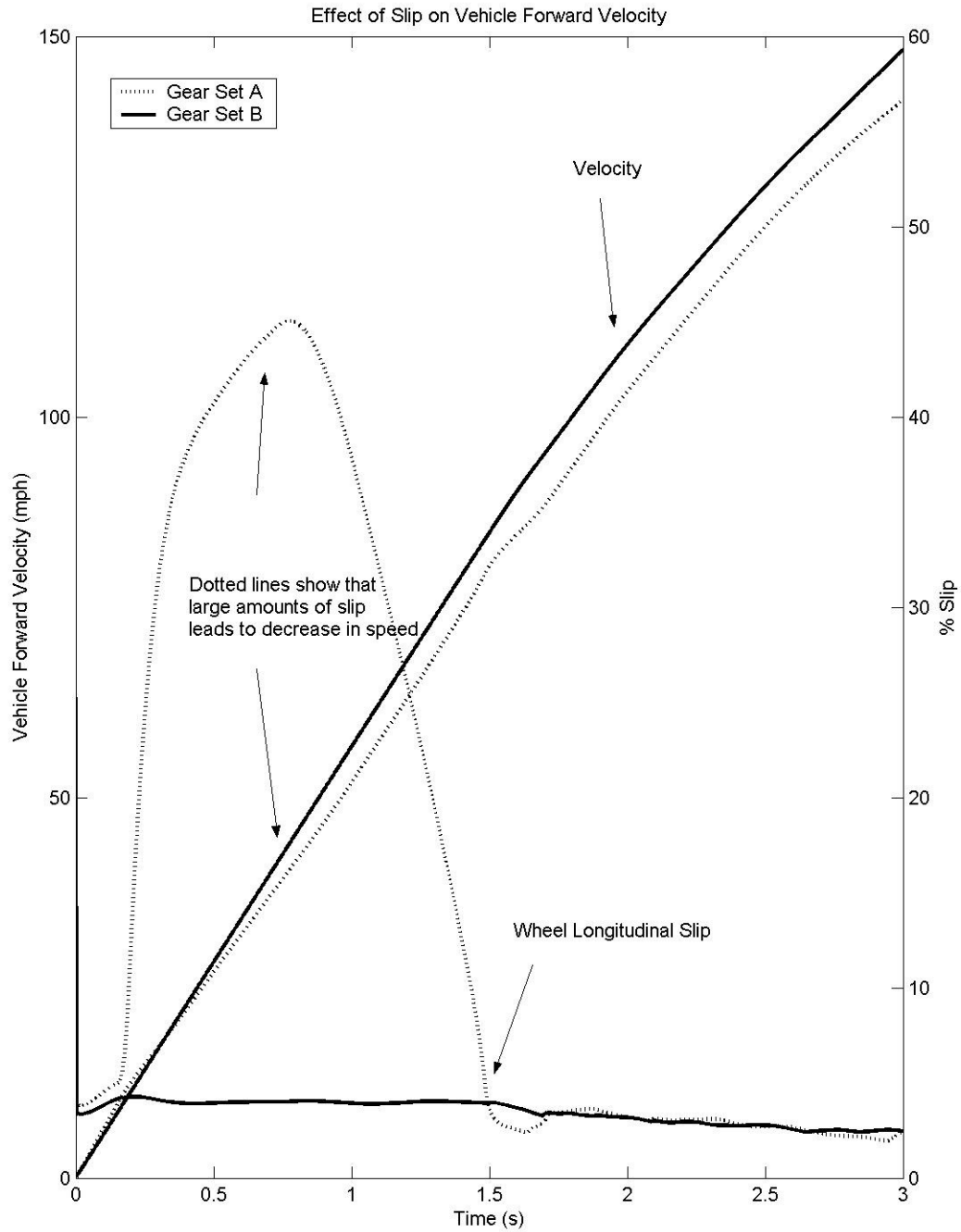
Figure 3.2: Wheel Slip Effect on Vehicle Velocity

CHAPTER FOUR

ROAD MODEL

Random Road Profile

A road surface that you would drive over on the highway would be considered a random surface. The same goes for a drag strip. These random "functions" do, however, exhibit some characteristic features. Wong [3] states that statistical properties of a certain type of road are consistent among all sections of the same type of road. Also, Ramji [4] states that one can perform a frequency analysis of a road profile to make an estimate of the amplitudes for various wavelengths present. Typically, this analysis is expressed in terms of its power spectral density, or PSD. From a surface profile of a particular type of road, an asphalt highway for example, a PSD of the profile may be determined as a function of spatial frequency. The spatial frequency content of each real road is used to recreate the vertical profile of the road in the model. Spatial frequency can be related to temporal frequency simply by dividing the temporal frequency by a constant velocity. The relationship of the road PSD to spatial frequency can be approximated by Equation (21), where S is the PSD, in ft²/(cycle/ft), and Ω is the spatial frequency, in cycles/ft.

$$S(\Omega) = C_{sp} * \Omega^{-N} \tag{21}$$

C_{sp} and N are the magnitude and exponent, respectively, of the approximate fitted curve of the road profile PSD to the experimentally determined curve. These constants for a given real road surface are found in Wong [3]. The values of C_{sp} and N used during this research are given in Table 4.1.

Table 4.1: Values of C_{sp} and N for Power Spectral Density of Surfaces

Road Description	N	C_{sp} (ft^2/cycle/ft)
Smooth Runway	3.8	1.60E-11
Smooth Highway	2.1	1.20E-06

The model used in this thesis includes the vehicle excitation due to randomly rough roads. The specific drag strip characteristics are selected to have a roughness severity between that of the smooth runway and the smooth highway.

The random road profile generator, implemented through MATLAB and Simulink was developed by David Moline [5]. The model creates a sum of 300 sine waves that are scaled using simple equations to give the desired road power spectral density. The MATLAB portion of the model generates 300 sine waves of random phases, created with a random number generator, and specified frequencies, linearly spaced from 0.1 to 100 Hz. The MATLAB and Simulink code is available in Appendix C.

The amplitude of each sine wave is dependent on the frequency of that particular sine wave and is governed by Equation (22). A_o is the constant, dependent on road surface, determined by a trial and error method to scale the randomly generated road profile to provide the correct magnitude of the PSD according to the road being simulated. The values of A_o are 0.03, 0.16, and 0.1 for the runway, drag strip, and highway respectively. The minimum and maximum frequency content of the random road is specified by the user, 0.1 and 100 Hz for this study, and the 300 frequencies are taken from this limit using linear spacing. Q is the exponent used in defining the slope of the power spectral density estimate of the randomly generated road profile. Q is related

to the slope of the power spectral density approximate fitted curve through a simple equation shown in Equation (23).

$$Amp_i = A_o * freq_i^Q \tag{22}$$

$$Q = \frac{N}{2} + 1 \tag{23}$$

$$profile = \sum_{i=1}^{300} Amp_i \sin(\omega_i t + \phi_i) \tag{24}$$

These attributes are then passed to Simulink to create the sine waves. The sine waves are then summed to create a surface which is used as the road profile input. The random road profile is generated in the spatial domain as shown in Equation (24). The longitudinal position of each contact point with the road surface, front and rear axles and wheelie bar contact, will be accessed at each moment in time using Equation (25).

$$x(t) = \int_0^t v(t)dt \tag{25}$$

This longitudinal position can then be related to a vertical displacement of the random road profile at that particular point. Thus, the road inputs to the vehicle model can be established.

Figure 4.1 shows an example of a desired road PSD, a smooth runway, and the simulated PSD of the road created by the simulation to match the desired road surface. As can be seen in this figure, the simulated road mimics the desired PSD fairly closely except for the lower frequency range. Real drag strips have PSDs that level off at low frequency, due to the flatness of the track, so the simulated PSD is in all likelihood closer to that of a real drag strip with a surface texture similar to that of a smooth runway.
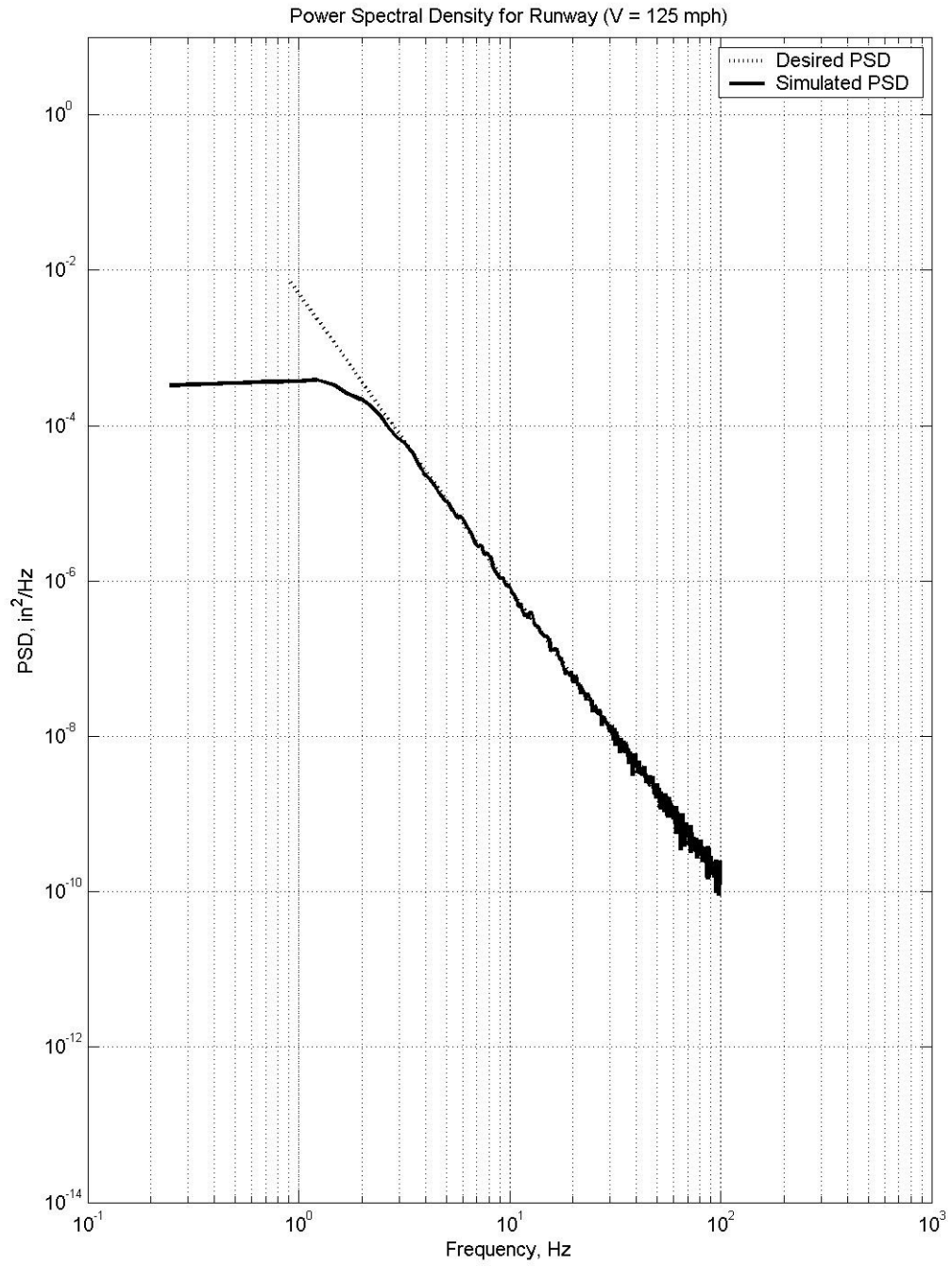
Figure 4.1: Power Spectral Density of Generated Runway

CHAPTER FIVE

RESULTS

<u>Introduction</u>

The results of this study will be described in this chapter. The first portion of the results sections will give the results of the case studies that were performed to investigate how the vehicle performance is affected by different road inputs. Case studies involving gear ratio selection are then discussed in detail.

The three road profiles used in the case studies involving road roughness effects on vehicle dynamics, listed in order of smoothest to roughest surface, are the smooth runway, simulated drag strip, and a smooth highway. The smooth runway and smooth highway will be referred to as the runway and highway respectively throughout this thesis. The gear ratio selection was performed for both a perfectly smooth flat road, with no vertical input from the road to the vehicle, and for the simulated drag strip. Gains in quarter mile performance are shown and discussed.

Another important aspect discussed in the results is the robustness of the gear ratio selection to different track-to-tire adhesion levels, or "mu" values. The drag performance of the vehicle with the improved gear ratios is compared to that with the original gears for tire-to-road adhesion levels +/- 20% from the nominal case. The gear ratio selection is also performed using these varying mu values, and the results are discussed later in this section.

Random Road Profile

Andrén [6] states that the vertical displacements of a road profile should be a member of a stationery random process, a signal whose statistical properties do not vary with length of road. Therefore, it is expected that the vertical displacements of the road profiles generated by MATLAB and Simulink will be normally distributed. In the case of a normal distribution, the majority of the data will remain within plus or minus three standard deviations of the data mean. In order for a set of data to be considered normally distributed approximately 68.2% of the data should be contained within + or - one standard deviation of the data mean, 95.4% within + or - two standard deviations, and 99.73% within + or - three standard deviations of the mean. Table 5.1 shows the vertical displacement data from the randomly generated road profiles. The standard deviations, root mean square (RMS) value, and the average value found from the random profiles generated through MATLAB are given.

Table 5.1: Random Road Vertical Profile Data

Road Type	σ (in)	RMS (in)	Avg (in)
Runway	0.03	.03	0.0015
Drag Strip	0.1802	0.1802	0.0027
Highway	0.1692	0.1692	0.0032

Table 5.2 indicates that the randomly generated road profiles are approximately normally distributed. This table contains the percentages of the data contained within the ranges of standard deviations from the mean. The percentages in parentheses are the percentages which would indicate a normally distributed data set.

Table 5.2: Normal Distribution Data for Randomly Generated Road Profiles

Road Type	+/- 3σ (99.73%)	+/- 2σ (95.4%)	+/- 1σ (68.2%)
Runway	99.28 %	94.11 %	73.09 %
Drag Strip	99.43 %	94.38 %	72.40 %
Highway	99.66 %	95.43 %	68.57 %

As can be seen, the profile data for all of the different road types that were randomly generated are approximately normally distributed. The randomly generated runway and drag strip deviate most from the normal distribution curve. The data, however, can still be considered approximately normally distributed because the data which is most skewed, i.e., the data within +/- one standard deviation from the mean, is less than 5% over the nominal 68.2% which should be within this range. This only means that slightly more data is contained within the range of +/- one standard deviation from the mean than a normally distributed curve.

Perhaps an easier way to visualize the normality of a set of data is to plot the data and compare it with a normal distribution curve. The percentages of data points within the standard deviation ranges discussed earlier are calculated and then plotted together with a normal (Gaussian) distribution curve for each of the three simulated road types in Figures 5.1-5.3. As can be seen in the plots, all of the data appear to be approximately normally distributed.

The simulated random roads need to also have the same power spectral density characteristics as the real roads. The power spectral densities of the real world roads can be estimated and plotted using Equation (21) and the values in Table 4.1. The curves given in Equation (21) are approximately fitted to the power spectral densities of real

road surfaces as described in Wong [3]. The aggressiveness, or roughness, of the drag strip is assumed to fall in between the surfaces of the runway and highway. It was determined through informal communications with the project sponsor that the maximum velocities across the shocks during a drag run would reach no more than approximately 1.5 ft/s. From simulations using the runway and highway random roads, the maximum velocities across the shocks were roughly 0.3 and 4.4 ft/s respectively.

Thus, it was assumed that the velocities across the shocks (and hence the road roughness) of the simulated drag strip would fall somewhere in between that of the runway and the highway. The road power spectral density for the simulated drag strip was determined through trial and error until the desired maximum velocity across the shocks, about 1.5 ft/s, was reached.
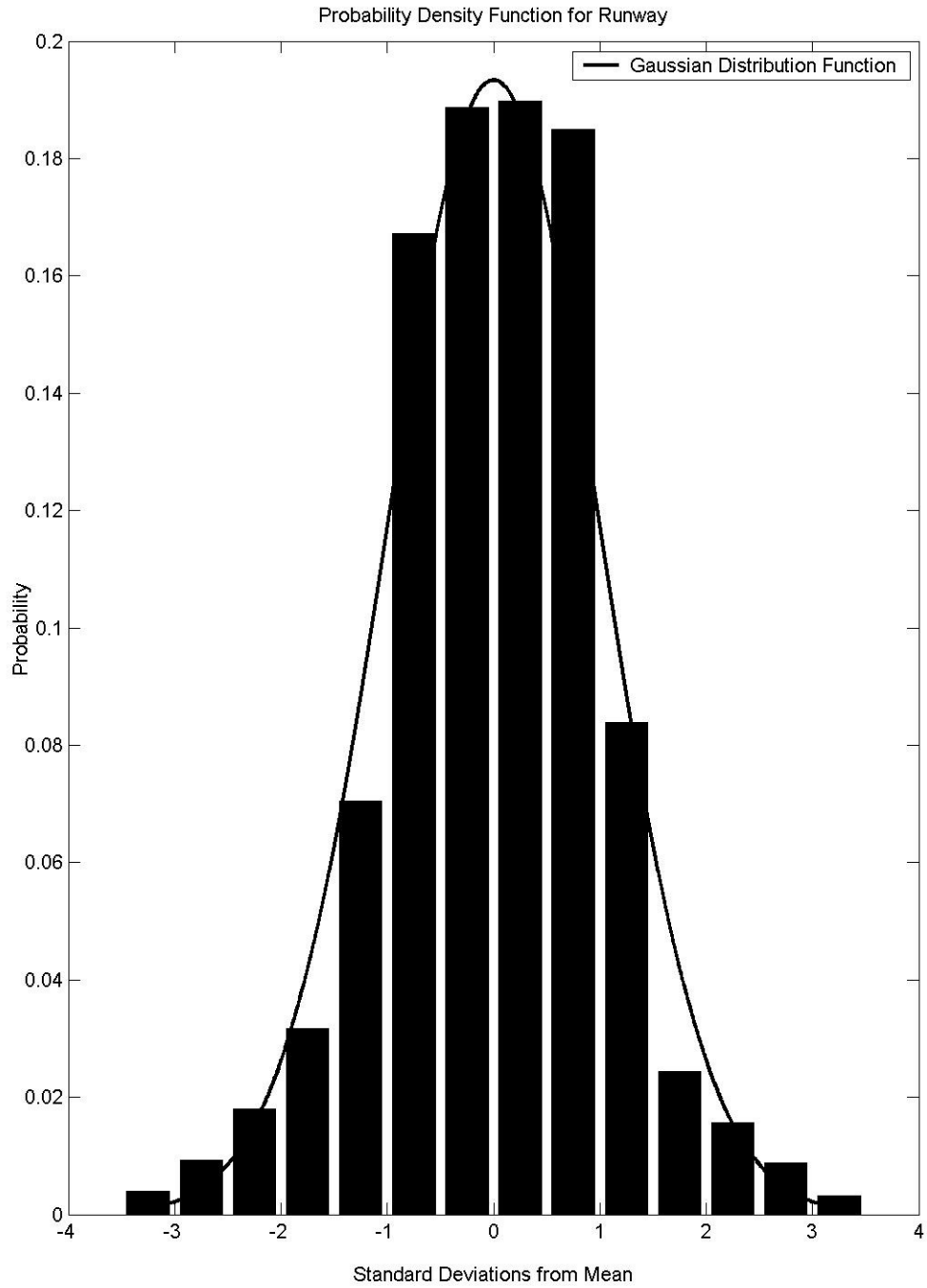
Figure 5.1: Probability Density Function for Runway
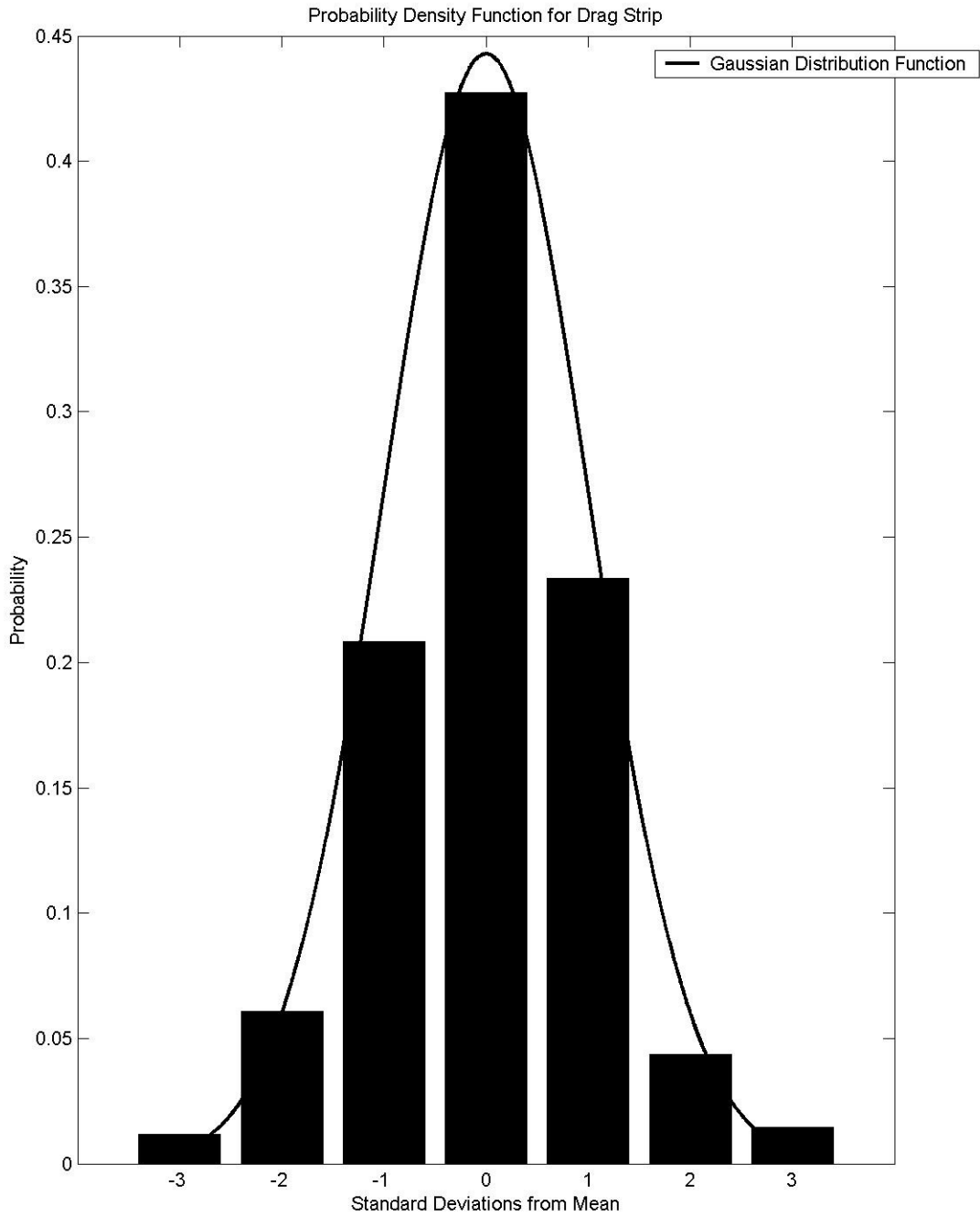
Figure 5.2: Probability Density Function for Drag Strip
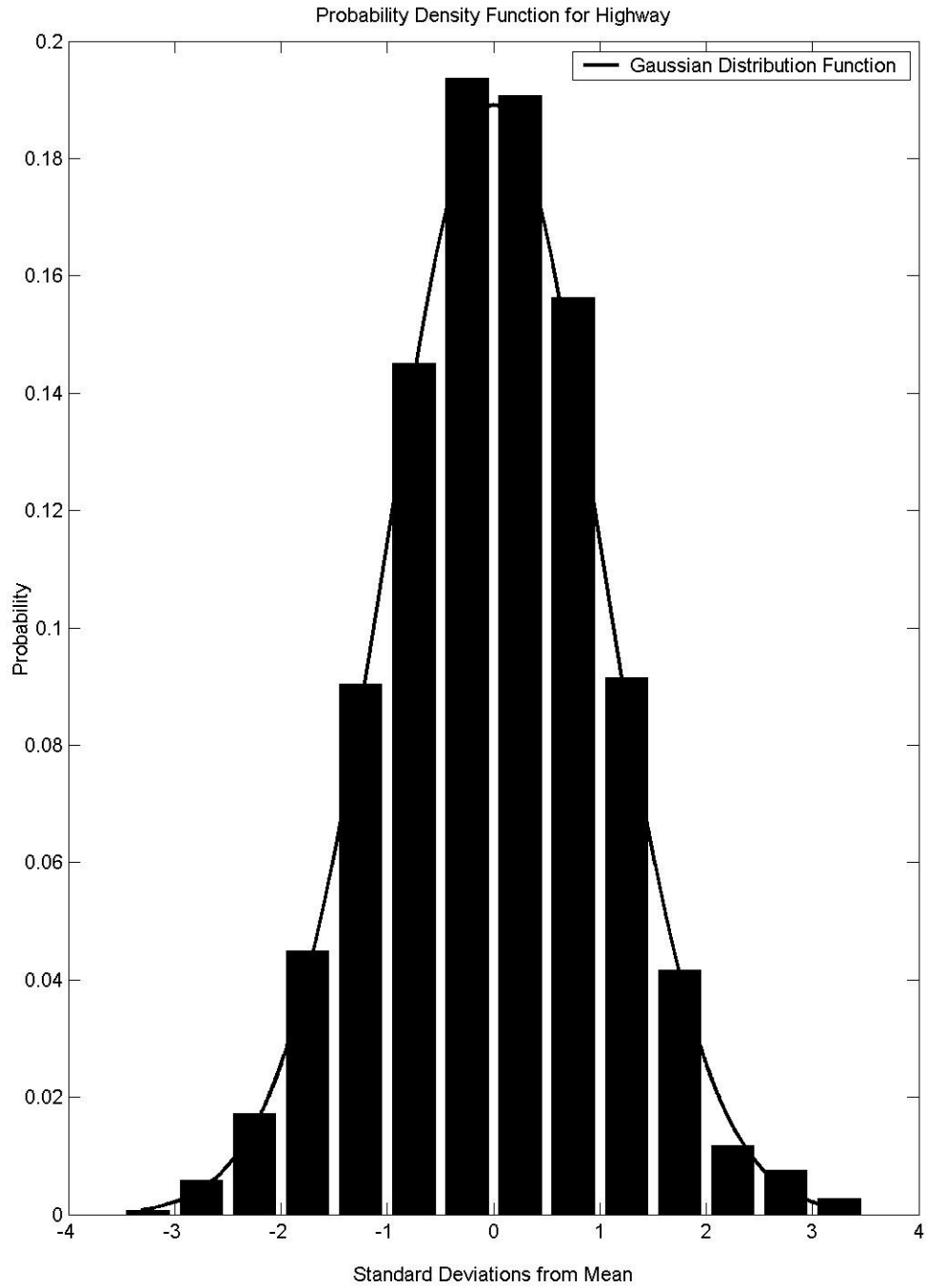
Figure 5.3: Probability Density Function for Highway

The road power spectral densities given in Wong [3] are plotted in Figures 5.4-5.6. These plots produce a straight line on the log-log plots because they are a curve fit to the measured data from the actual roads. The power spectral densities of the randomly generated road profiles are plotted over the curve fits for the actual roads. The randomly generated roads are filtered to eliminate the large bumps associated with the low frequency portion of the power spectral density plot. This causes the left portion of the power spectral density of the randomly generated road profiles to level off, decreasing the magnitude of the bumps in the lower frequency range. This is more indicative of the roads encountered on drag strips, since they have no large, long wavelength (or low frequency) bumps and are relatively flat.

As can be seen by the plots of the road power spectral densities, the generated roads match almost exactly the real road power spectral densities. The conclusion drawn from these plots is that the generated roads accurately depict the road profiles of the surfaces we want to study. The vertical road profiles and slopes of the three simulated roads are shown in Figures 5.7-5.9. As can be seen by the figures, the highway is the most aggressive road, followed in decreasing severity by the drag strip and then the runway.

Figure 5.4: Power Spectral Density of Generated Runway

Figure 5.5: Power Spectral Density of Generated Drag Strip
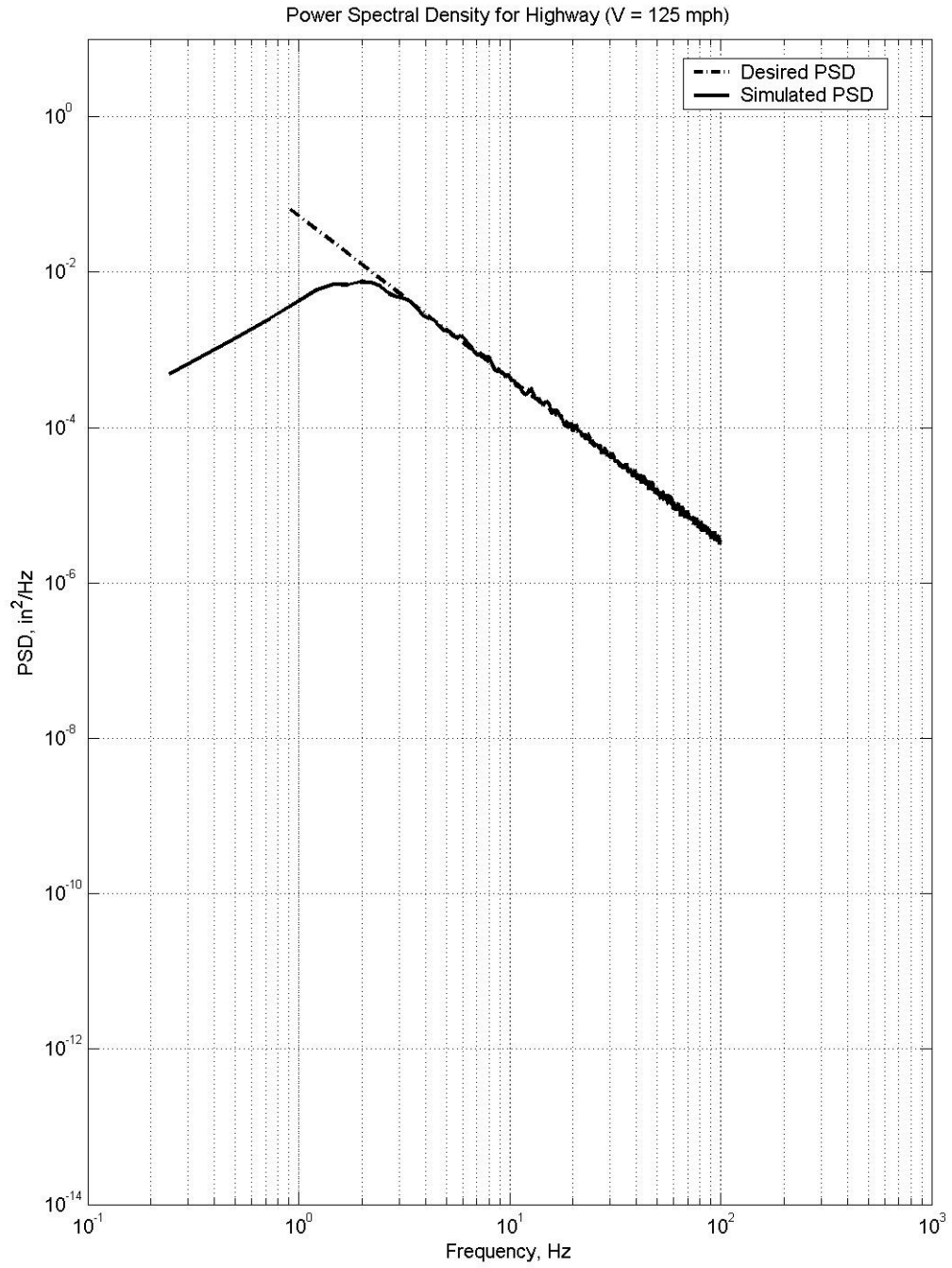
Figure 5.6: Power Spectral Density of Generated Highway
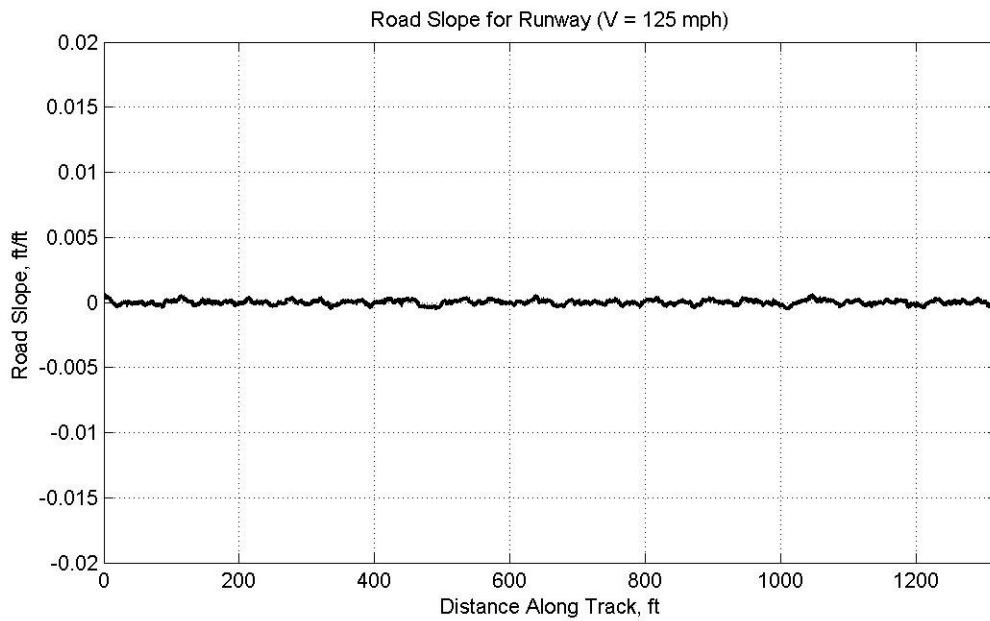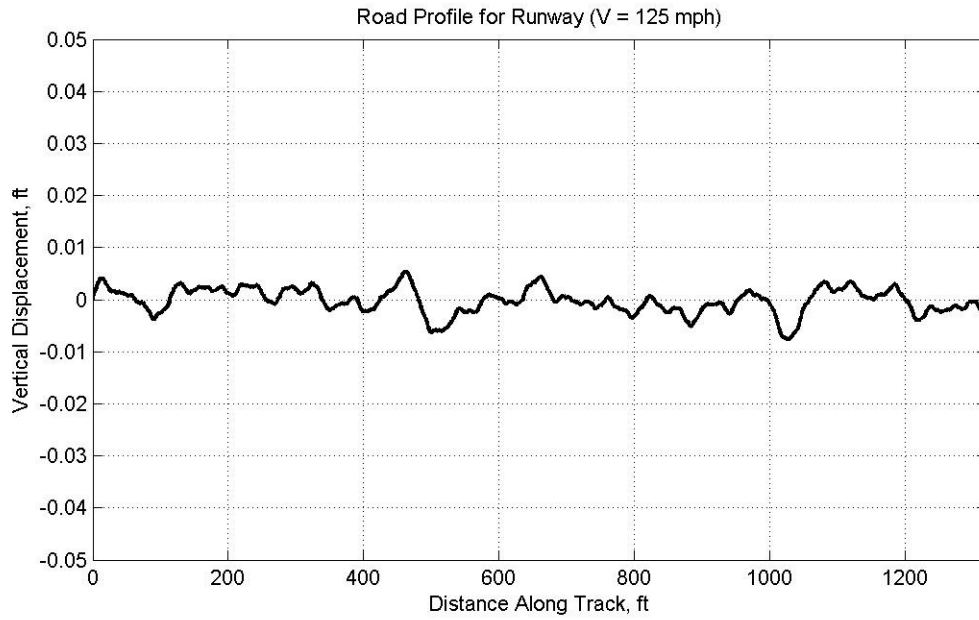
Figure 5.7: Simulated Runway Vertical Profile and Road Slope
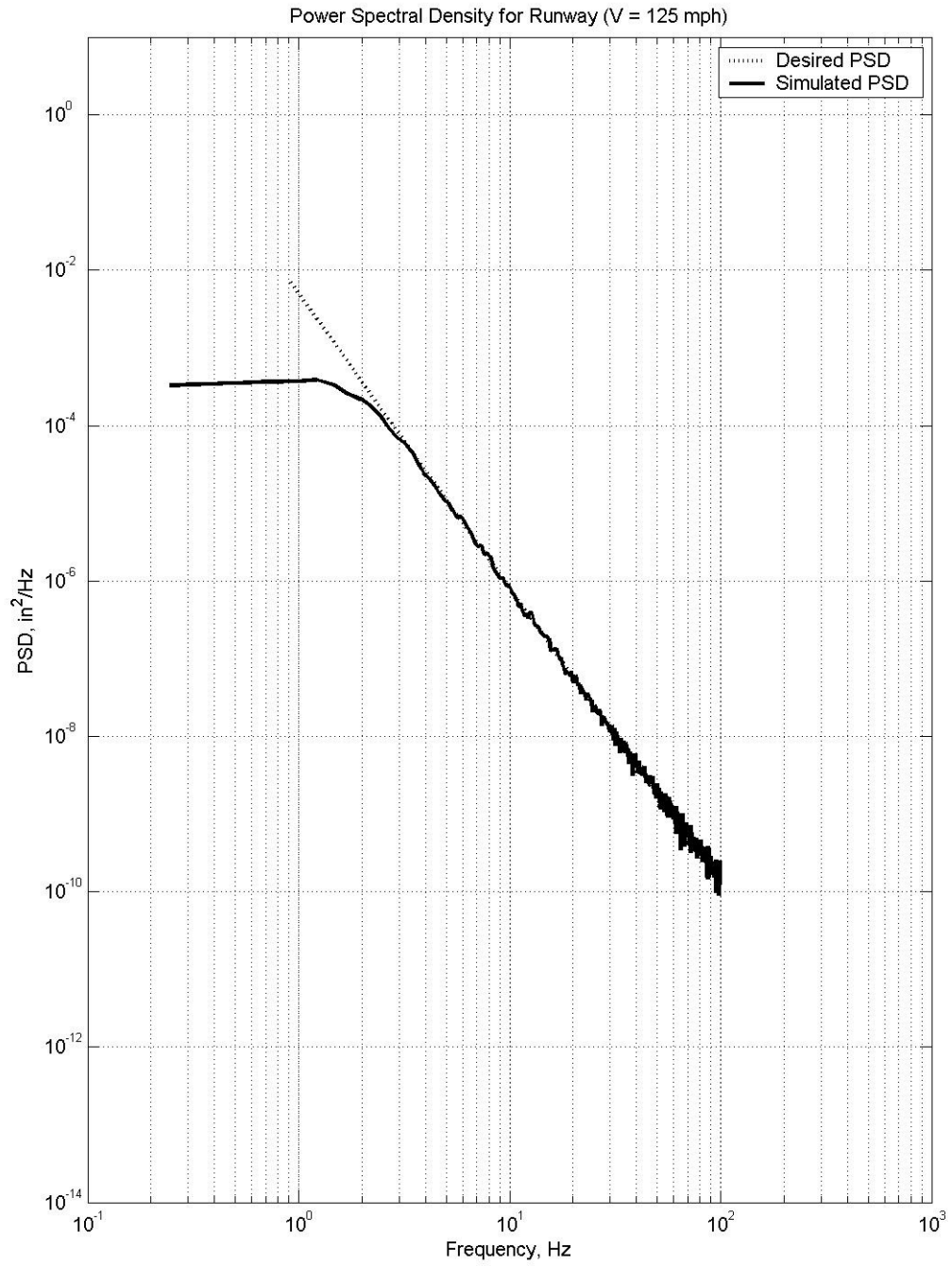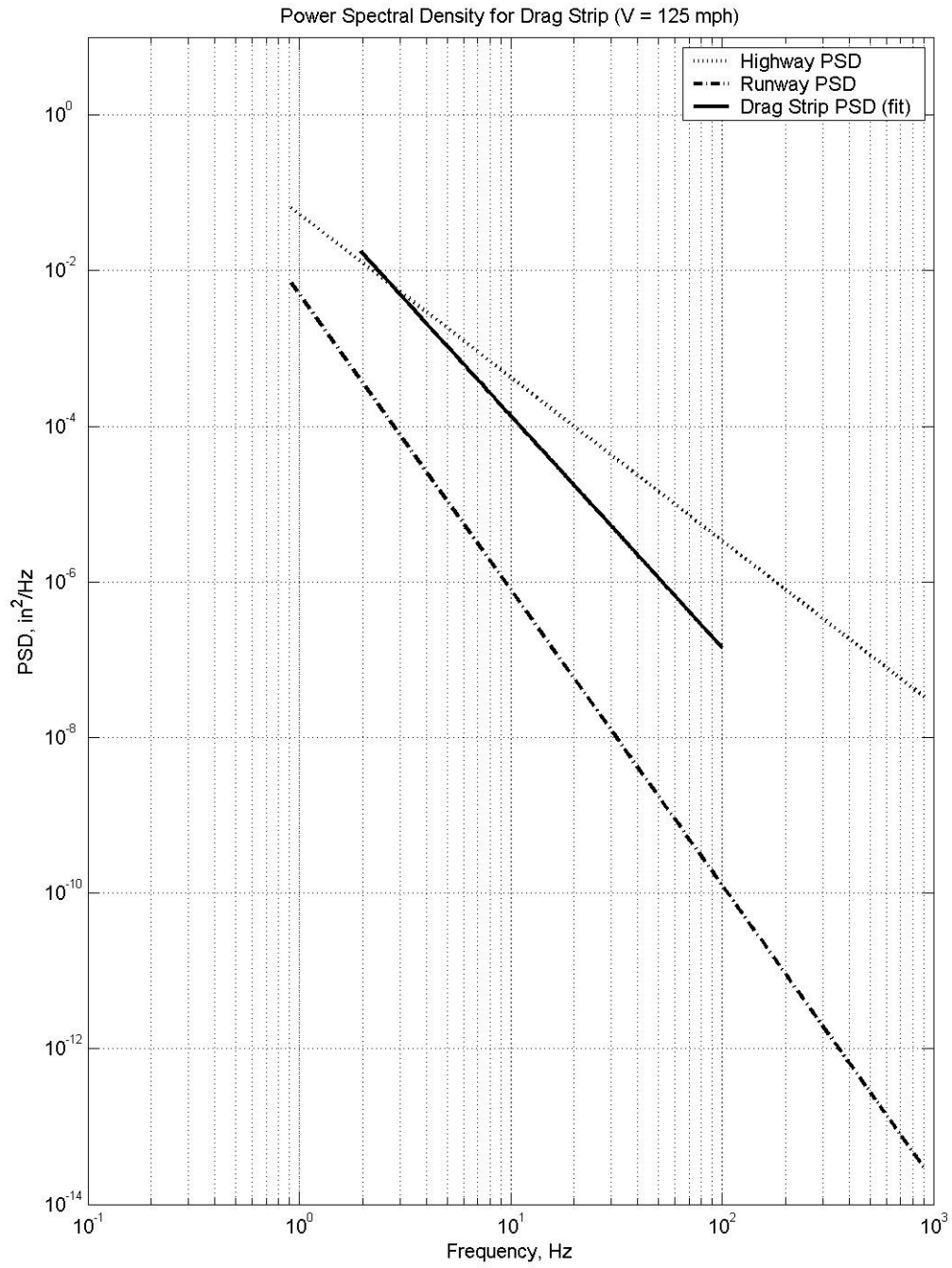
38
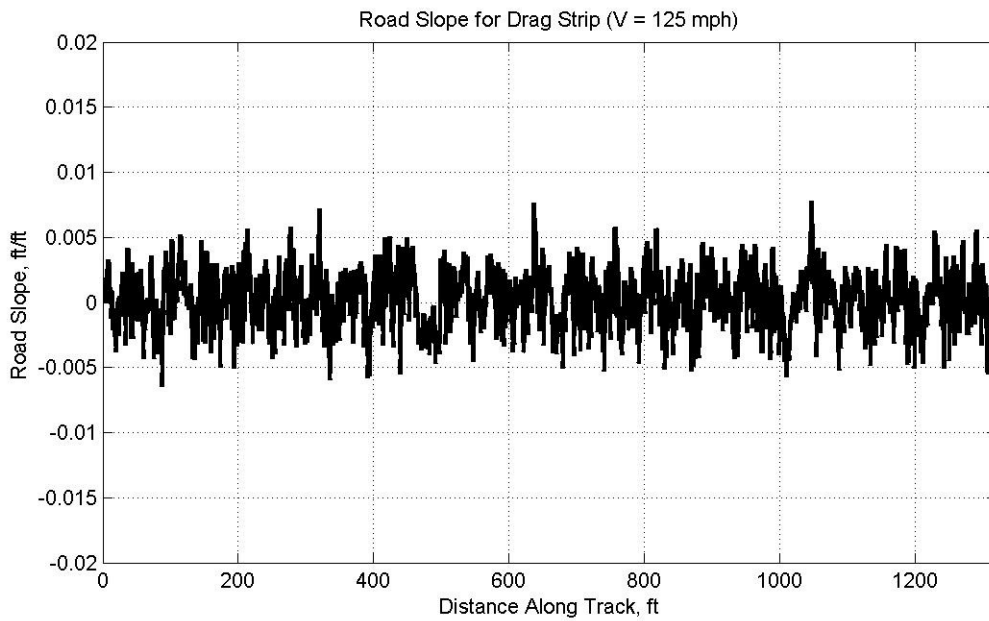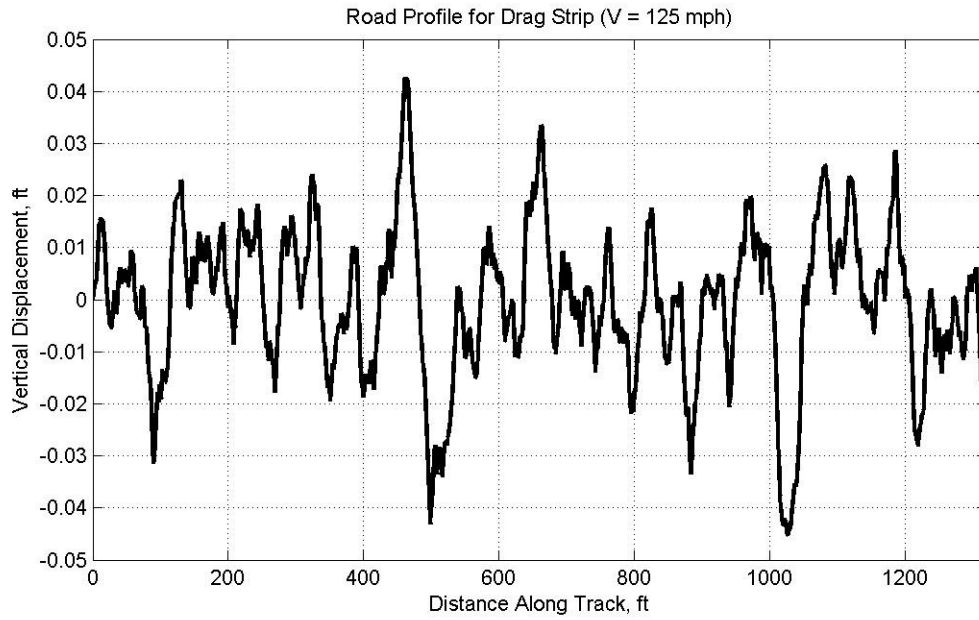
Figure 5.8: Simulated Drag Strip Vertical Profile and Road Slope

39
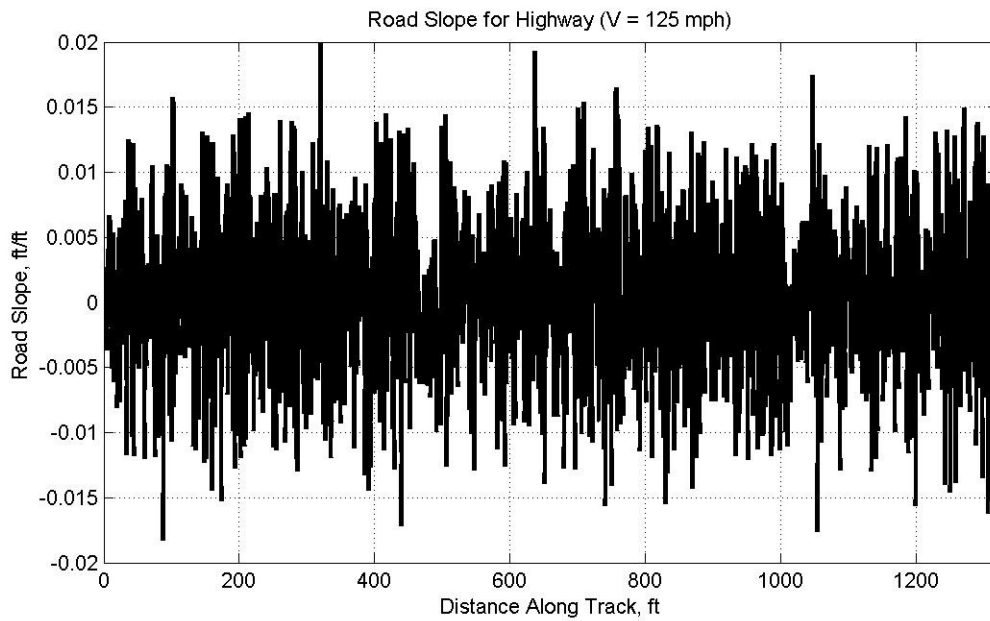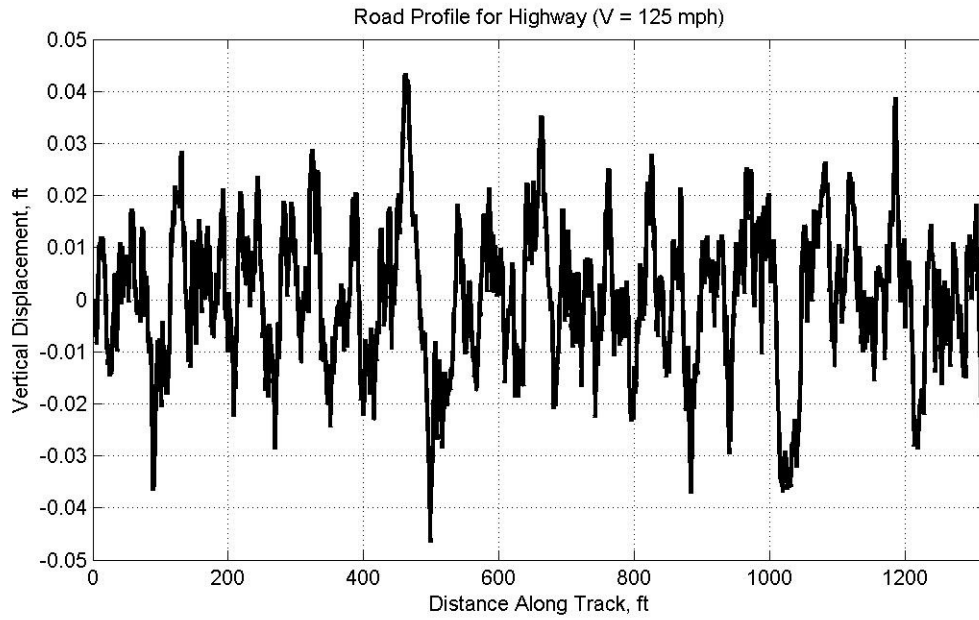
Figure 5.9: Simulated Highway Vertical Profile and Road Slope

Case Studies / Road Roughness

Perfectly Smooth, Flat Road (Nominal Case)

The nominal case for the track surface of a drag strip would be a perfectly smooth, flat road. This would reduce the dynamic response of the vehicle considerably since there would be no displacement inputs from the road surface to the tires or wheelie bar. Using this track surface as the nominal case, it can be shown, through the rough road case, that roughness characteristics of the track surface greatly affect the dynamic response of a drag racing vehicle. The quarter mile performance over the perfectly smooth, flat road is shown in Table 5.3. The elapsed time is the time it takes the drag vehicle to complete the simulated quarter mile run. The trap speed is the speed, in miles per hour, the simulated vehicle is traveling as it crosses the quarter mile point.

Figures 5.10-5.14 show results for the simulated drag run using the nominal vehicle parameters given in Appendix B. There are no vertical displacement inputs to the vehicle for this nominal case and the original gear set is used.

Figure 5.10 shows time histories for the nominal case of: (a) position, (b) speed, and (c) available traction force in each gear (assuming no slip) together with the total resistive force (aerodynamic and rolling). The large drops in available tractive force are due to the change in gear ratio. As the driver shifts to higher gears, the torque provided to the drive axle decreases.

The total resistance is calculated using the drag forces calculated from Equation (1). Aerodynamic drag can become important at very high speeds, but the traction force

available at the speeds reached in this race car is much higher than the force from aerodynamic drag. The drag does have an effect however, but the effect is minimal.

Figure 5.10 also shows the estimated tractive effort coefficient in relation to slip. This coefficient is the ratio of instantaneous longitudinal traction force (Fx) to instantaneous vertical normal force (Fz). As can be seen in the figure, the tractive effort coefficient increases linearly until the slip of the tire becomes significant. The tractive effort coefficient for the simulated drag tires reaches a peak at around three, a rather startling value since most street tires only reach about one, and begins to slightly decrease. Therefore, the slip that the front tires should maintain to achieve the greatest traction force is around 5% slip. The Fx/Fz vs. slip curve used for this simulation is the estimated characteristic for these particular drag tires on this particular surface. Since no data was available for the mu-slip curves, the values for tractive effort coefficient were determined through trial and error of the vehicle simulation to reproduce quarter mile times similar to those of the actual vehicle modeled.

Figure 5.11 shows the time histories of the vehicle longitudinal acceleration, the normal forces acting on the front and rear tires, and the wheelie bar. The normal force values are normalized using the static loading on each individual component. The results are plots that give ratios of dynamic normal forces versus static loading at any point in time for the points where the vehicle contacts the track surface. As the vehicle accelerates from the start line, the longitudinal weight shift of the vehicle unloads the front axle and decreases the front normal force. As the acceleration of the vehicle decreases at the higher speeds, the front normal force approaches the steady state value of

42

one. The normal force at the rear also drops below one initially but approaches one as the acceleration decreases. This indicates that the wheelie bar is counteracting the weight shift of the vehicle at higher accelerations, but the effect lessens as the acceleration decreases.

Figure 5.12 shows the heave of the vehicle CG, the vertical displacements of the front and rear axles, and the pitch angle of the vehicle. The pitch angle increases, to approximately 0.3 degrees, as the car is launched from the start line, and then decreases as the acceleration of the vehicle decreases. This very small pitch angle is due to the assumed rigid body of the vehicle, the stiff suspension, and the pinned joint at the rear of the vehicle where the wheelie bar contacts the road surface.

Figure 5.13 shows the wheel slip and how it affects the traction available to the vehicle. At the beginning of the run, the front drive tires approach 50% slip. As can be seen from the assumed mu-slip curve in Figure 5.10, this decreases the amount of traction available to the car. At this point of the quarter mile run, as can be seen in the plot of wheel speed and velocity versus time, the front tires are spinning at almost twice the rate that the vehicle is traveling. The solution to this problem is found in carefully selecting the gear ratios, which will be discussed in the following chapter. The torque of the motor as a function of rpm is also shown in this figure. The vehicle is launched from a stand still position at 8000 rpm, which generates approximately 450 ft-lbs of torque at the flywheel. This torque, when transmitted to the drive axle, is enough to overcome the available traction at the wheels, which in turn causes the excessive amount of wheel spin.

Figure 5.14 shows the actual torque produced at the drive wheels and the traction force produced at the front axle during the quarter mile run. The motor torque generates a force at the wheel to road contact that is greater than traction available at the beginning of the run. The lower gear ratios used at the beginning of the quarter mile run create this higher torque at the drive tires which causes excessive wheel slip at the beginning of the run. The "jumps" in the traction force can be attributed to the shift points during the drag run. Figure 5.13 shows that there is only a small interval of engine rpm that provides maximum torque. As the vehicle is shifted into the next gear, the engine rpm decreases, which moves the engine rpm out of this maximum torque range.

Table 5.3: Quarter Mile Performance for Perfectly Smooth, Flat Road

Original Gears	
	Flat Road
Elapsed Time (seconds) =	8.307
Trap Speed (miles per hour) =	166.45
1/8 Mile Time (seconds) =	5.427
1/8 Mile Speed (miles per hour) =	141.85
330 Foot Time (seconds) =	3.662
60 Foot Time (seconds) =	1.510
Max Vel. Across Shocks (ft/s) =	0.305
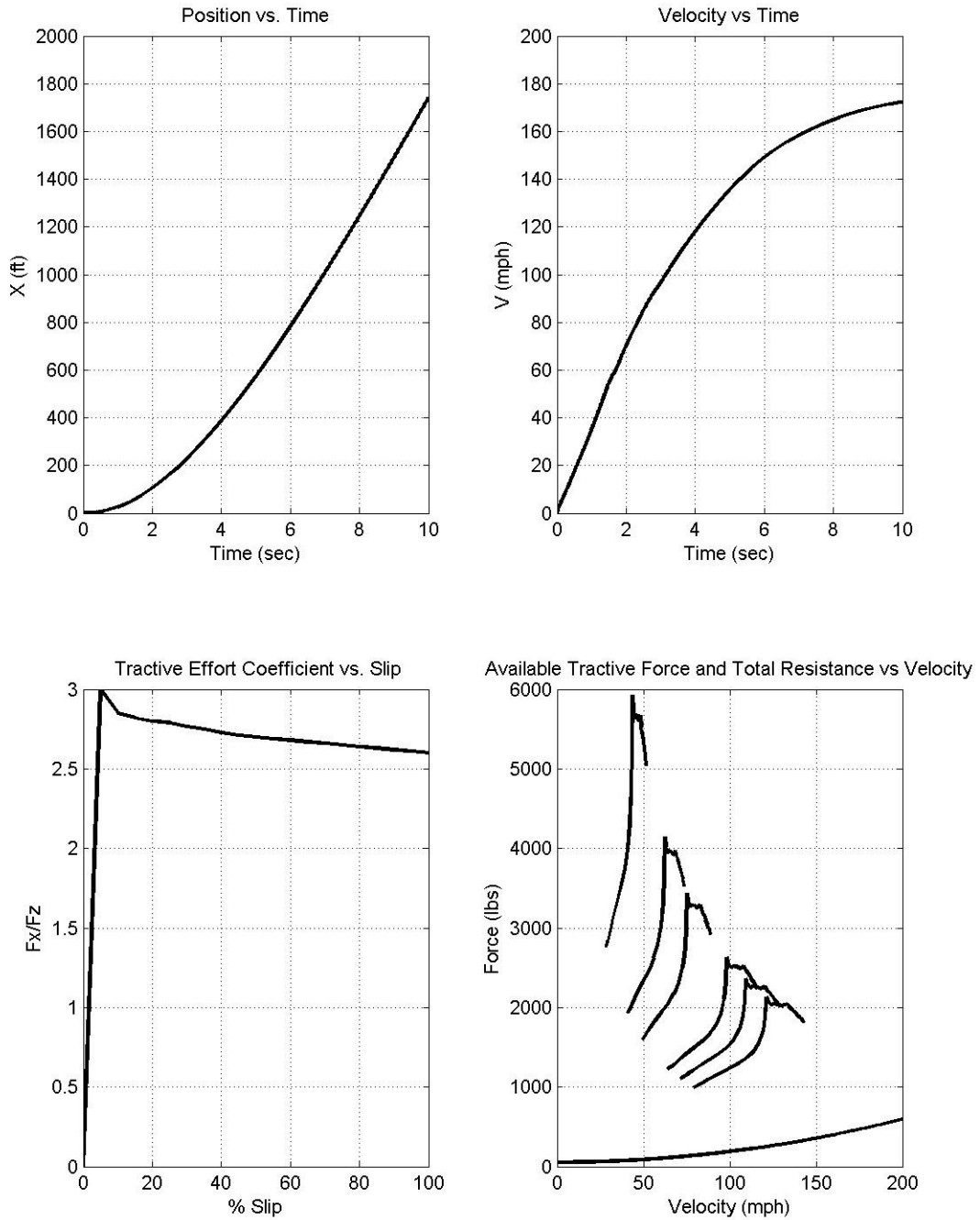
Figure 5.10: Vehicle Dynamics Plot 1 over Perfectly Smooth, Flat Road
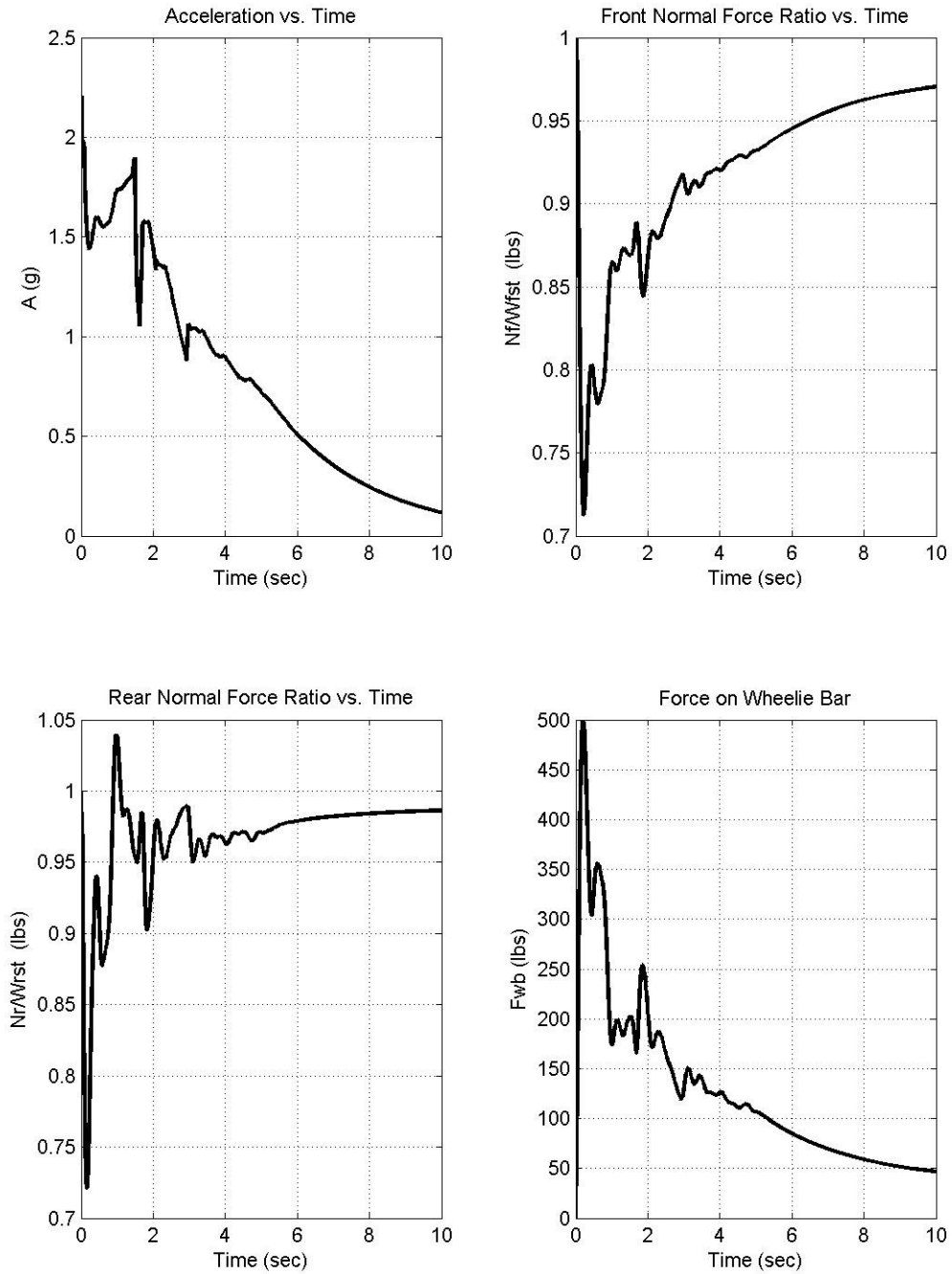
Figure 5.11: Vehicle Dynamics Plot 2 over Perfectly Smooth, Flat Road
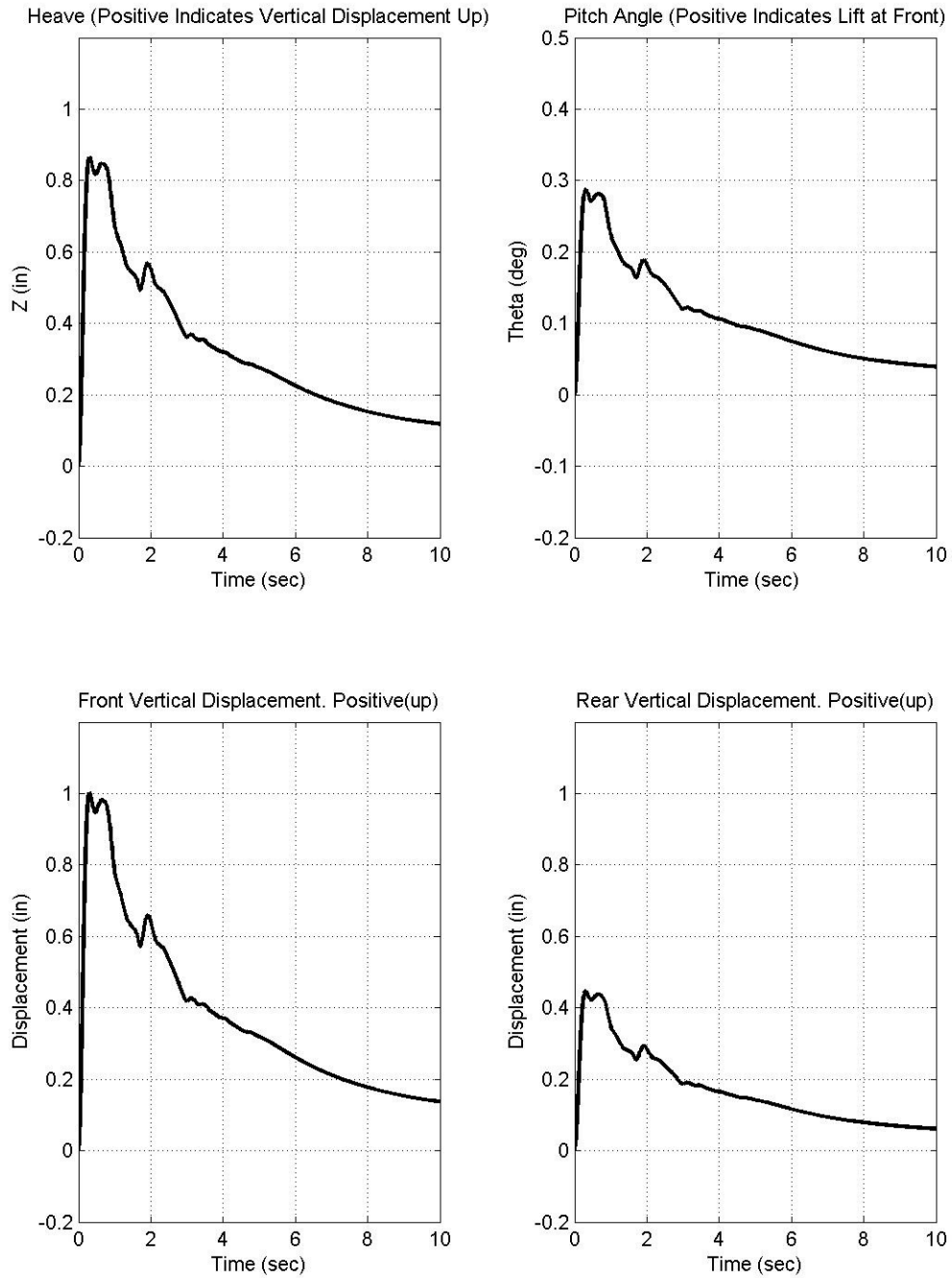
Figure 5.12: Vehicle Dynamics Plot 3 over Perfectly Smooth, Flat Road
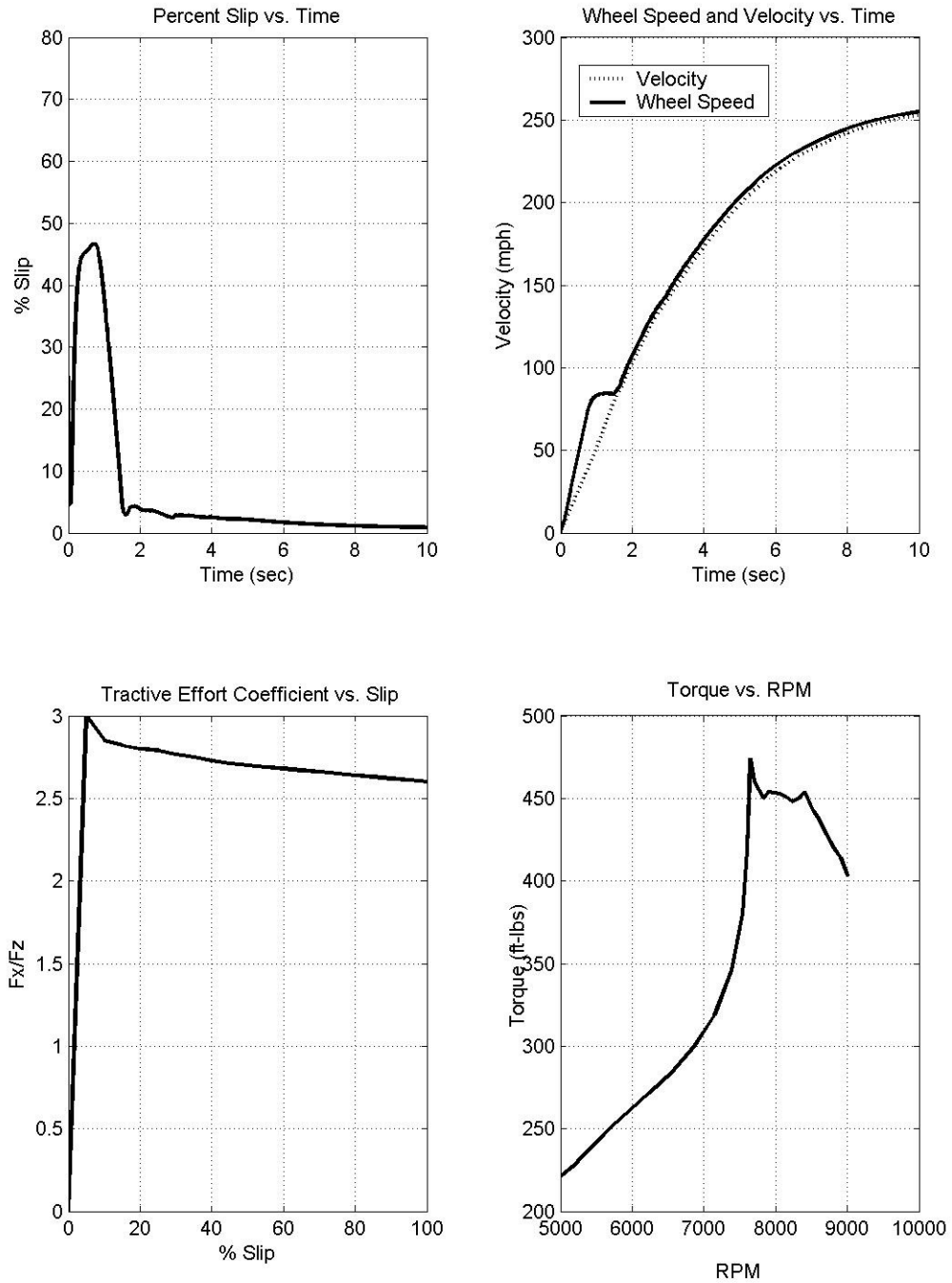
Figure 5.13: Vehicle Dynamics Plot 4 over Perfectly Smooth, Flat Road

48
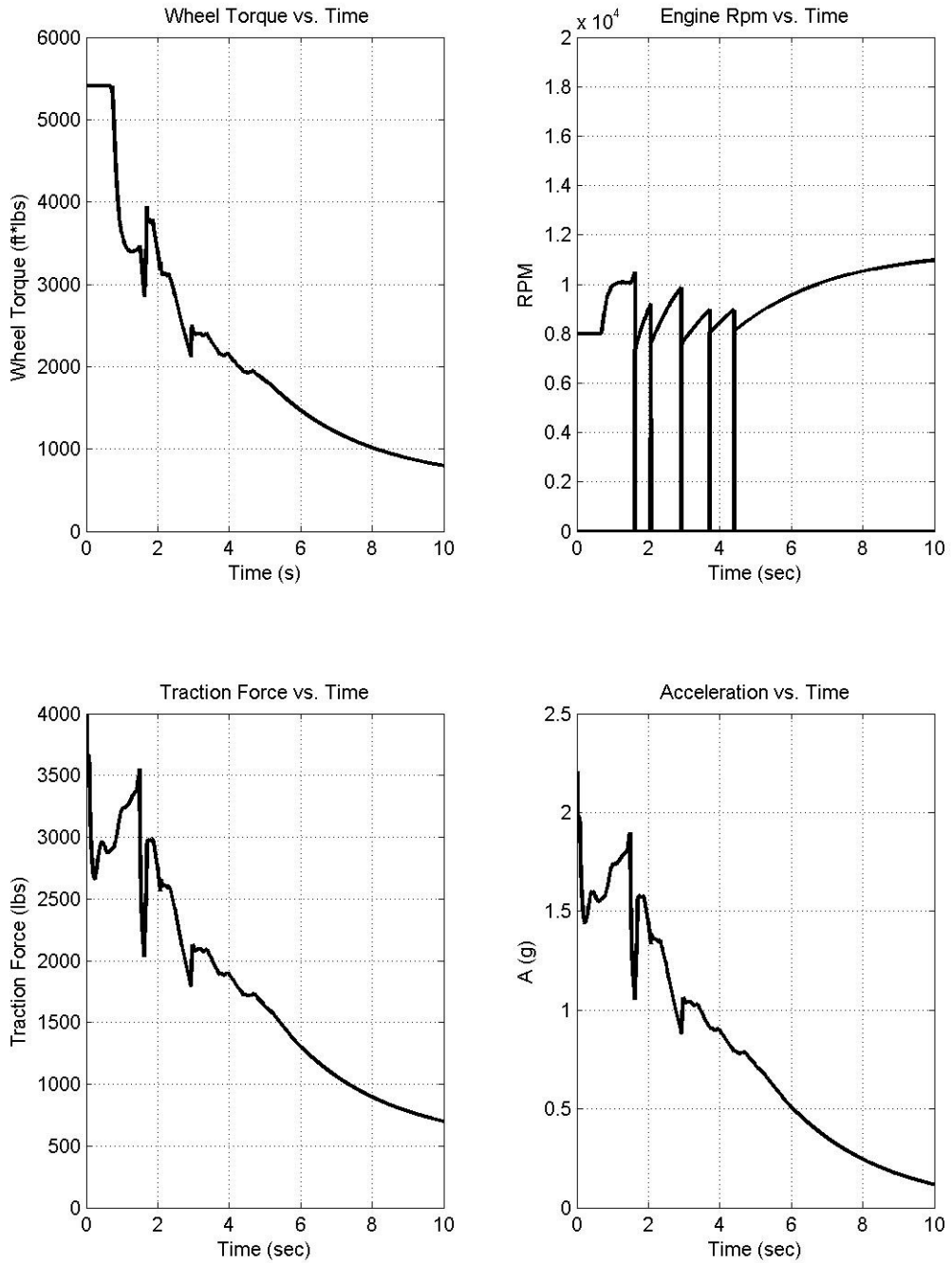
Figure 5.14: Vehicle Dynamics Plot 5 over Perfectly Smooth, Flat Road

Highway

The second case that is studied in depth is that of the car traversing the quarter mile strip of the simulated highway. This highway consists of the roughest vertical profile that was studied in this research project. The plots shown in Figures 5.15-5.19 give an overall depiction of the dynamic response of the front wheel drive drag racing car during the quarter mile simulation over the highway. The quarter mile performance, as compared with the nominal case, is shown in Table 5.4.

The position and velocity vs. time plots in Figure 5.15 looks very similar to those of the nominal case. The scale that is used to show the speeds of the entire drag run do not capture the small differences in quarter mile performance between the nominal case and the highway. These differences, although small compared to the magnitude of the speed and quarter mile time (8.326 vs. 8.307 seconds for the quarter mile), are very important in the drag racing world.

Figure 5.16 shows the main effect that the road roughness has on the vehicle dynamics. The normal forces associated with the vehicle contacts with the road surface are directly related to the roughness of the road surface. As can be seen in the plots, the normal force ratio goes negative for both the rear axle and wheelie bar. This would indicate a tension force between the tire or wheelie bar and the road, which is not possible. In this model, the wheelie bar is a pin that is not allowed to depart from the track surface. The tension generated at the wheelie bar contact with the track surface then adversely affects the normal forces at the rear axle. This is one negative aspect of modeling the wheelie bar as a pin joint that is fixed to the road. This problem only

occurs when the vehicle is traversing an aggressive road surface like the highway. Figure 5.16 also shows the longitudinal acceleration of the drag car over the course of the quarter mile run. The maximum acceleration of the drag car happens in peaks and the magnitude is around 2.3 longitudinal g's, or about 22 m/s^2. Compared with the nominal case, the maximum acceleration of the vehicle is greater over the highway. This is caused by the downward heaving of the sprung mass, which in turn creates a larger normal force on the front axle and creates more traction force available. On the other hand, however, as the sprung mass heaves upwards, the amount of normal force on the drive tires decrease and the longitudinal acceleration decreases as well. This oscillation of the sprung mass, which is caused by the road surface roughness, causes the normal forces and vehicle accelerations to oscillate as well.

Figure 5.17 shows the vertical displacements of the car, including the heave of the CG, the displacements of the front and rear axles, and the pitch angle of the vehicle. The oscillation that was discussed in the previous paragraph can be seen very clearly in these plots. The pitch angle of the car climbs to approximately 0.2 degrees as the vehicle launches. This angle is less than that of the nominal case, due to the average longitudinal acceleration magnitude being less.

Figure 5.18 shows very similar responses compared to those of the nominal case. The road surface roughness can be detected in the oscillation of wheel slip. The magnitude of the wheel slip at the beginning of the drag run still approaches 50%, which does not use the maximum traction available from the tire to track interface.

Results shown in Figure 5.19 also look similar to those of the nominal case. The traction force and wheel torque both exhibit the dynamic oscillations that were discussed previously.

The vehicle dynamic response, when compared between the perfectly smooth, flat road and the highway, is quite different. Since there are no vertical excitations from the flat road, the pitch and heave of the vehicle over the flat surface are only affected, in this model, by the longitudinal acceleration of the vehicle. The vertical inputs from the highway to the front and rear axles, along with the longitudinal acceleration of the vehicle, cause the car to exhibit more complicated dynamics and more oscillation around the equilibrium positions. These dynamics affect the forces applied to the vehicle, which affect many properties, such as front axle normal force, which are used to determine the available tractive force at the drive axle.

Table 5.4: Quarter Mile Performance Perfectly Smooth, Flat Road vs. Highway

Original Gears		
	Flat Road	**Highway**
Elapsed Time (seconds) =	8.307	8.326
Trap Speed (miles per hour) =	166.45	166.33
1/8 Mile Time (seconds) =	5.427	5.444
1/8 Mile Speed (miles per hour) =	141.85	141.64
330 Foot Time (seconds) =	3.662	3.676
60 Foot Time (seconds) =	1.510	1.515
Max Vel. Across Shocks (ft/s) =	0.305	4.36
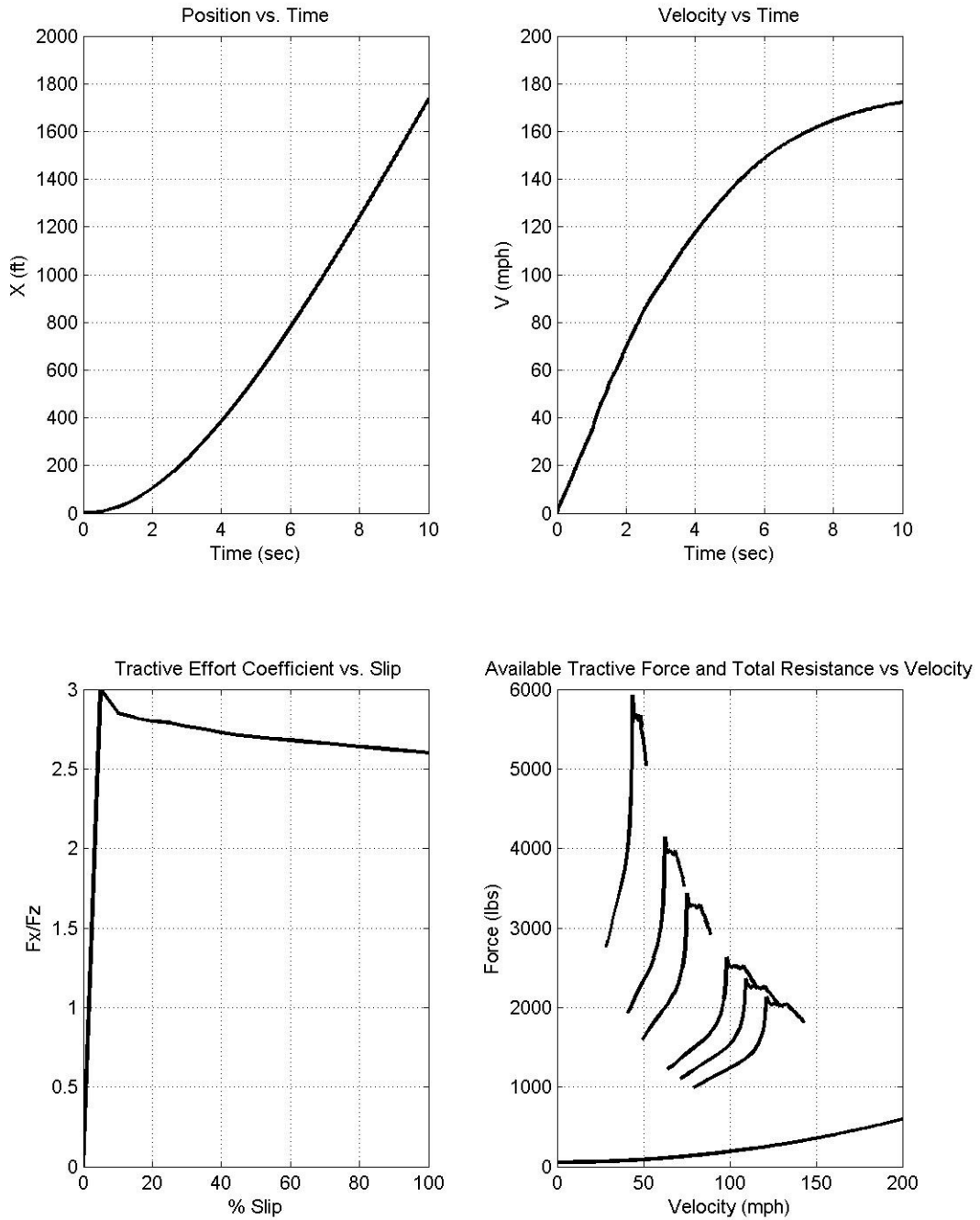
Figure 5.15: Vehicle Dynamics Plot 1 over Highway
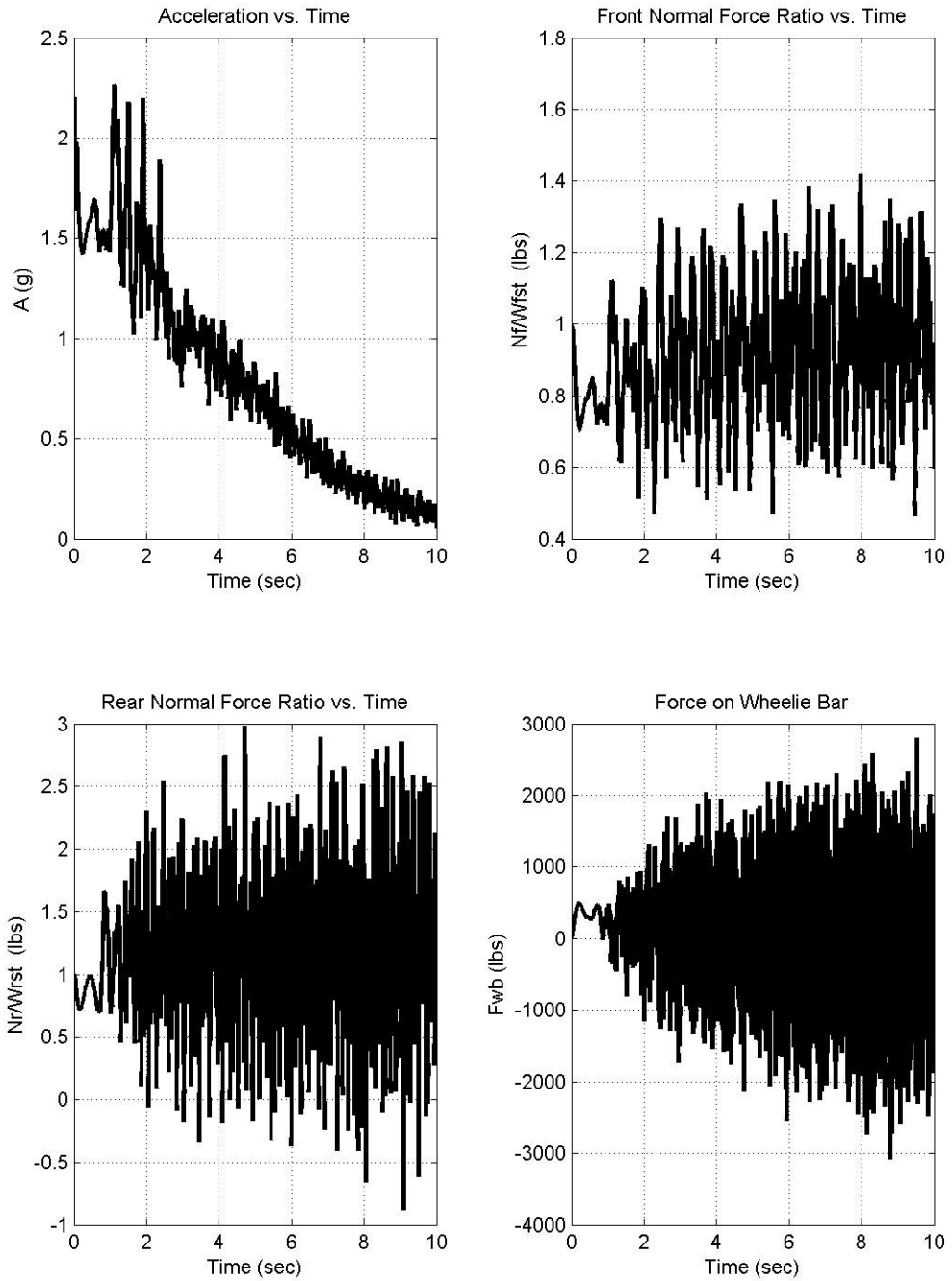
Figure 5.16: Vehicle Dynamics Plot 2 over Highway
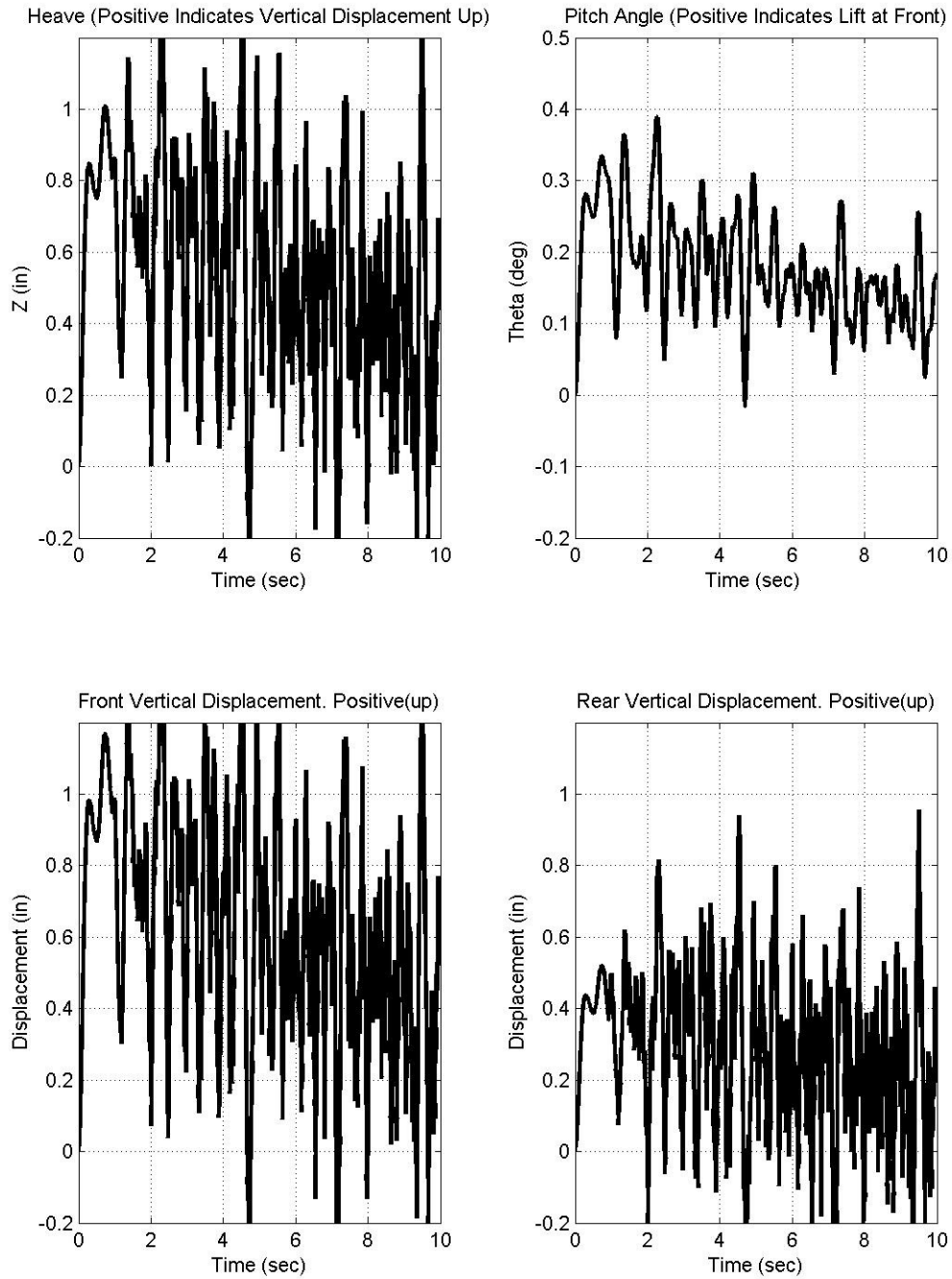
Figure 5.17: Vehicle Dynamics Plot 3 over Highway
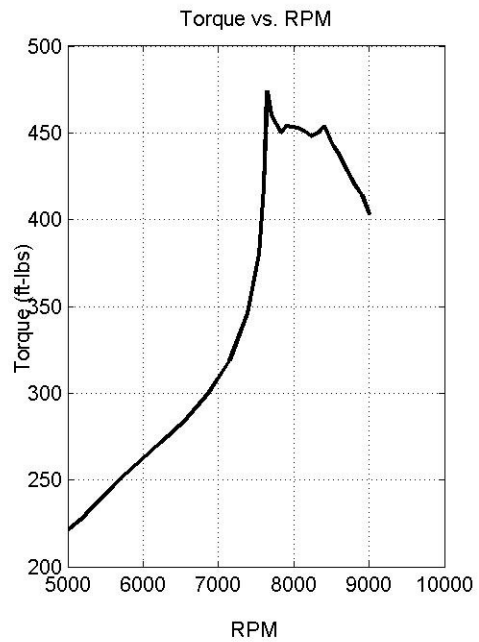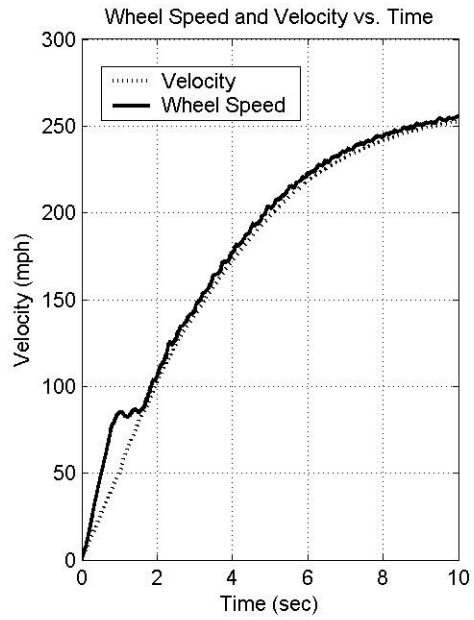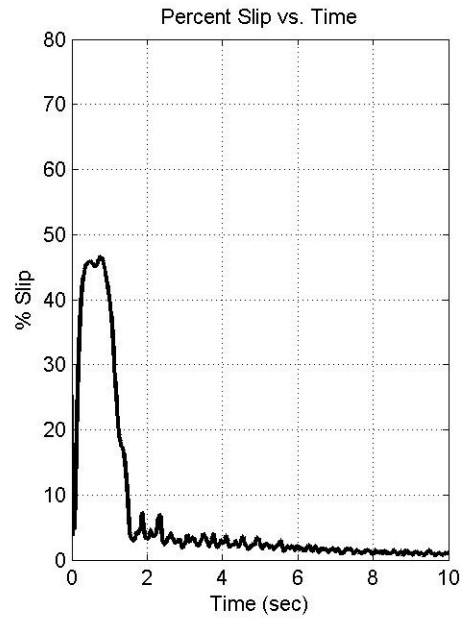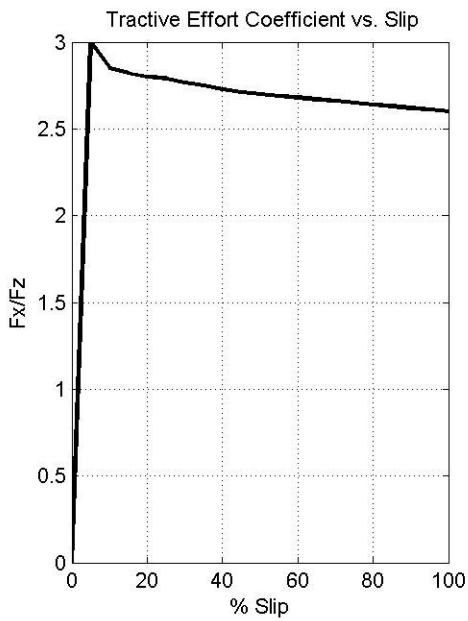
Figure 5.18: Vehicle Dynamics Plot 4 over Highway
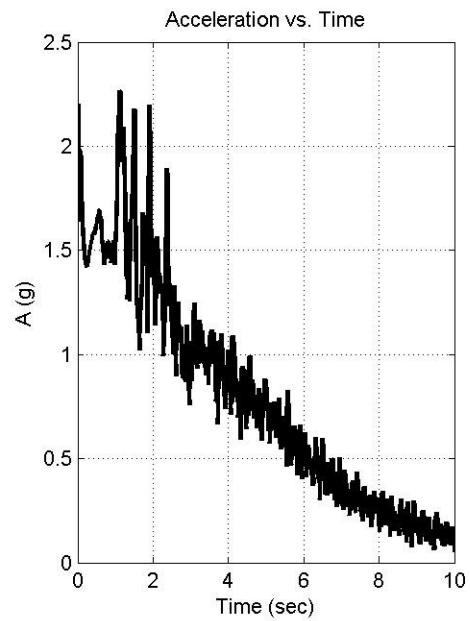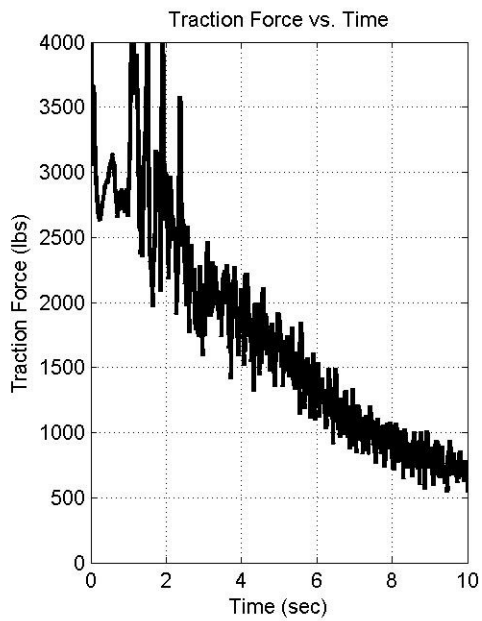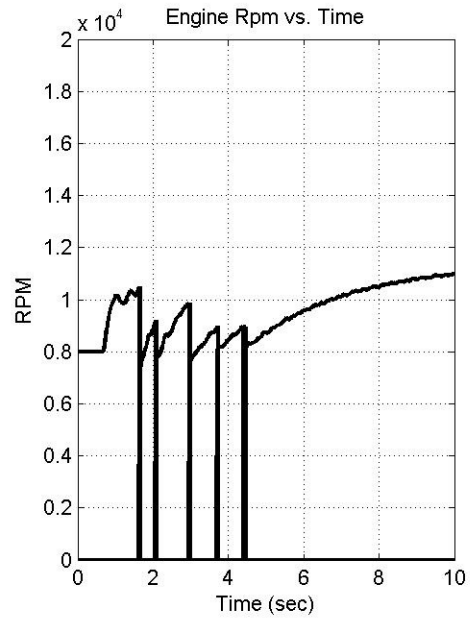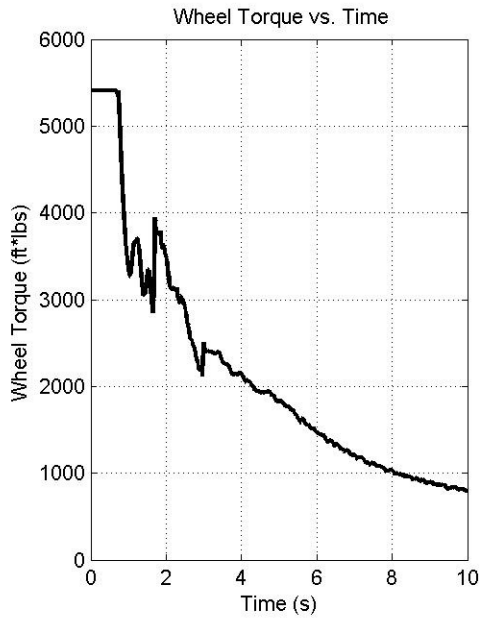
Figure 5.19: Vehicle Dynamics Plot 5 over Highway

Runway

The vehicle exhibits less dynamic response while traversing the runway in comparison to the highway. This is because the runway is not as rough as the highway. The vehicle dynamic response plots over the runway are given in the same order as those for the highway. This order is used for ease of comparison when contrasting the differences of the vehicle response over the different surfaces. The vehicle behaves in a more stable manner and completes the quarter mile run faster on the runway than when traversing the highway. Table 5.5 shows the quarter mile performance of the drag racing vehicle on the simulated surfaces discussed thus far.

Figure 5.20, showing vehicle position and velocity versus time for the runway, is very similar to that of the highway. The only difference is that the vehicle traveling over the runway completes the quarter mile run faster and with a higher top speed. This faster time and higher speed can be contributed to the amount of time the front normal force ratio remains at a high level, without dropping too low, for the runway. When compared with the runway, the front normal force ratio for the highway drops well below that of the runway. However, the front normal force ratio for the highway also exhibits values greater than that of the runway. The lower values of the front normal force ratio are much more penalizing to the vehicle's forward motion than the larger values aid it. The traction force available is dependent on the front axle normal force. The torque available from the engine has a limit, however, and hence there is a point where the engine does not produce enough torque to overcome the available traction and induce wheel spin. Therefore, by remaining at a fairly high traction level, the front normal force ratio on the

runway allows the vehicle slightly more time at a high level of traction, which allows the vehicle to traverse the road quicker and faster.

Figure 5.21 shows the normal forces on the front and rear axles and wheelie bar in relation to the static weight on the bodies. As can be seen from the plots, the dynamic response of the vehicle is less than that of the previous case due to the decreased road roughness. However, the force on the wheelie bar still becomes negative when the vehicle approaches the end of the quarter mile run. At this point of the simulation, the weight transfer towards the rear of the vehicle is minimized and weight actually starts to shift towards the front of the vehicle due to road surface irregularities. This causes the vehicle to pitch forward, trying to "lift" the wheelie bar point contact from the track surface, thus creating a tension force between the wheelie bar point contact and track surface. This is a characteristic of the vehicle model, since the wheelie bar is modeled as a pin joint that is rigidly attached to the road surface. In an actual drag racing condition, the wheelie bar will lift off of the road surface in this situation. When this happens in the simulation, the wheelie bar cannot lift off the ground and therefore produces a tension force. It is very easy to see the differences between the runway and highway when comparing Figures 5.21 and 5.16. The plots for the runway give a smaller response due to the lower excitation.

Figure 5.22 shows the vehicle attitude during the drag run on the runway. The pitch angle is much smaller and less oscillatory than when the vehicle was traveling over the highway. This is due to the decreased level of excitation. The effects of the smoothness of the runway as compared to the highway can be seen in these figures. The

dynamic response of the vehicle is smoother and the magnitude of the vibration seen by the front and rear axles is significantly reduced.

The vehicle still experiences large amounts of wheel slip at the beginning of the quarter mile run. As can be seen in Figure 5.23, the longitudinal wheel slip approaches 50%. This is similar to that of the vehicle traveling over the highway. This indicates that the wheel slip is more a function of gear ratios than a function of road surface roughness. The wheel slip at the beginning of the drag run has a great effect on the performance of the vehicle during the quarter mile run.

Figure 5.24 is very similar to the plots for the highway run, with the main differences being the oscillations of the traction force and acceleration time histories for the highway. The average magnitudes of the longitudinal acceleration and traction force on the runway are, however, similar to those on the highway.

It can also be noted that the engine RPM is much smoother due to less variation of magnitude in the traction force versus time curve. As can be seen in Figure 5.19, the traction force has peaks and valleys that vary greatly and occur in a very short period of time as the vehicle traverses the highway. The simulation runs the engine at wide open throttle throughout the drag run. Therefore, as the available traction force decreases, due to a decrease in front normal force, the engine RPM increases due to less resistive force on the engine, causing the torque to increase and exceed the available traction. The opposite happens as the normal force increases. As the vehicle travels over the runway, the traction force curve remains much smoother and therefore the engine RPM does not fluctuate as much, which can be seen in Figure 5.24.

Table 5.5: Quarter Mile Performance Flat Road, Runway and Highway

Original Gears			
	Flat Road	**Runway**	**Highway**
Elapsed Time (seconds) =	8.307	8.307	8.326
Trap Speed (miles per hour) =	166.45	166.45	166.33
1/8 Mile Time (seconds) =	5.427	5.428	5.444
1/8 Mile Speed (miles per hour) =	141.85	141.84	141.64
330 Foot Time (seconds) =	3.662	3.663	3.676
60 Foot Time (seconds) =	1.510	1.501	1.515
Max Vel. Across Shocks (ft/s) =	0.305	0.303	4.36
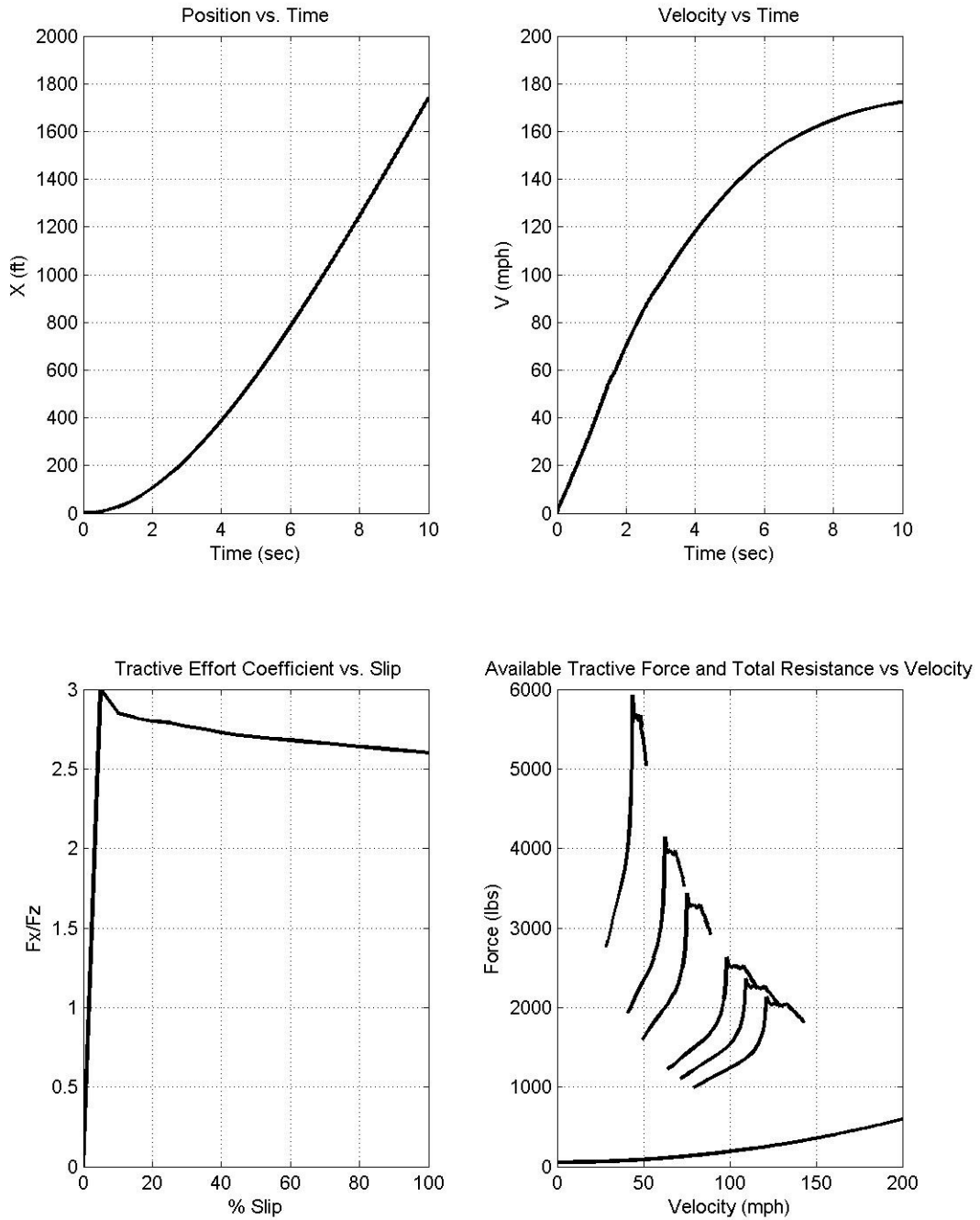
Figure 5.20: Vehicle Dynamics Plot 1 over Runway
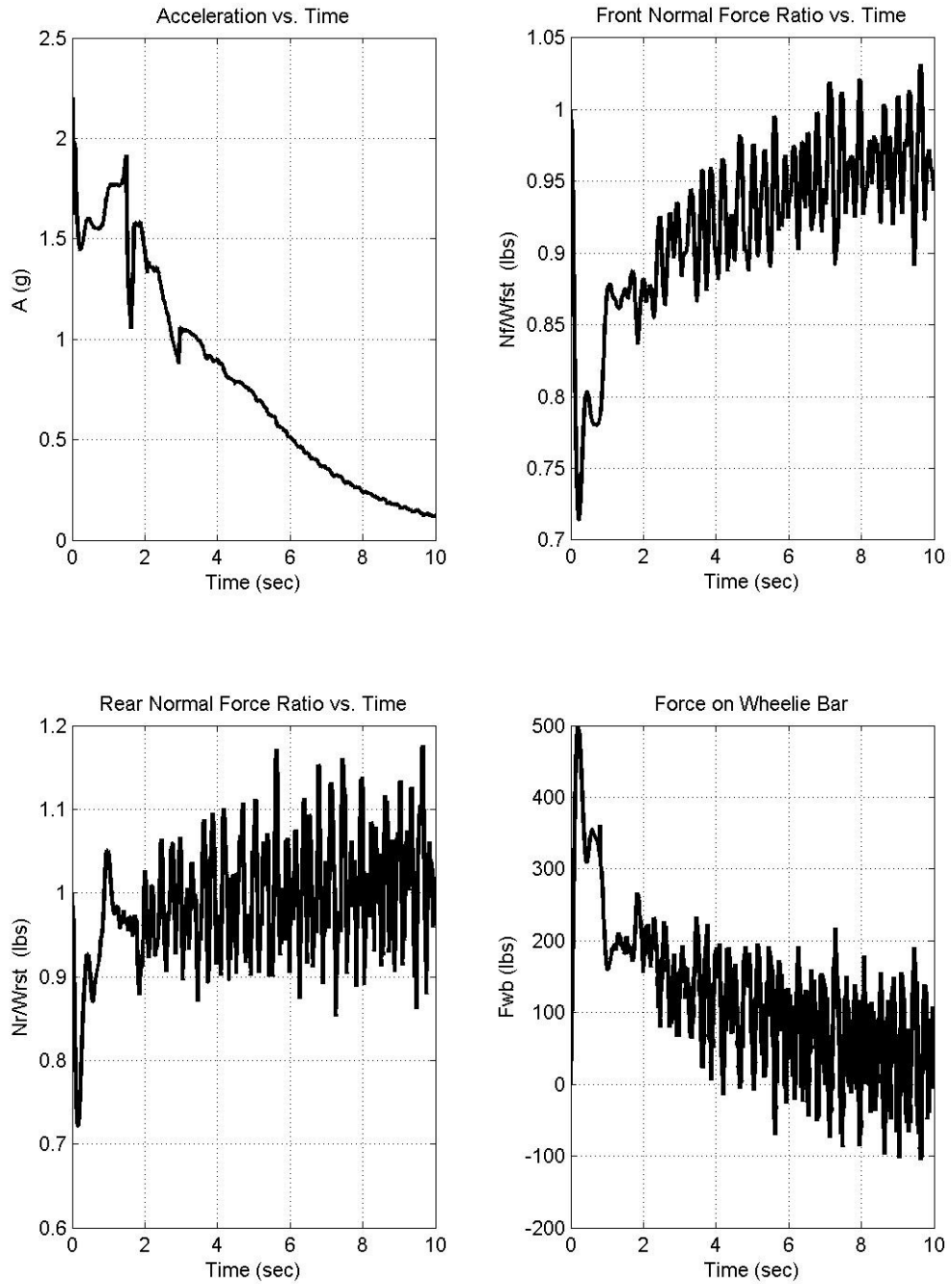
Figure 5.21: Vehicle Dynamics Plot 2 over Runway
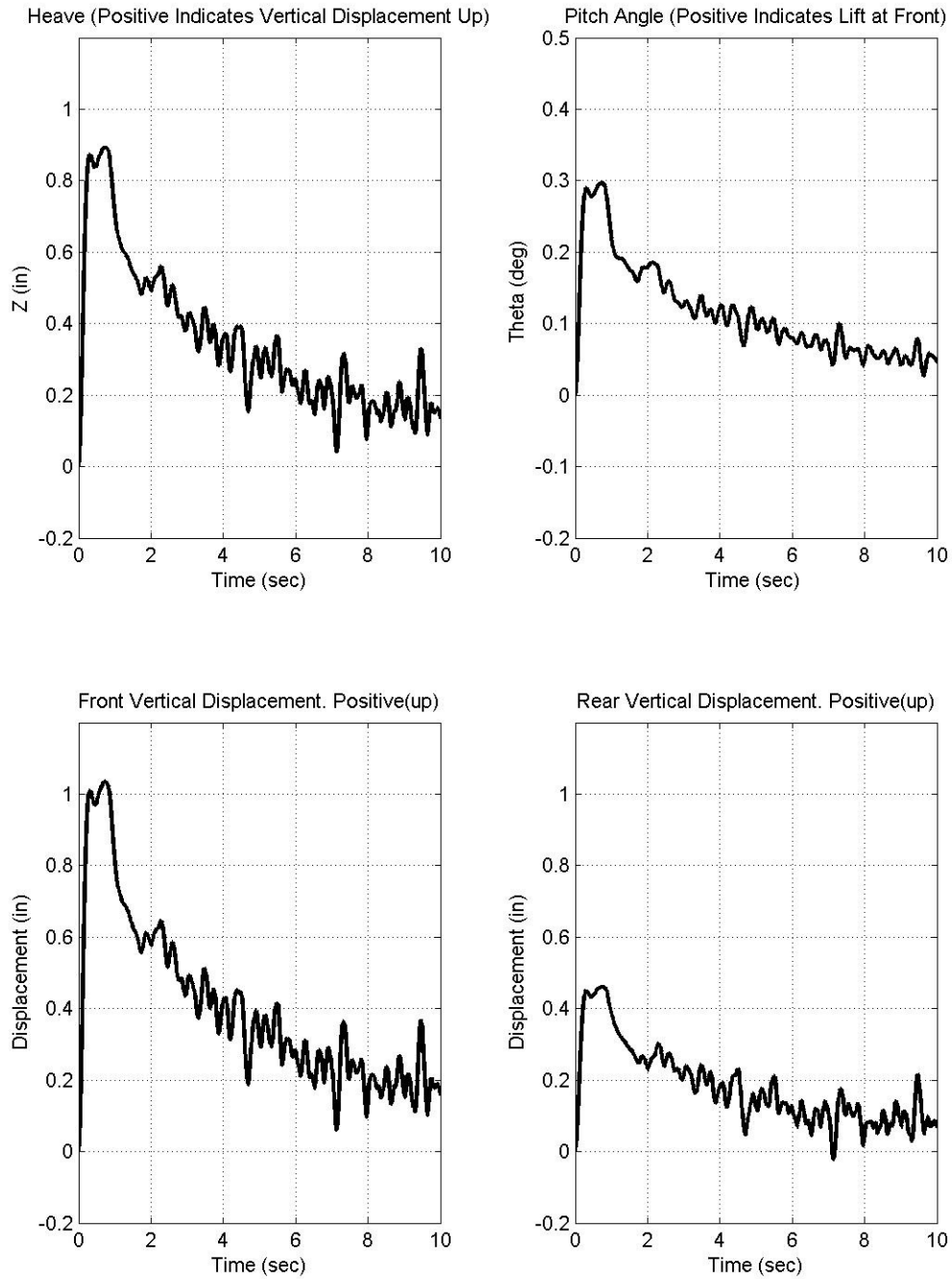
Figure 5.22: Vehicle Dynamics Plot 3 over Runway
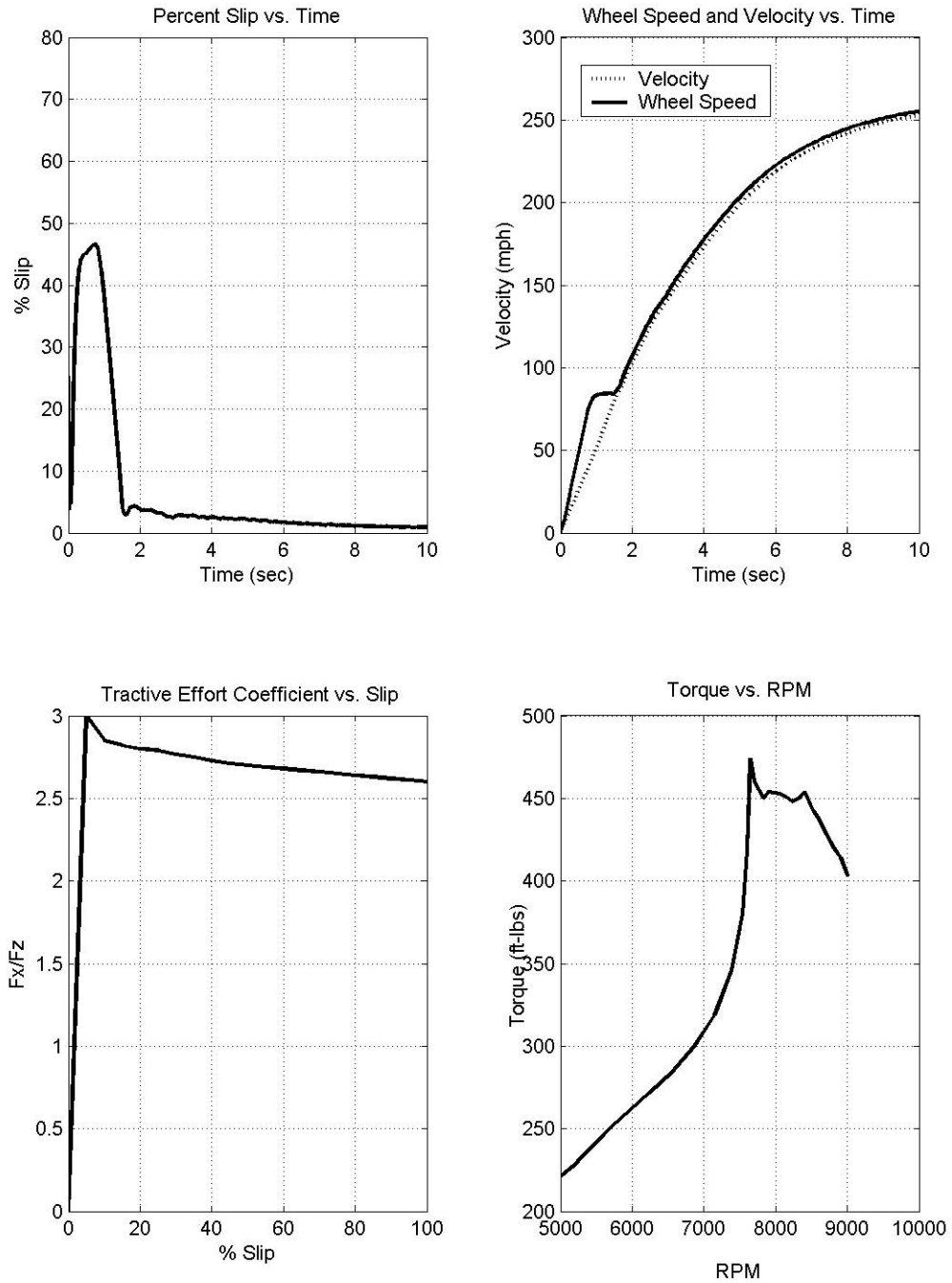
Figure 5.23: Vehicle Dynamics Plot 4 over Runway
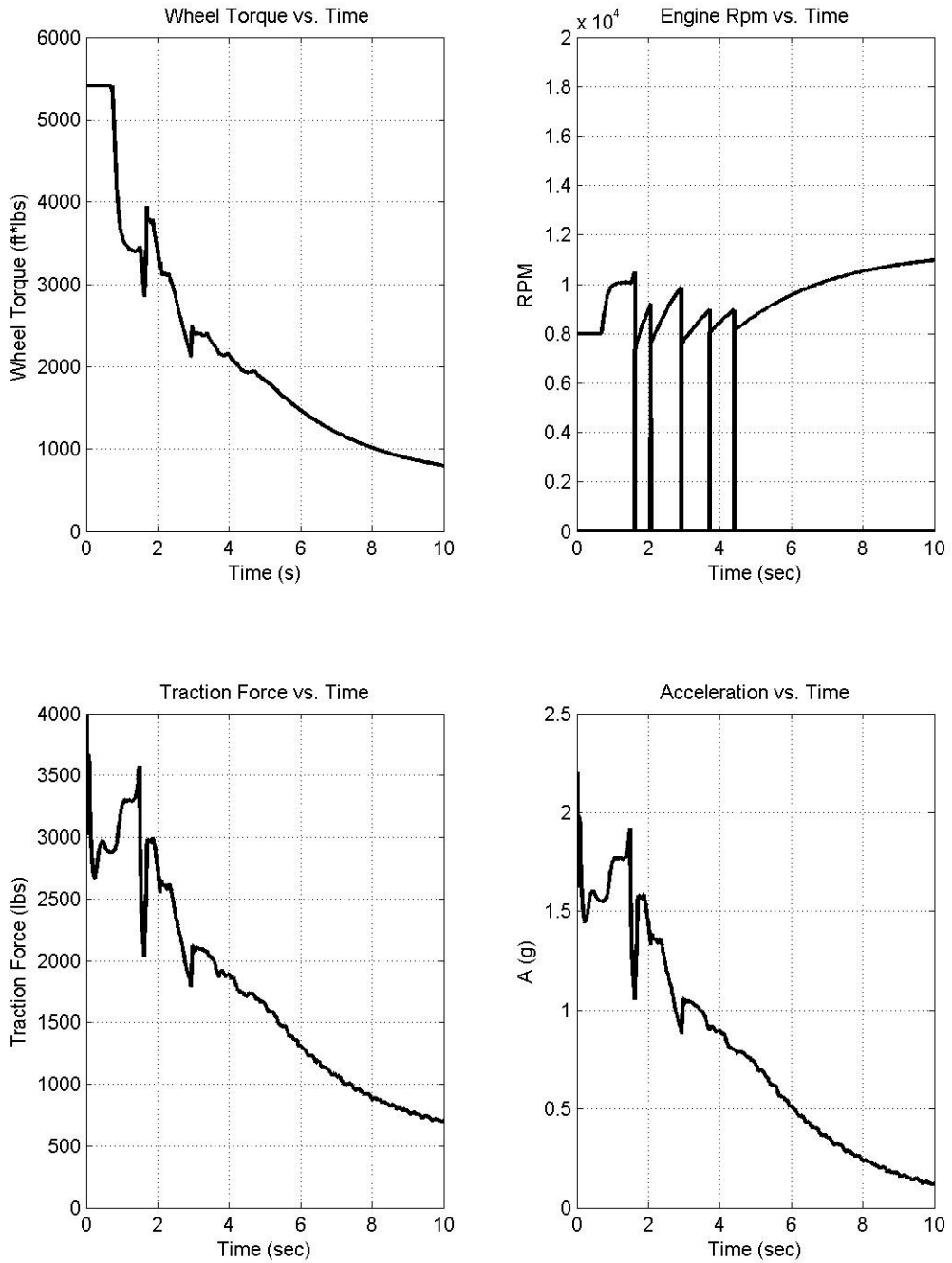
Figure 5.24: Vehicle Dynamics Plot 5 over Runway

Simulated Drag Strip

As discussed earlier in this section, it was determined that the simulated drag strip should have a roughness level between that of the runway and the highway in order to give a maximum value of approximately 1.5 ft/s for the shock velocities. A trial and error method was used to create the road profile that provided this. The PSD's of the three road surfaces are shown in Figure 5.5. After determining the PSD of the simulated drag strip surface, the drag run was simulated to determine the dynamic response. The results are given in Figures 5.25-5.29. Table 5.6 shows the quarter mile performance of the vehicle on all of the simulated surfaces.

Figure 5.25 shows the time histories of the vehicle position and velocity for the quarter mile run. These plots are similar to those for the previous two road profiles. The only difference is a slight change in quarter mile time and speed between the different profiles.

Figure 5.26 shows that the vehicle behaves similarly on both the simulated drag strip and the highway. The front normal force ratio for the drag strip simulation exhibits minimum values between those of the run over the runway and the highway. As was discussed earlier, the minimum values of the front normal force ratio penalize the quarter mile times. The minimum values exhibited for the drag strip are lower than those for the runway, but greater than those over the highway. This would lead to the hypothesis that the quarter mile times over the drag strip would be faster than over the highway, but slower than over the runway. This is the trend seen when comparing the three road surfaces.

Figure 5.27 shows the attitude of the vehicle. The pitch and vertical lift of the front and rear while traveling over the simulated drag strip falls in between the levels found on the runway and highway. The reaction of the vehicle, however, is very similar to that on each of the other roads, with the magnitude being the main difference.

The wheel slip is shown in Figure 5.28. The slip still reaches almost 50% as with the other road surfaces, further justifying the statement that the road surface roughness does not affect the slip of the wheels as much as the gear ratio selection. Notice how the vehicle speed approaches the wheel rotational speed as the wheel slip decreases.

Figure 5.29 shows the traction force and longitudinal acceleration of the vehicle. The magnitudes of the oscillations in these plots tend to fall between the magnitudes of the peaks for the runway and highway plots.

Table 5.6: Quarter Mile Performance Flat Road, Runway, Drag Strip, and Highway

Original Gears				
	Flat Road	Runway	Drag Strip	Highway
Elapsed Time (seconds) =	8.307	8.307	8.315	8.326
Trap Speed (miles per hour) =	166.45	166.45	166.35	166.33
1/8 Mile Time (seconds) =	5.427	5.428	5.434	5.444
1/8 Mile Speed (miles per hour) =	141.85	141.84	141.68	141.64
330 Foot Time (seconds) =	3.662	3.663	3.667	3.676
60 Foot Time (seconds) =	1.510	1.501	1.511	1.515
Max Vel. Across Shocks (ft/s) =	0.305	0.303	1.46	4.36

Figure 5.25: Vehicle Dynamics Plot 1 over Simulated Drag Strip
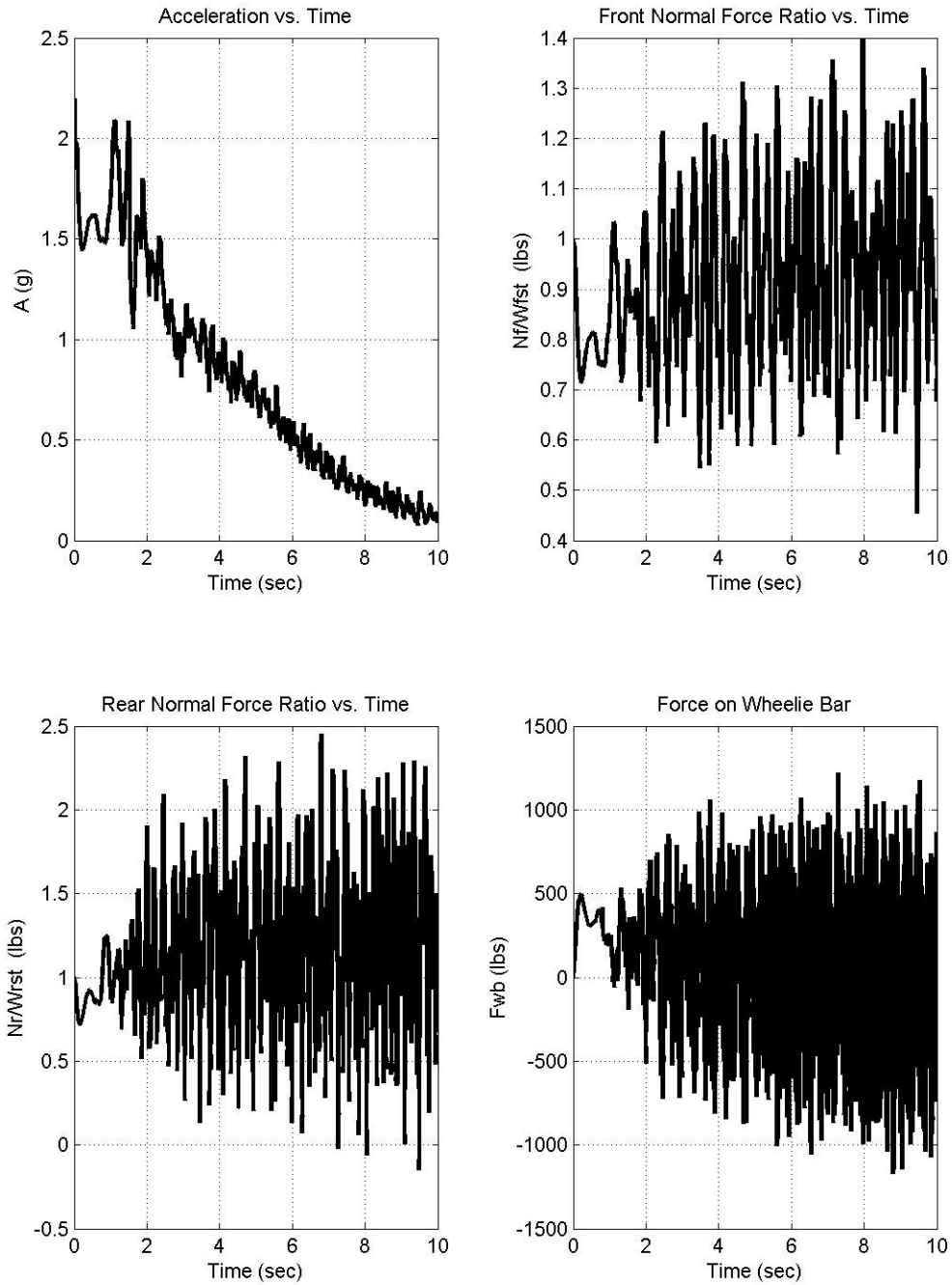
Figure 5.26: Vehicle Dynamics Plot 2 over Simulated Drag Strip
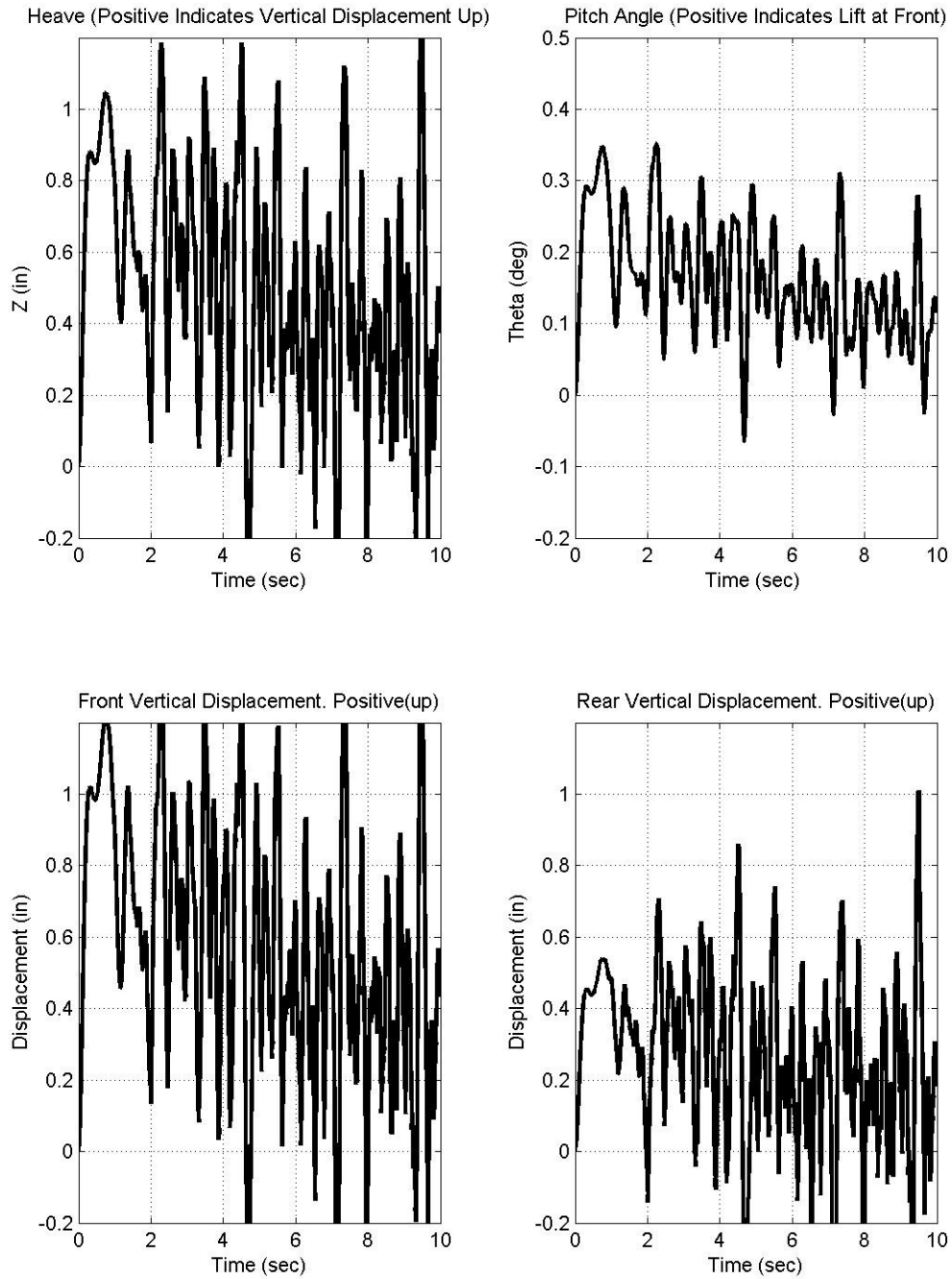
Figure 5.27: Vehicle Dynamics Plot 3 over Simulated Drag Strip
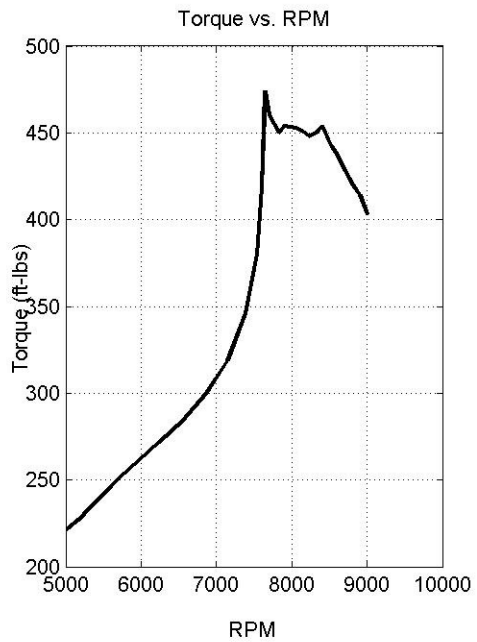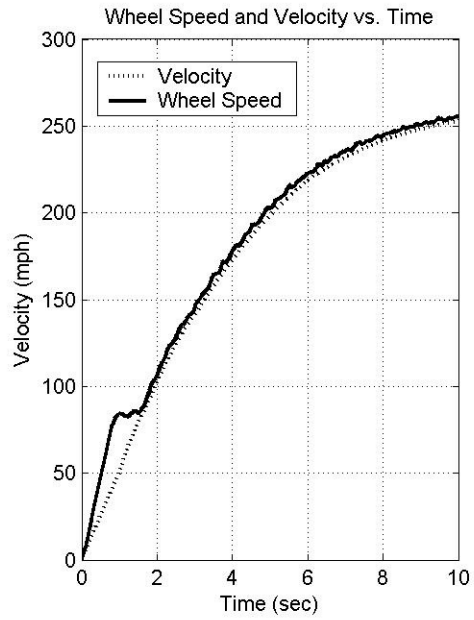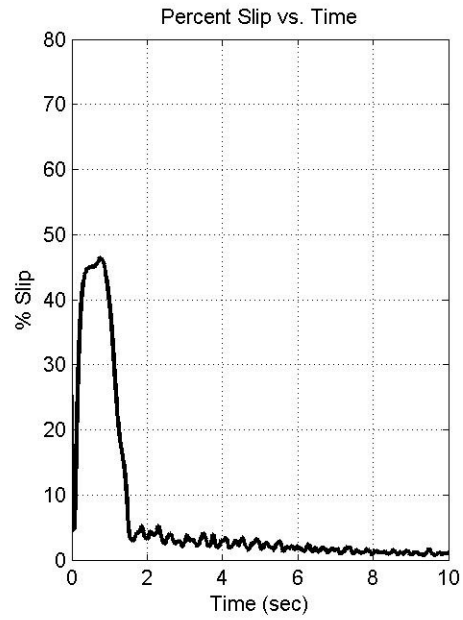
Figure 5.28: Vehicle Dynamics Plot 4 over Simulated Drag Strip
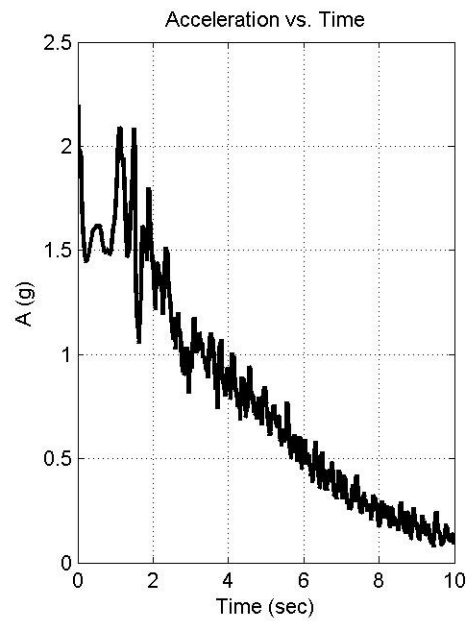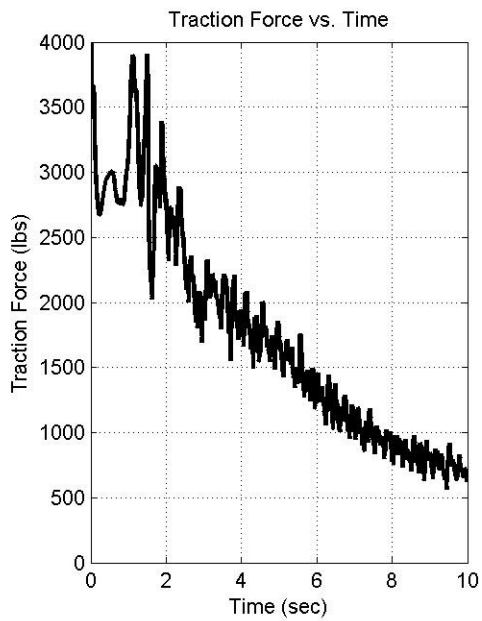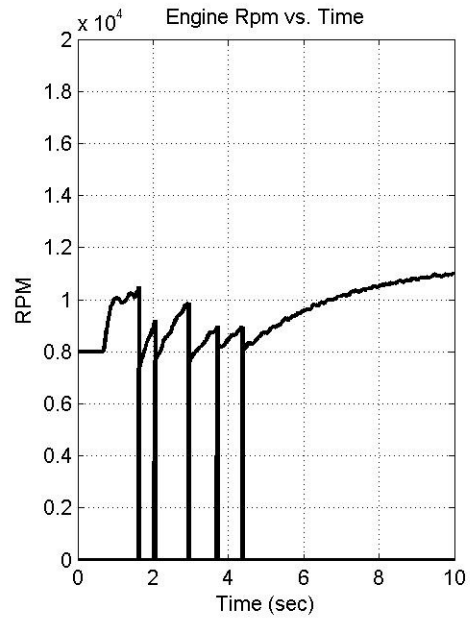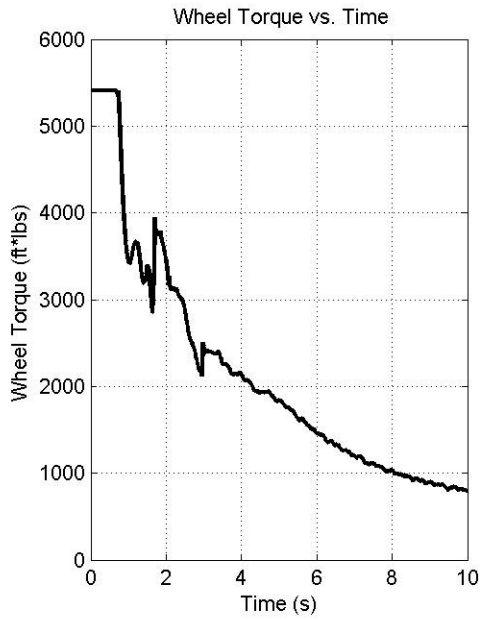
Figure 5.29: Vehicle Dynamics Plot 5 over Simulated Drag Strip

Drag Performance Comparisons

The front wheel drive drag racing car was run over four different surfaces to compare quarter mile performance. The four surfaces investigated were a perfectly flat surface and the aforementioned runway, highway, and simulated drag strip. Table 5.6 shows the quarter mile performance of the front wheel drive drag racing car over the four simulated surfaces.

Table 5.6, shown again on the next page, illustrates the results from the simulated drag runs. The Elapsed Time is the time it takes for the drag racing vehicle to traverse the quarter mile track. The Trap Speed indicates the speed in miles per hour at which the vehicle crosses the finish line. The 1/8 Mile Time and Speed designate the time it takes to reach the eighth mile mark and the speed at which the drag racing vehicle crosses the eighth mile marker. Other times that are important to the drag racing community are the time it takes the vehicle to reach 330 feet and sixty feet. The maximum velocities across the shocks are also noted to indicate the roughness of the surface being traversed.

The level of aggressiveness of the road profile is a direct indicator of the quarter mile elapsed time. The more aggressive surfaces caused slower quarter mile times. This change in quarter mile time is due to the difference in vehicle dynamic response for the different road profiles, mainly the front normal force which dictates available traction. The same trend can be seen in the time it takes the drag car to reach an eighth mile and the 330 foot mark.

The time it takes for the drag car to reach the sixty foot mark shows a similar trend. However, the run on the runway produced a slightly faster sixty foot time. This is

caused by the vehicle getting more traction due to higher normal forces on the drive axle of the vehicle as compared to when the vehicle travels over the perfectly smooth, flat road. The roughness integrated into the runway causes the vehicle to pitch forward at times, which creates higher normal forces on the front axle than seen on the perfectly smooth surface. The roughness of the road, when more pronounced however, causes an increase in magnitude of vehicle positive heave. This dynamic causes a decrease in the front normal force and traction available, causing the vehicle to be slower when traveling over the rougher surfaces. This extra traction shows up in the sixty foot time where the speed of the vehicle off the line is primarily traction-limited. The roughness of the other two road surfaces creates less front normal force than the smoother surfaces, which in turn leaves less traction force available and causes slower times.

Table 5.6: Quarter Mile Performance Flat Road, Runway, Drag Strip, and Highway

Original Gears				
	Flat Road	Runway	Drag Strip	Highway
Elapsed Time (seconds) =	8.307	8.307	8.315	8.326
Trap Speed (miles per hour) =	166.45	166.45	166.35	166.33
1/8 Mile Time (seconds) =	5.427	5.428	5.434	5.444
1/8 Mile Speed (miles per hour) =	141.85	141.84	141.68	141.64
330 Foot Time (seconds) =	3.662	3.663	3.667	3.676
60 Foot Time (seconds) =	1.510	1.501	1.511	1.515
Max Vel. Across Shocks (ft/s) =	0.305	0.303	1.46	4.36

Case Studies / Gear Ratio Improved Selection

Theory

The plots of the dynamic response of the front wheel drive drag racing car indicate that the drive axle experiences a significant amount of wheel slip during the initial stages of each drag run, as seen in the upper left plot in Figures 5.13, 5.18, 5.23, and 5.28. This inefficient use of the drive torque increases the quarter mile times. A case study is done here to determine, through a logical progression, improved gear ratios that will improve quarter mile time in the simulation of the drag car model. The main point made in this section is that there is a noticeable gain available if the gear ratios of the front wheel drive drag racing car are selected to make effective use of the available traction.

The gear ratio improvement is carried out by running the drag racing car simulation in a loop. The ratio of first gear is varied, while fixing the other five gears at the original gear ratios, to give a quarter mile time for each of the first gear values or ratios in the specified range. The gear ratio giving the fastest quarter mile time is then selected.

Once the improved first gear ratio is found, it is fixed at that ratio and the second gear ratio is run through the same improvement loop, keeping the rest of the gears at the original gear ratios. The improvement loop is run until all of the six gears have been improved. This will be referred to as the "first improvement". Once the first improvement is complete, the gear ratio improvement is carried out again, using the gear ratios from the first improvement as the "original" gears for the second improvement.

This procedure is completed twice to determine the improved set of gears. After two passes through the loop, the improved gear ratios only change in the thousandths place. Therefore, after two passes through the improvement loop, the improved gear ratios are considered to be accurate to +/- one hundredth. A flow chart explaining the gear ratio improvement process is given below in Figure 5.30.

Start

improve	orig.	orig.	orig.	orig.	orig.
1st	2nd	3rd	4th	5th	6th

Select Improved 1st Gear

new	improve	orig.	orig.	orig.	orig.
1st	2nd	3rd	4th	5th	6th

Select Improved 2nd Gear

new	new	improve	orig.	orig.	orig.
1st	2nd	3rd	4th	5th	6th

Select Improved 3rd Gear

new	new	new	improve	orig.	orig.
1st	2nd	3rd	4th	5th	6th

Select Improved 4th Gear

new	new	new	new	improve	orig.
1st	2nd	3rd	4th	5th	6th

Select Improved 5th Gear

new	new	new	new	new	improve
1st	2nd	3rd	4th	5th	6th

Select Improved 6th Gear

Improved Set of Gear Ratios

new	new	new	new	new	new
1st	2nd	3rd	4th	5th	6th

Return for Second Improvement

Figure 5.30: Gear Ratio Improvement Process

Gear Ratio Improvement (Perfectly Smooth, Flat Road)

The gear ratio improvement (GRI) was performed for the drag racing car on a perfectly smooth, flat road. This case study was used to determine if, in fact, there could be a significant gain in quarter mile time through using the GRI program. The GRI was carried out using the procedure outlined in the previous section. The plots of the surface correlating gear ratios with quarter mile times are shown in Figures 5.31 and 5.32, the first improvement and second improvement respectively. After the first improvement, the improved gear ratios are determined with an accuracy of +/- one tenth. After the second improvement, the improved gear ratios are determined to +/- one hundredth. By continuing the improvement process, the numerical value of the gear ratios becomes more precise, but the physical application of these differences becomes impractical. Therefore, it is deemed sufficient to perform only two loops for the GRI process.

As can be seen from the plots, there certainly is a well defined set of gear ratios that provide the fastest quarter mile time in the simulation. An interesting fact to note is that on the surface relating the first gear ratio with quarter mile time, there is a point where the slope of the curve is discontinuous. This is the point where the torque from the motor provides enough force at the drive wheel to exceed the available traction force at the front axle. Due to the fact that the "driver" in the drag racing simulation launches from the starting line at 8000 rpm, the GRI, in essence, is finding the gear ratio that utilizes all of the available traction force and creates a minimum amount of wheel spin.
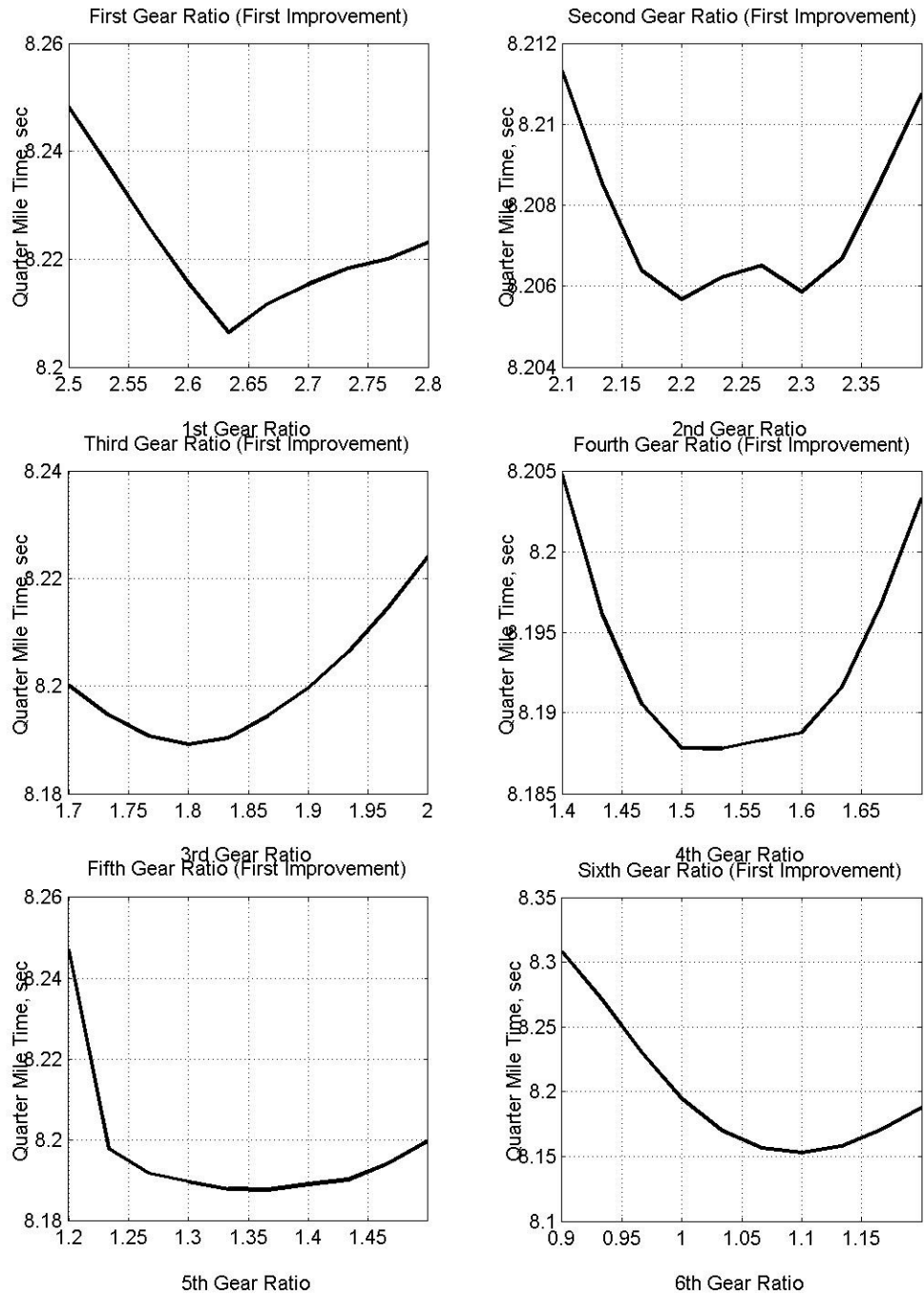
Figure 5.31: First Improvement of Gear Ratios (Perfectly Smooth, Flat Road)
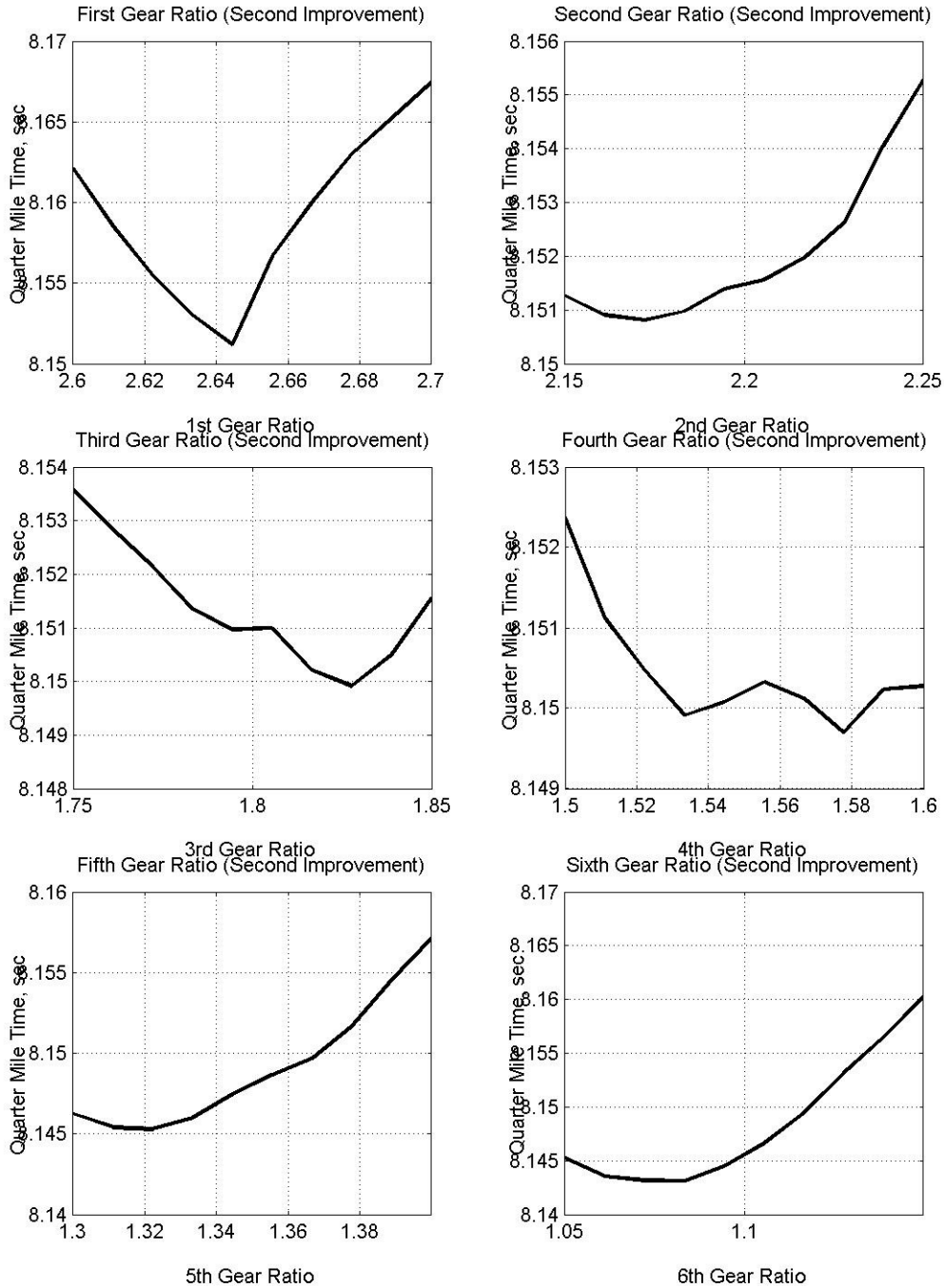
Figure 5.32: Second Improvement of Gear Ratios (Perfectly Smooth, Flat Road)

Figures 5.33 and 5.34 show the engine rpm, vehicle longitudinal speed, and wheel rotational speed for the original and improved gear ratios. The plots show a definite decrease in the difference between wheel rotational speed and vehicle longitudinal velocity, or wheel spin. Figure 5.33 shows the large amount of wheel spin the front axle encounters using the original gear ratio setup. The improved gear ratios reduce this effect and therefore decrease the time it takes to complete the quarter mile run.

The engine rpm is also a good indicator of how the gear ratio setup of the vehicle is performing. The spacing of the original gears does not take advantage of the torque curve provided by the motor. The bottom right plot in Figure 5.25 shows the available tractive effort versus vehicle longitudinal velocity, assuming no slip using the original gears. We see that the spacing between first and second gear creates a large drop in force when moving between the gears. This is not desirable since the race car needs to be in the engine rpm range that produces the maximum torque for as long as possible. The shift between first and second gear would create an unnecessary decrease in engine rpm, thus limiting power to the wheels. The same phenomenon is observed between third and fourth gears as well.

The improved gears approach a geometric progression configuration that would keep the engine in the same rpm range, which creates the most torque. Figure 5.34 shows that while the vehicle is in the improved first through fifth gears, the engine rpm ranges from about 7800 to 9000 rpm. By looking at the torque vs. rpm curve of the motor in Figure 5.28, it can be seen that this rpm range is the range where the motor provides the most consistent and powerful torque. The improved gears allow the motor to stay in this

rpm range. Figures 5.33 and 5.34 also show how the improved gears exhibit excellent spacing, which is not shown by the original gears. This approximately geometric spacing allows the motor to use the entire portion of the torque curve that creates maximum torque in each gear, which in turn provides faster quarter mile times.

The gear ratios and performance improvements of the front wheel drive drag racing vehicle are shown in Table 5.7 and will be discussed in the "Drag Performance Comparisons" section later in this chapter.

Table 5.7: Quarter Mile Performance Gains with Improved
Gears on the Perfectly Smooth, Flat Road

Perfectly Smooth, Flat Road					
	Original Gears	1st Improvement	Gain	2nd Improvement	Total Gain
1st Gear Ratio =	3.33	2.6333		2.6444	
2nd Gear Ratio =	2.33	2.2		2.1722	
3rd Gear Ratio =	1.93	1.8		1.8278	
4th Gear Ratio =	1.48	1.5333		1.5778	
5th Gear Ratio =	1.33	1.3667		1.3222	
6th Gear Ratio =	1.2	1.1		1.0833	
Elapsed Time (seconds) =	8.307	8.153	0.154	8.143	**0.164**
Trap Speed (miles per hour) =	166.45	171.55	5.10	172.30	**5.85**
1/8 Mile Time (seconds) =	5.427	5.322	0.105	5.318	0.109
1/8 Mile Speed (miles per hour) =	141.85	142.08	0.23	142.20	0.35
330 Foot Time (seconds) =	3.662	3.568	0.094	3.566	0.096
60 Foot Time (seconds) =	1.510	1.461	0.049	1.463	0.047

Figure 5.33: Engine RPM and Vehicle/Wheel Speed for Original Gears
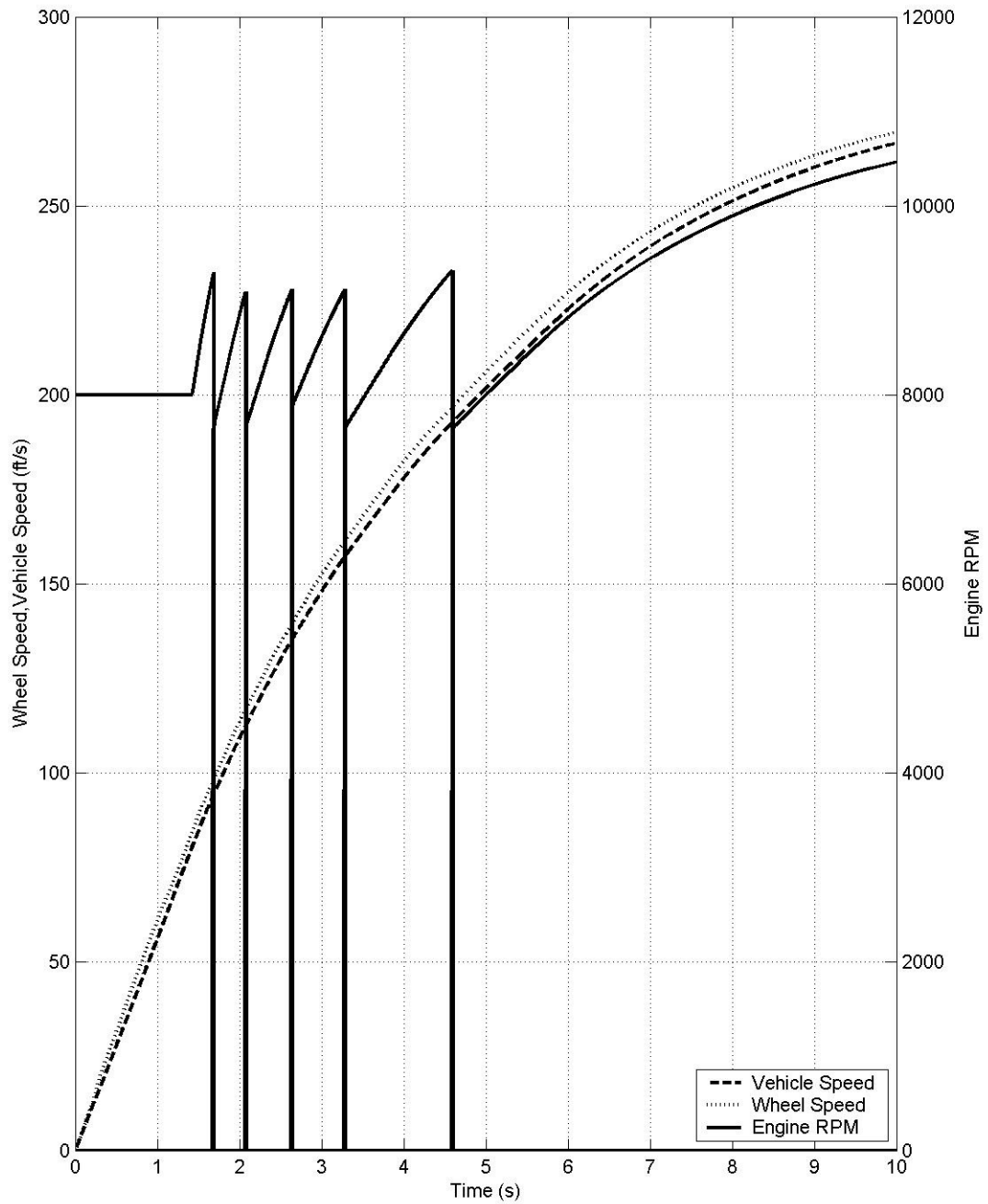
Figure 5.34: Engine RPM and Vehicle/Wheel Speed for Improved Gears

Gear Ratio Improvement (Drag Strip)

The same GRI program was run on the randomly generated drag strip road profile. As was the case with perfectly smooth, flat road, there are definable gear ratios that give a minimum quarter mile time in the simulation. All of the characteristics exhibited from the improvement on the perfectly smooth, flat road are displayed in the plots for the improvement carried out on the drag strip. The plots of the first and second GRIs are given in Figures 5.35 and 5.36 respectively.

The five plots of the vehicle dynamics over the simulated drag strip are given in Figures 5.37–5.41 in the same order as those previously discussed in this chapter. These plots can be used to evaluate the differences between the runs over the simulated drag strip using the original and improved gears. The vehicle dynamics plots over the drag strip with the original gears are shown in Figures 5.25-5.29.

The overall dynamics of the vehicle do not change much after the gear ratio improvement. The attitude of the vehicle, or pitch angle, heave, and vertical axle displacements, are all almost identical between the runs with the original and improved gear ratios. This is to be expected since the simulation is using the identical physical parameters between the two runs and the vehicle is traversing the same road over both runs. This would give a similar dynamic response. The main difference seen in the pitch attitude of the vehicle is near the beginning of the run, during the first second. The vehicle behaves slightly differently due to more traction being produced by the front tires that slip less with the improved gears. The other differences later on in the quarter mile run are due to the higher speeds the vehicle reaches with the improved gears.

The main difference between the run with the original gears and the improved gears can be seen in Figure 5.42, which shows the effect of the improved gear ratios on wheel slip. The improved gear ratio set exhibits a large improvement in wheel slip at the beginning of the run. The 30% reduction in wheel slip between gear sets, when associated with the tractive effort coefficient vs. slip curve (Figure 5.37), correlates to an increase in tractive effort coefficient from approximately 2.7 to around 2.85, about a 5% improvement. This extra tractive effort coefficient equates to a more effective use of available grip at the start of the drag run with the improved gear ratios. This causes the vehicle to be faster off the start line, which in turn decreases the overall elapsed time for the drag run.

Figure 5.43, shows the traction force throughout the run provided by the front tires for the original gears as well as the improved gears. As can be seen, the improved gears provide more traction force during a majority of the drag run. The most significant gains, however, are seen in the first second and then again in the last four seconds of the run. The gains at the beginning of the run can be attributed to less wheel spin due to the higher first gear ratio of the improved gear set. The gains at the end of the quarter mile run are due to the increase in wheel torque, without inducing excessive wheel slip, which occurs because the engine remains in the high torque rpm range with the improved sixth gear ratio.

Figure 5.44 shows the available tractive force, assuming zero wheel slip, versus velocity for the front wheel drive drag racing vehicle for each of the improved gear ratios and original gear ratios. The available tractive force exhibits excellent spacing for the

improved gear ratios. As the available tractive force trails off for one gear, there is a seamless transition to the maximum traction force available for the next gear. This excellent spacing is a product of the GRI program finding the gear ratios that will produce the fastest quarter mile time. The original gear ratios exhibit large gaps between gears where the traction force available decreases substantially as the next gear is selected. This can be seen between first and second gear as well as third and fourth gears. These gaps between gears do not allow the drive tires to use all of the available traction and therefore will result in worse quarter mile performance.
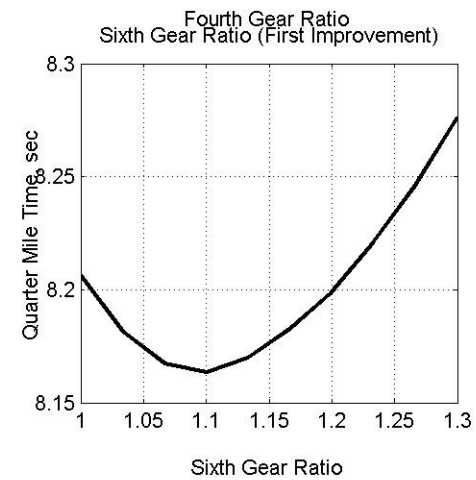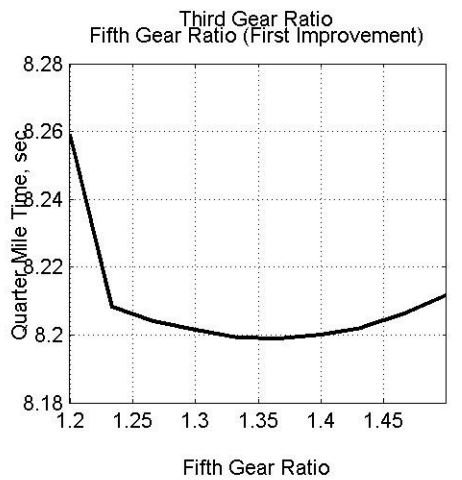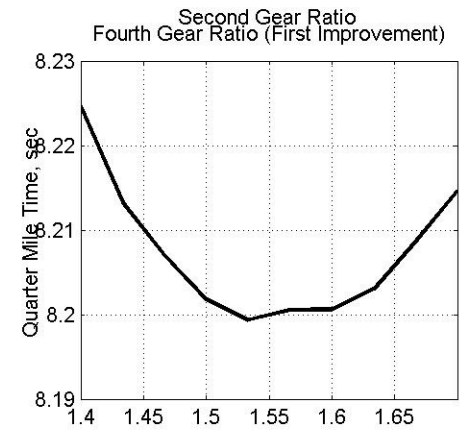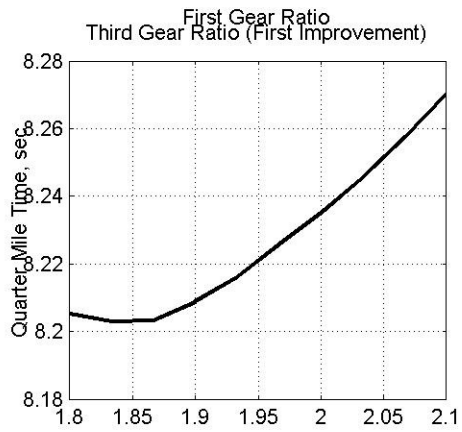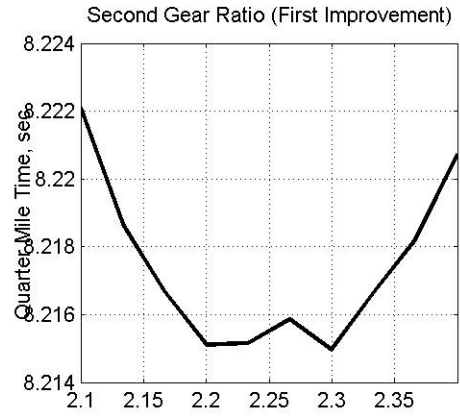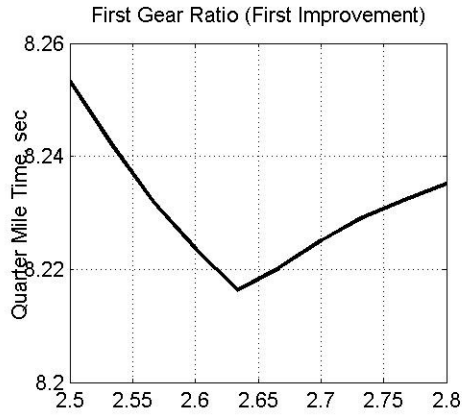
Figure 5.35: First Improvement of Gear Ratios (Drag Strip)

89
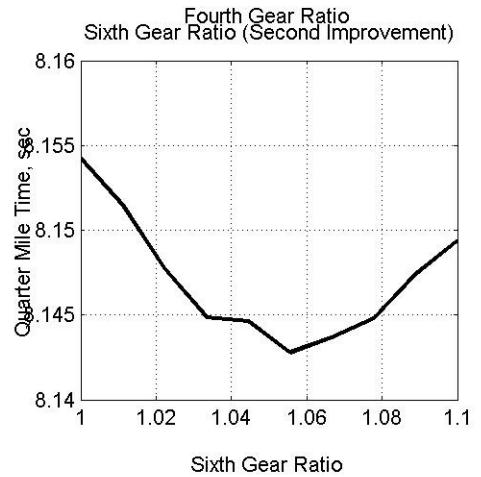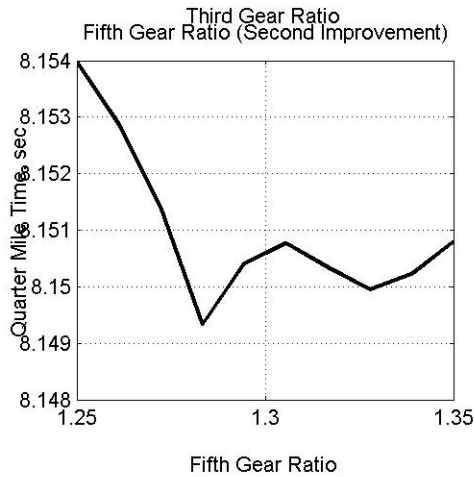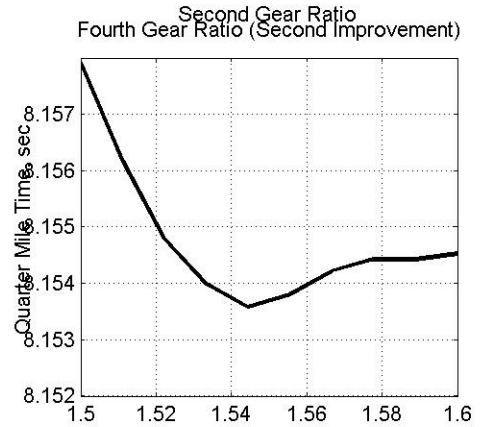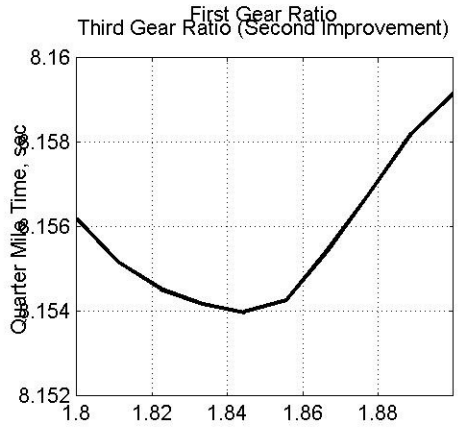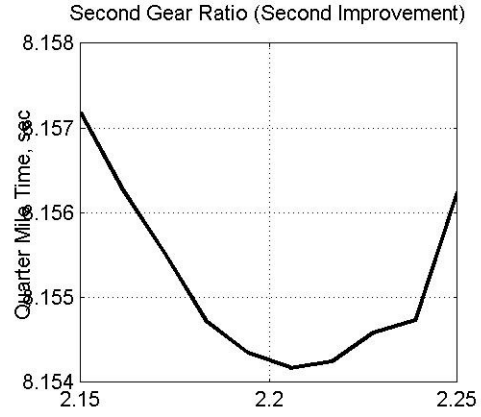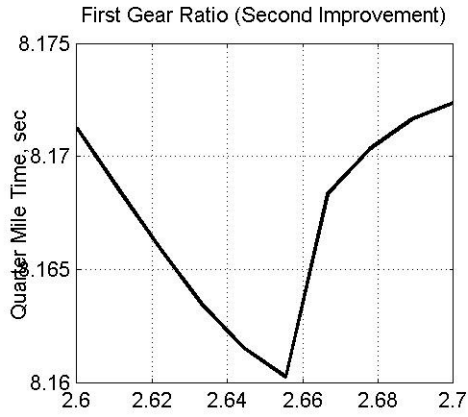
Figure 5.36: Second Improvement of Gear Ratios (Drag Strip)
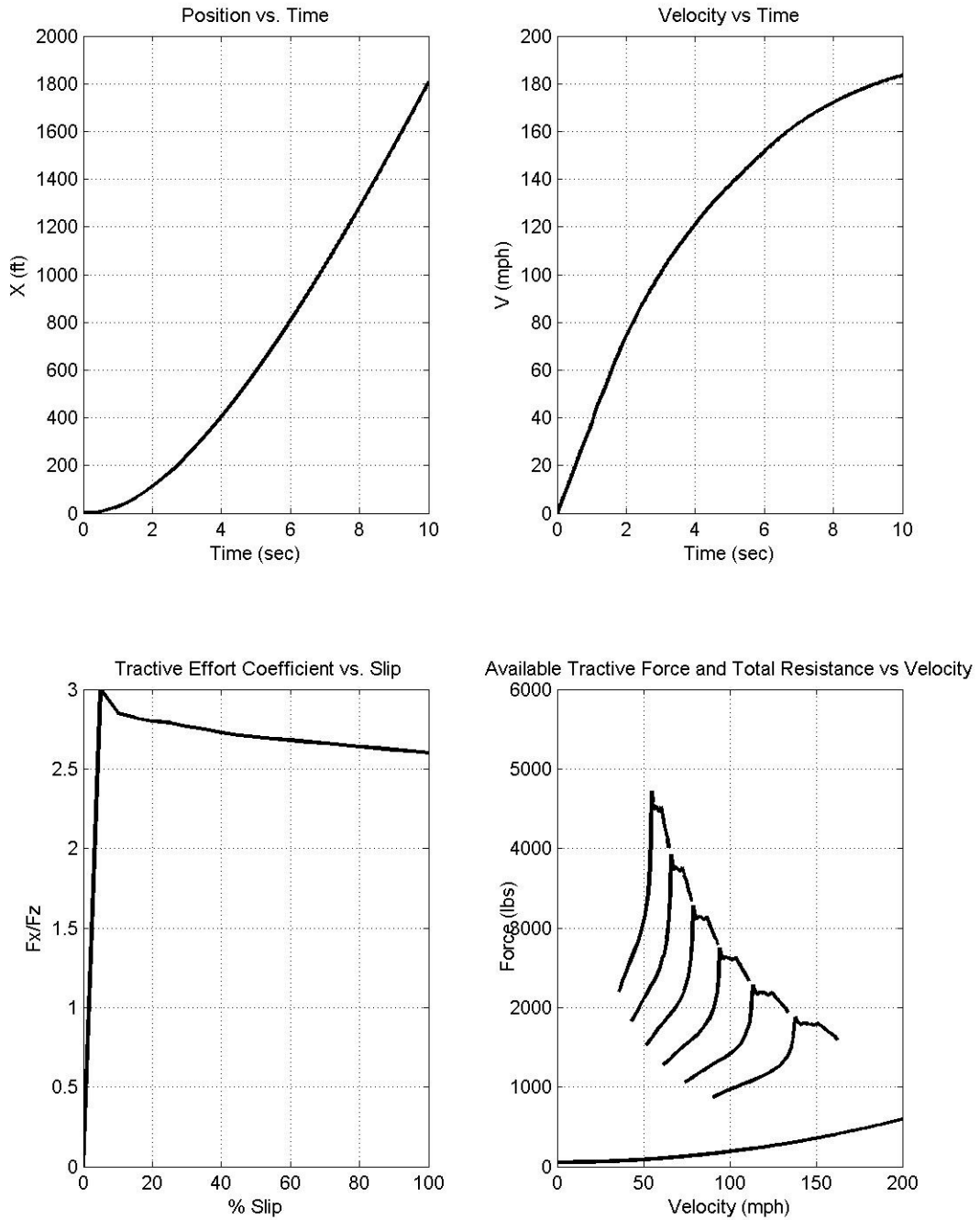
Figure 5.37: Vehicle Dynamics Plot 1 with Improved Gears (Drag Strip)
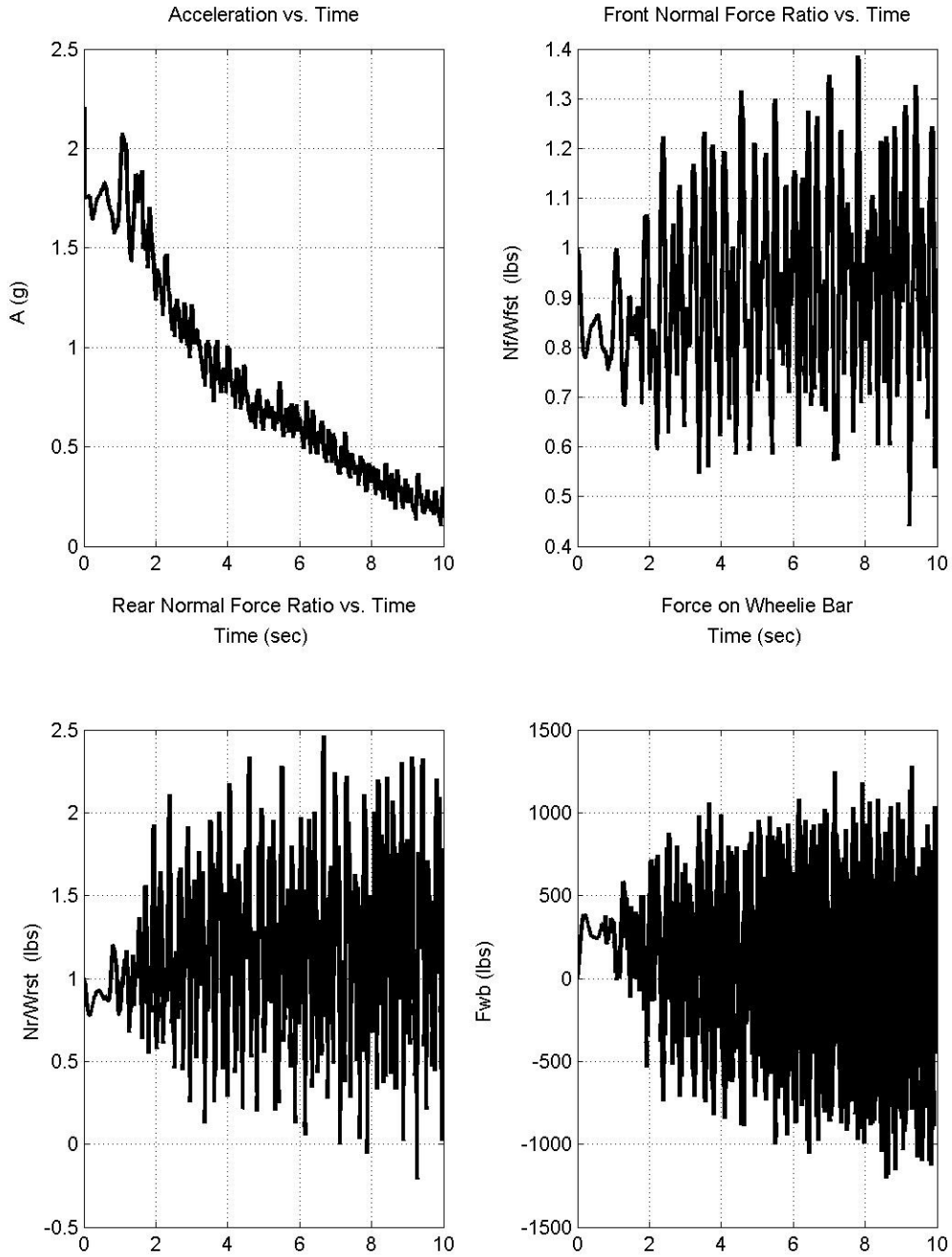
Figure 5.38: Vehicle Dynamics Plot 2 with Improved Gears (Drag Strip)

Heave (Positive Indicates Vertical Displacement Up)

Pitch Angle (Positive Indicates Lift at Front)

Vertical Displacement of the Front of the Car. Positive(up)

Vertical Displacement of the Rear of the Car. Positive(up)
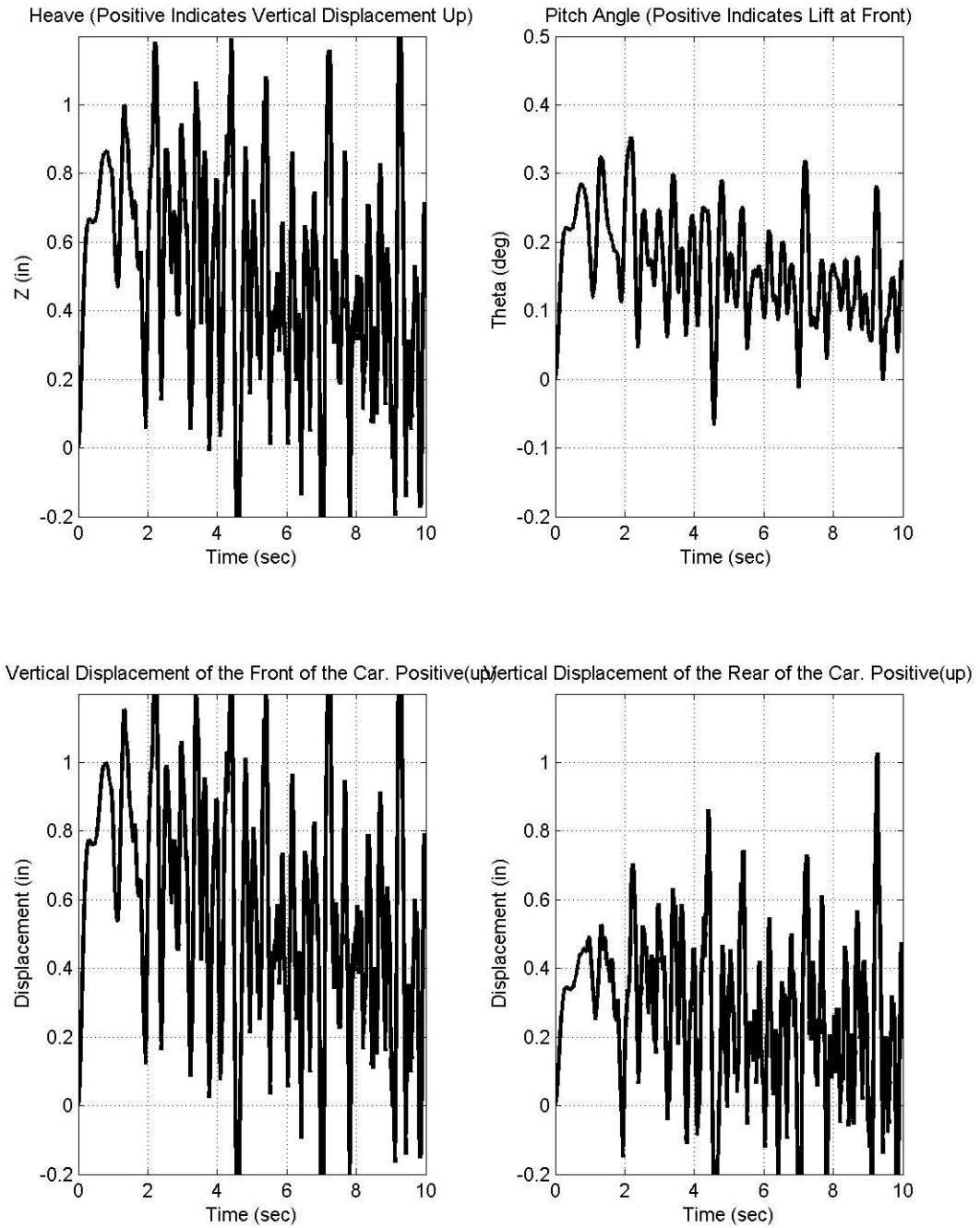
Figure 5.39: Vehicle Dynamics Plot 3 with Improved Gears (Drag Strip)

93
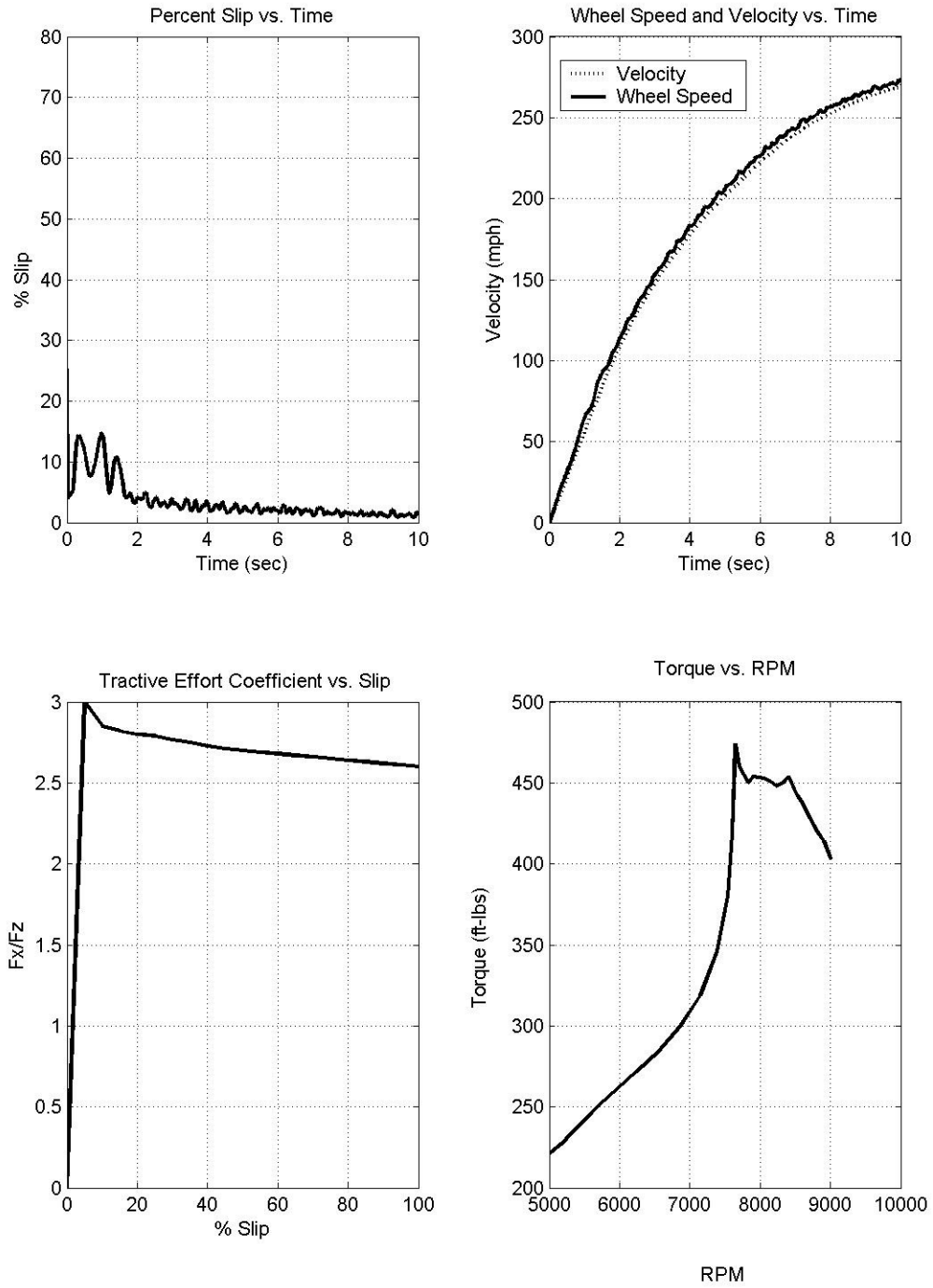
Figure 5.40: Vehicle Dynamics Plot 4 with Improved Gears (Drag Strip)
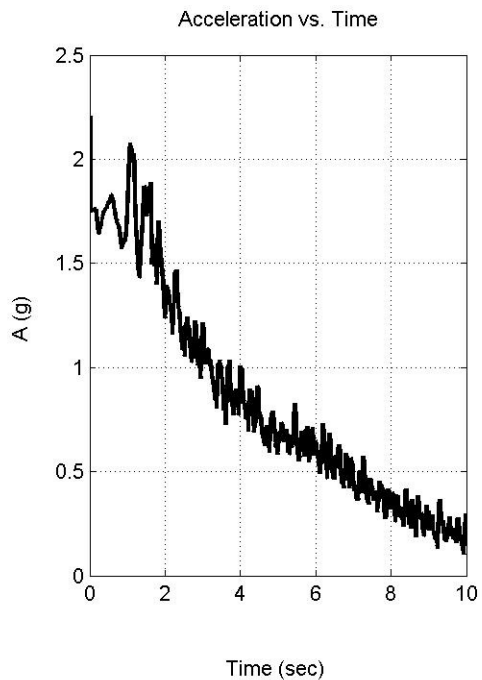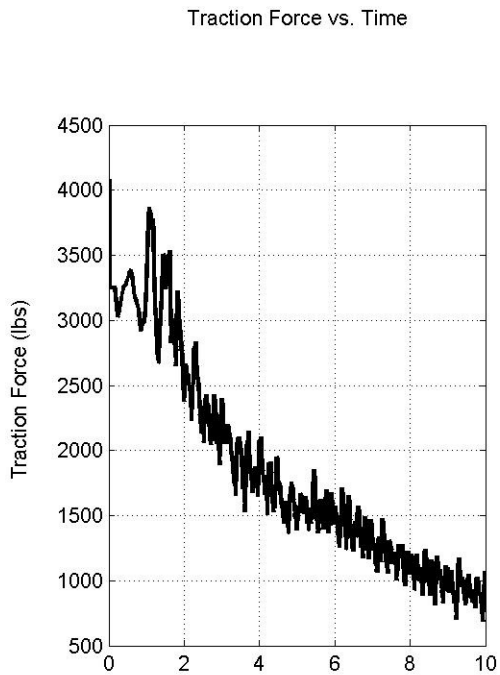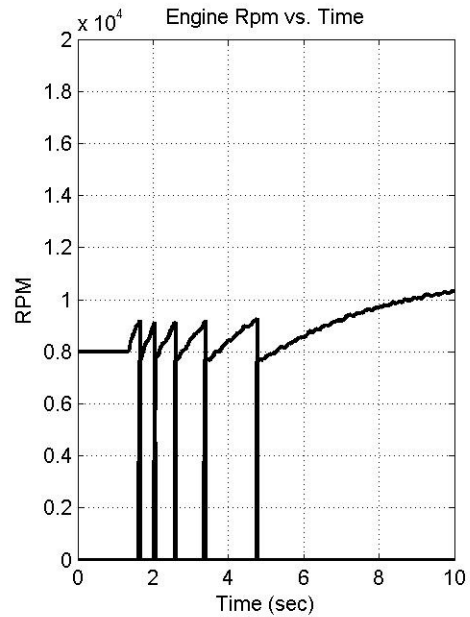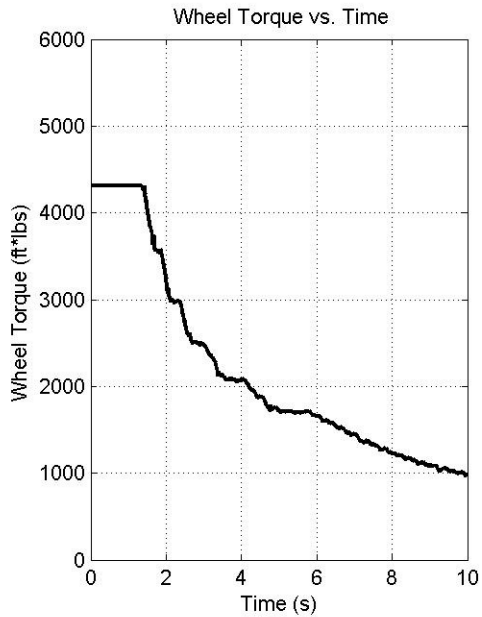
Figure 5.41: Vehicle Dynamics Plot 5 with Improved Gears (Drag Strip)
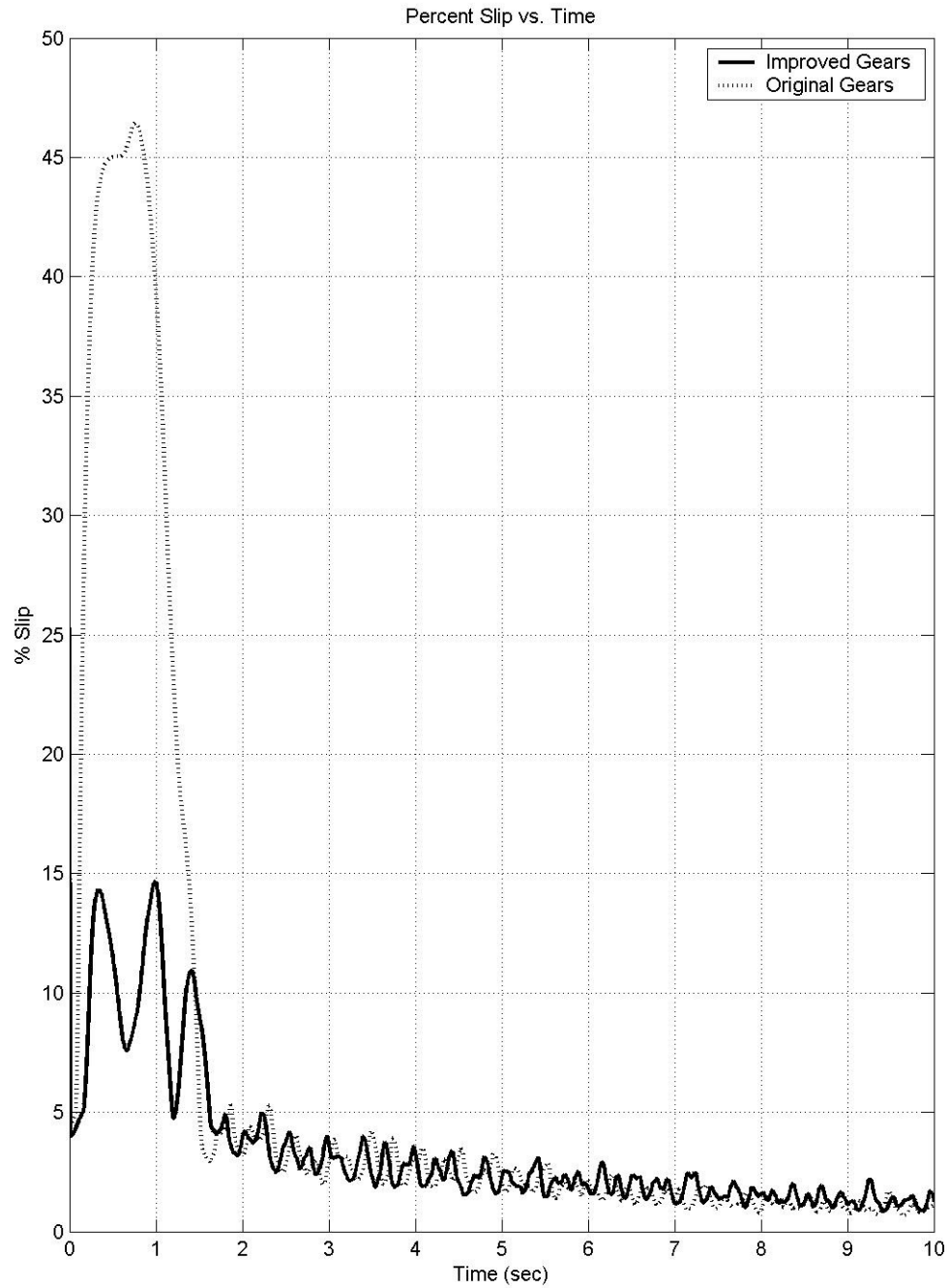
Figure 5.42: Gear Ratio Effect on Wheel Slip (Drag Strip)
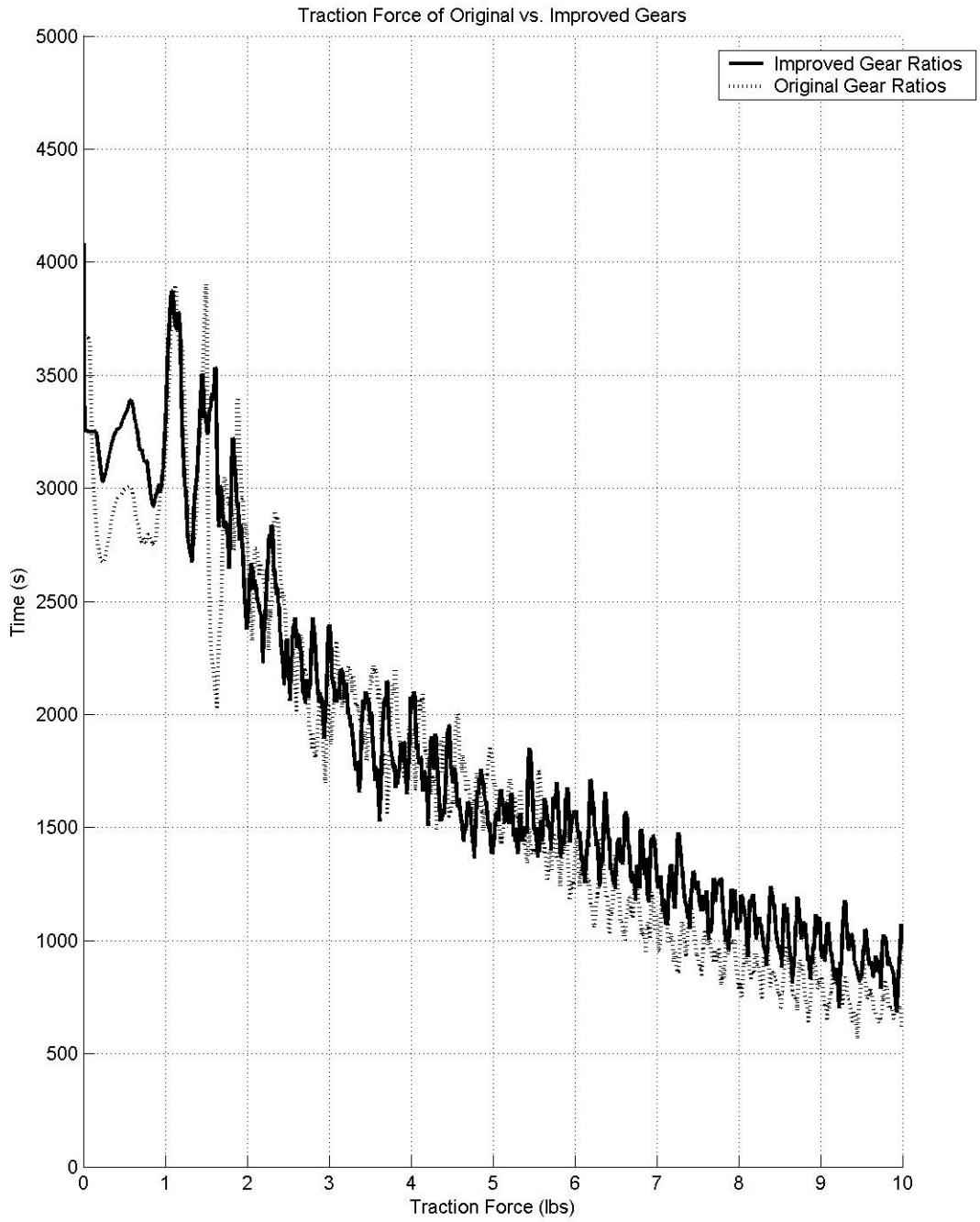
Figure 5.43: Traction Force for Original and Improved Gear Ratios (Drag Strip)
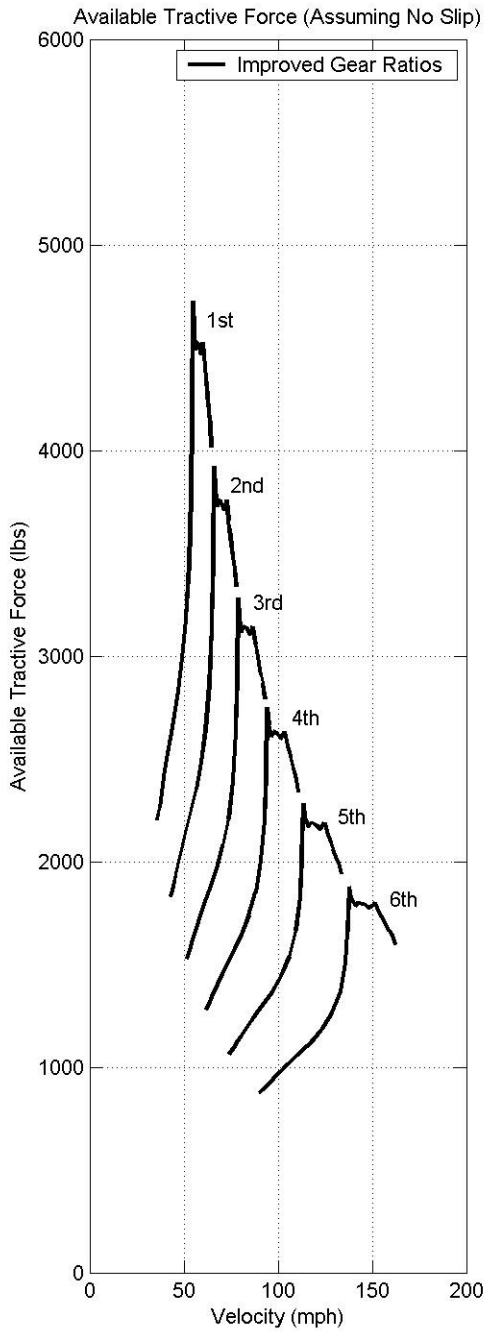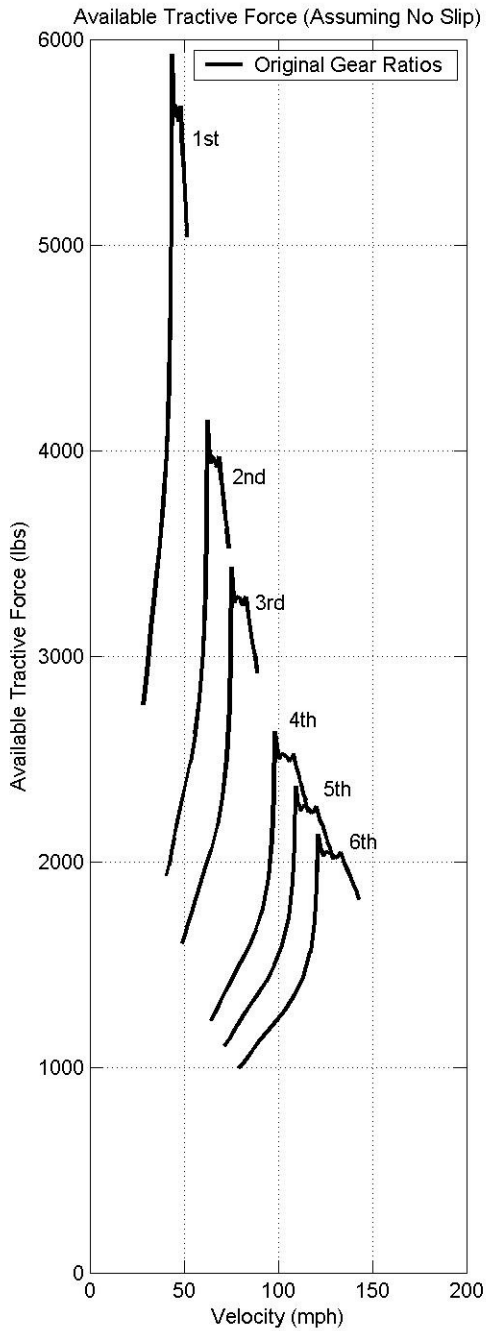
Figure 5.44: Gear Ratio Effect on Available Tractive Force (Drag Strip)

Drag Performance Comparisons

The quarter mile performance characteristics of the front wheel drive drag racing car using the original and improved gear ratios are broken down into the same categories as described earlier in this chapter. These categories, Elapsed Time, Trap Speed, etc., are shown in Table 5.8 for the drag racing vehicle traversing both the perfectly smooth, flat road and the simulated drag strip with the original gear ratios, first improvement gear ratios, and second improvement gear ratios. The gains for each performance category are also shown.

As can be seen from the performance table for the vehicle on the perfectly smooth road, the GRI procedure reduced the elapsed time for the quarter mile run by 0.164 seconds. This may seem insignificant, but to a drag racer it is an eternity. Races are won and lost by thousandths of a second and a gain of almost two tenths is outstanding. The final speed of the vehicle across the finish line increased from the original to improved gear ratios by almost six miles per hour, which is another significant gain in the world of drag racing. The speed gained is mostly due to the significant change of the higher gear ratios. Sixth gear changes from a 1.2:1 to a 1.08:1 ratio. This allows the engine to operate in the RPM range with the highest amount of torque. This also allows the wheels to turn faster and create more speed near the quarter mile mark. Table 5.8 shows gains in all categories, but the main gains associated with the final result of the drag run are highlighted.

Table 5.8: Quarter Mile Performance Gains with Improved Gears

Perfectly Smooth, Flat Road					
	Original Gears	1st Improvement	Gain	2nd Improvement	Total Gain
1st Gear Ratio =	3.33	2.6333		2.6444	
2nd Gear Ratio =	2.33	2.2		2.1722	
3rd Gear Ratio =	1.93	1.8		1.8278	
4th Gear Ratio =	1.48	1.5333		1.5778	
5th Gear Ratio =	1.33	1.3667		1.3222	
6th Gear Ratio =	1.2	1.1		1.0833	
Elapsed Time (seconds) =	8.307	8.153	0.154	8.143	**0.164**
Trap Speed (miles per hour) =	166.45	171.55	5.10	172.30	**5.85**
1/8 Mile Time (seconds) =	5.427	5.322	0.105	5.318	0.109
1/8 Mile Speed (miles per hour) =	141.85	142.08	0.23	142.20	0.35
330 Foot Time (seconds) =	3.662	3.568	0.094	3.566	0.096
60 Foot Time (seconds) =	1.510	1.461	0.049	1.463	0.047

Simulated Drag Strip					
	Original Gears	1st Improvement	Gain	2nd Improvement	Total Gain
1st Gear Ratio =	3.33	2.6333		2.6556	
2nd Gear Ratio =	2.33	2.3		2.2056	
3rd Gear Ratio =	1.93	1.8333		1.8444	
4th Gear Ratio =	1.48	1.5333		1.5444	
5th Gear Ratio =	1.33	1.3667		1.2833	
6th Gear Ratio =	1.2	1.1		1.0556	
ET (seconds) =	8.315	8.163	0.152	8.143	**0.172**
Elapsed Time (seconds) =	166.35	171.46	5.11	173.25	**6.90**
Trap Speed (miles per hour) =	5.434	5.331	0.103	5.323	0.111
1/8 Mile Time (seconds) =	141.68	141.98	0.30	142.10	0.42
1/8 Mile Speed (miles per hour) =	3.667	3.576	0.091	3.570	0.097
330 Foot Time (seconds) =	1.511	1.463	0.048	1.465	0.046

The GRI performed for the drag car on the simulated drag strip shows very similar trends to that on the perfectly smooth, flat road. The quarter mile time decreases by 0.172 seconds and the speed at which the vehicle crosses the finish line increases by almost seven miles per hour. These gains are slightly greater than those seen on the perfectly smooth, flat road.

Every category that is used to evaluate the performance of the drag run showed improvement with the improved gear ratios. The main change in gear ratio is found in first gear. The gear ratio changed from a 3.33:1 ratio to a 2.66:1 ratio. This decrease in gear ratio effectively decreases the amount of torque seen at the drive wheels, since the vehicle is launched at a constant 8000 rpm, and therefore creates less wheel slip when the vehicle starts the run. Less longitudinal slip translates into more traction force and thus decreased quarter mile times and increased speed.

The Effect of Tire-to-Road Adhesion Level on
Simulated Drag Performance and GRI

One question that arises is how robust the improved gear ratios will prove to be when used for different tracks. Drag racing events are held at different locations and each track has different characteristics. One of the most important characteristics of a track is the coefficient of friction between the track surface and the drive tires. The coefficient of friction is most commonly referred to as μ, or mu. In order to see the effects of μ on the gear ratio selection, the μ of the simulated drag strip is varied by + / - 20%. This will give a broad range of surfaces ranging from the slicker surfaces to the more "tacky" surfaces.

The improved gear ratios exhibited an improvement in quarter mile elapsed time and final velocity for all studied variations in tire-to-road adhesion level. As can be seen in Table 5.9, the improvements were not as significant at the varied mu levels. The least significant gain was at the higher mu value. Less wheel slip is generated by the original gears since there is more longitudinal grip on the higher mu surface. The intermediate times are better for the original gears, due to the ability to effectively use the extra torque provided by the original gears. The improved gears, however, provide more torque at faster speeds and thus generate faster speeds toward the end of the drag run.

In the lower mu evaluation, the improved gears again showed an improvement over the original gears. The gains are greater than those seen over the higher mu surface and exhibit a trend similar to those over the nominal surface.

The GRI procedure seems to create gear ratios that are reasonably robust for surfaces with mu levels less than nominal. As the mu level increases, however, the positive effects of the improved gear ratios become smaller.

Table 5.9: The Effect of Tire-to-Road Adhesion Level on Improved
Gear Ratio Robustness to Drag Performance

Simulated Drag Strip μ +/- 20%			
	Original Gears with μ	Improved Gears with μ	Difference
Elapsed Time (seconds) =	8.315	8.143	-0.172
Trap Speed (miles per hour) =	166.35	173.25	6.9
1/8 Mile Time (seconds) =	5.434	5.323	-0.111
1/8 Mile Speed (miles per hour) =	141.68	142.1	0.42
330 Foot Time (seconds) =	3.667	3.57	-0.097
60 Foot Time (seconds) =	1.511	1.465	-0.046
	Original Gears with μ + 20%	Improved Gears with μ + 20%	Difference
Elapsed Time (seconds) =	8.124	8.122	-0.002
Trap Speed (miles per hour) =	166.73	173.51	6.78
1/8 Mile Time (seconds) =	5.252	5.306	0.054
1/8 Mile Speed (miles per hour) =	142.3	142.32	0.02
330 Foot Time (seconds) =	3.496	3.556	0.06
60 Foot Time (seconds) =	1.379	1.454	0.075
	Original Gears with μ - 20%	Improved Gears with μ - 20%	Difference
Elapsed Time (seconds) =	8.646	8.541	-0.105
Trap Speed (miles per hour) =	165.7	172.31	6.61
1/8 Mile Time (seconds) =	5.748	5.698	-0.05
1/8 Mile Speed (miles per hour) =	140.53	140.49	-0.04
330 Foot Time (seconds) =	3.961	3.918	-0.043
60 Foot Time (seconds) =	1.704	1.675	-0.029

Performing the GRI program for each of the mu values should give a good indication of how the friction coefficient of each track would affect the gear ratio selection. Therefore, if the μ for a given track surface is known, an improved gear ratio selection could be made for each different surface.

As can be seen in Table 5.10, the selection of the gear ratios is logical; more torque is provided to the front wheels when there is more traction available at the road surface. The road surface affects the gear ratio selection significantly. All gears selected through the improvement program see either an increase or decrease depending on the trend of the μ value of the racing surface. Also notice that, even with the improved gears, the performance of the drag car decreases in every category as μ decreases. This is understandable because the vehicle can only use the traction that is available, and if there is less traction available, the quarter mile time will be slower.

Table 5.10: The Effect of Tire-to-Road Adhesion Level
on Improved Gear Ratio Selection

Simulated Drag Strip μ +/- 20%					
	Improved Gears with μ	Improved Gears with μ + 20%	Gear Ratio Diff.	Improved Gears with μ - 20%	Gear Ratio Diff.
1st Gear Ratio =	2.6556	3.3	.6444 (+24.3%)	2.0556	-0.6 (-22.6%)
2nd Gear Ratio =	2.2056	2.4667	.2611 (+11.8%)	1.8111	-0.3945 (-17.9%)
3rd Gear Ratio =	1.8444	1.9667	.1223 (+6.6%)	1.5778	-0.2666 (-14.4%)
4th Gear Ratio =	1.5444	1.6222	.0778 (+5.0%)	1.4222	-0.1222 (-7.9%)
5th Gear Ratio =	1.2833	1.3444	.0611 (+4.8%)	1.2222	-0.0611 (-4.8%)
6th Gear Ratio =	1.0556	1.0778	.0222 (+2.1%)	1.0222	-0.0334 (-3.2%)
Elapsed Time (seconds) =	8.143	8.045		8.421	
Trap Speed (miles per hour) =	173.25	172.60		173.49	
1/8 Mile Time (seconds) =	5.323	5.221		5.588	
1/8 Mile Speed (miles per hour) =	142.10	142.02		141.09	
330 Foot Time (seconds) =	3.570	3.469		3.814	
60 Foot Time (seconds) =	1.465	1.377		1.599	

We can check the validity of the gear ratio improvement program with a simple calculation. If we assume that the improved first gear ratio, for the original μ, uses 100% of the available traction, we can estimate the gear ratio needed to use all of the traction available for +/- 20% of the original μ by adding and subtracting 20% from the original gear ratio. Using this calculation we find that the first gear ratios for the +/- 20% μ surfaces are 3.19 and 2.12 respectively. These values are very close to the values chosen by the gear ratio improvement program. This estimation will only be valid for the first gear ratio because this is the only point in the drag run where the longitudinal wheel slip is significant.

CHAPTER SIX

SUMMARY AND RECOMMENDATIONS

Summary

Front wheel drive drag racing is becoming an ever popular sport with import car enthusiasts as well as domestic car fans. The simulation that is created for this thesis gives a fairly accurate depiction of the dynamics exhibited by a front wheel drive drag racing car as it traverses a drag strip during a quarter mile run.

In summary, randomly generated roads were created to simulate three roads of different levels of roughness. The simulated roads had the same power spectral density characteristics as the real world roads. The similarities of the simulated roads to the real roads are confirmed by comparing power spectral densities and checking for normality.

The GRI program in the simulation of the front wheel drive drag racing car shows that a definite improvement in quarter mile performance can be found in the selection of the gear ratios. The gear ratios determined by the GRI may not produce the fastest quarter mile times in a true racing application, but could be used as a starting point. The purpose of the study was to note the fact that improvement in performance could be made in that area of the drag racing car. The trend of the improved gear ratios being close to a geometrical progression should be noted as a possible solution to improving quarter mile performance.

The selection of gear ratios is sensitive to the coefficient of friction between the track surface and drive tires. As mu increases, the gear ratios can be designed to deliver more torque to the drive wheels to take advantage of this increase in traction. But as mu

decreases, the gear ratios need to be chosen to minimize the amount of wheel spin that is generated due to the decrease in traction.

<div align="center">Recommendations</div>

The five DOF vehicle model of the front wheel drive drag racing car is a very simple model. Perhaps a more detailed model would be useful in future studies of the drag racing car.

Lateral dynamics are ignored in this thesis since drag racing mainly excites the longitudinal dynamics of the vehicle. Lateral degrees of freedom could, however, be added in future works to improve the accuracy of the model.

The drag racing vehicle is modeled as a rigid body for this study. A race car chassis is normally very stiff, which makes this a valid assumption. However, a race car chassis will flex a little under the extreme loadings experienced during a drag racing run. If there is interest in studying the influence of chassis flex on this model, Knauff derived and investigated chassis flex for this application in [1].

Another assumption that was made for this model involves the wheelie bar. The wheelie bar is modeled as a pin joint that is fixed directly to the surface of the road, free to rotate, and must follow the vertical displacement of the road in the z-direction. This causes the force exerted from the wheelie bar to the chassis of the vehicle to become negative at points during the quarter mile run. There are two cases that can occur during a true drag racing run. One case occurs when the wheelie bar is in contact with the road surface and the other occurs when the wheelie bar is not touching the road surface. The reason the wheelie bar is modeled as a pin joint fixed to the road surface was to simplify

the model. To avoid having the model switch between the two different sets of equations of motion, one was chosen that would create the correct vehicle motion at the most critical point of the drag run, the launch. Another dynamic model, one of the drag vehicle with the wheelie bar not in contact with the track surface, could be added to the simulation. The simulation could then switch between the two models, depending on if the wheelie bar is in contact with the road.

If a race team knows the mu versus slip curve for a given tire / track combination, the GRI simulation could be used to determine an approximate set of gears for the drag car. Also, measuring the PSD of the actual drag strip surface to be run could allow the simulation to recreate the track surface and be used in the simulation. It would be very interesting to see how the simulation's predicted quarter mile performance would compare to the results of the actual drag run.

APPENDICES

Appendix A

Equations of Motion

The equations of motion of the 5 DOF vehicle model and their derivation are described in this appendix. The longitudinal dynamic equations are derived using Newton's Second Law.

The free body diagram of the front wheel drive drag racing vehicle is shown in Figure 2.1. For an easier explanation of the equations of motion, the figure is repeated below.

Figure 2.1: Front Wheel Drive Drag Racing Car 5 DOF Model

111
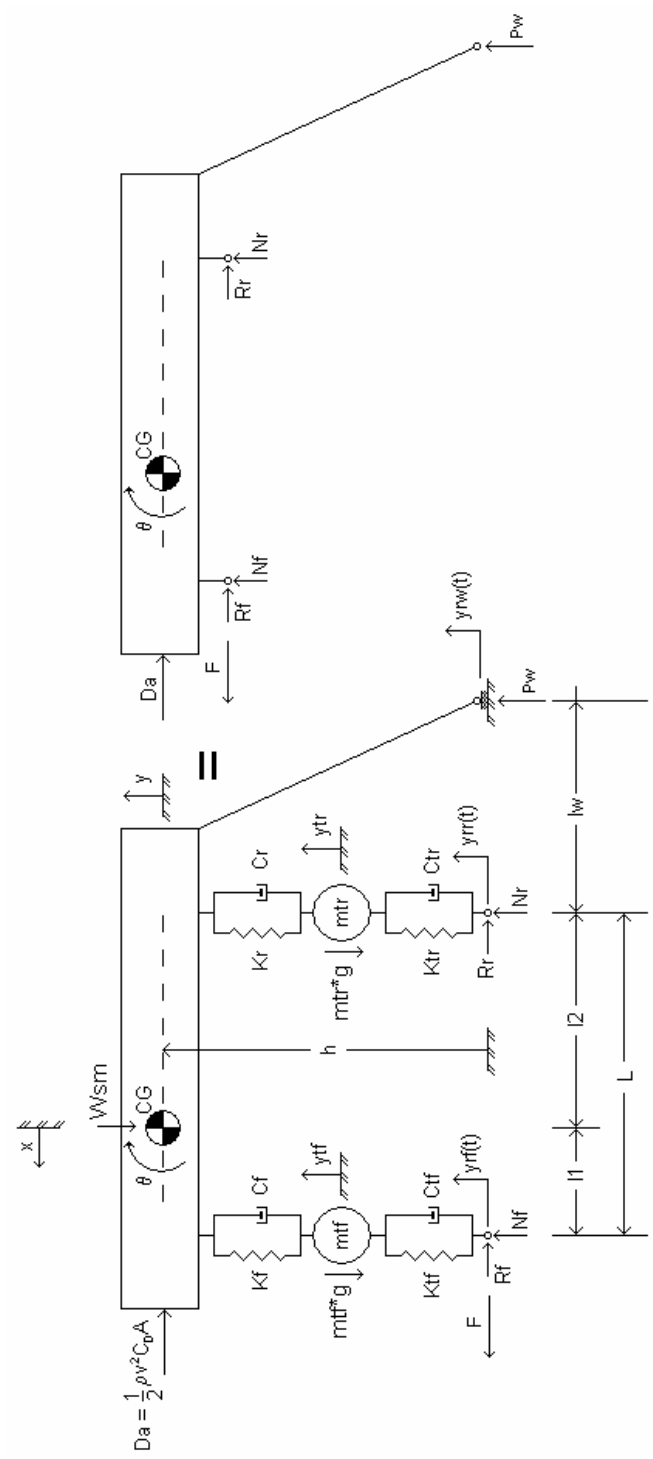
Assuming that the wheelie bar is pinned to the road, the vertical displacement of the vehicle front (y_f), center of gravity (y), and rear (y_r) can be calculated using the vehicle pitch angle (Θ) and distance the associated position on the vehicle is from the pivot that the wheelie bar creates around the road. The time derivative of these equations can be taken to give the sprung vertical velocity and acceleration. These equations are shown below in Equations A.1-A.7, and are used in substitutions throughout the derivation of the equations of motion used for the front wheel drive drag racing car.

$$y = (l_2 + l_w)\theta + y_{rw}(t) \tag{A.1}$$

$$\dot{y} = (l_2 + l_w)\dot{\theta} + \dot{y}_{rw}(t) \tag{A.2}$$

$$\ddot{y} = (l_2 + l_w)\ddot{\theta} + \ddot{y}_{rw}(t) \tag{A.3}$$

$$y_f = (L + l_w)\theta + y_{rw}(t) \tag{A.4}$$

$$\dot{y}_f = (L + l_w)\dot{\theta} + \dot{y}_{rw}(t) \tag{A.5}$$

$$y_r = l_w\theta + y_{rw}(t) \tag{A.6}$$

$$\dot{y}_r = l_w\dot{\theta} + \dot{y}_{rw}(t) \tag{A.7}$$

The equation of motion for the longitudinal dynamics of the vehicle is found by summing the forces in the longitudinal, or x, direction on the free body diagram of the drag racing car. The summation is shown in Equation (A.8) below.

$$F - D_a - R_f - R_r = m\ddot{x} \tag{A.8}$$

F is the traction force, D_a is the aerodynamic drag force, R_f and R_r are the rolling resistances of the front and rear respectively, m is the vehicle total mass and x is the

displacement in the longitudinal direction. The rolling resistances and aerodynamic drag can be quantified using the equations given in Equations A.9-A.11.

$$D_a = \frac{1}{2}\rho \cdot \dot{x}^2 \cdot C_D \cdot A \tag{A.9}$$

$$R_f = f \cdot N_f \tag{A.10}$$

$$R_r = f \cdot N_r \tag{A.11}$$

ρ is the density of air, C_D is the drag coefficient of the vehicle, A is the frontal area of the drag racing car, f is the coefficient of friction, and N is the normal force at the front or rear axles.

Knowing that the mass of the vehicle is simply the vehicles weight (W) divided by gravity (g), we can solve Equation (A.8) for the longitudinal acceleration and substitute Equations A.9-A.11 to derive our first equation of motion for the five degrees of freedom vehicle model. This equation is shown in Equation (A.12).

$$\ddot{x} = \frac{g}{W}F - fg\left(\frac{N_f + N_r}{W}\right) - \frac{1}{2}\rho \cdot \dot{x}^2 \cdot C_D \cdot A \tag{A.12}$$

The equation of motion for the drive axle can be derived using the free body diagram of the front axle. This equation is used to determine amount of wheel spin the vehicle experiences and the rotational velocity of the drive axle. The free body diagram of the front axle of the front wheel drive drag racing vehicle is shown in Figure 2.4, but is also shown below to aid in the derivation.
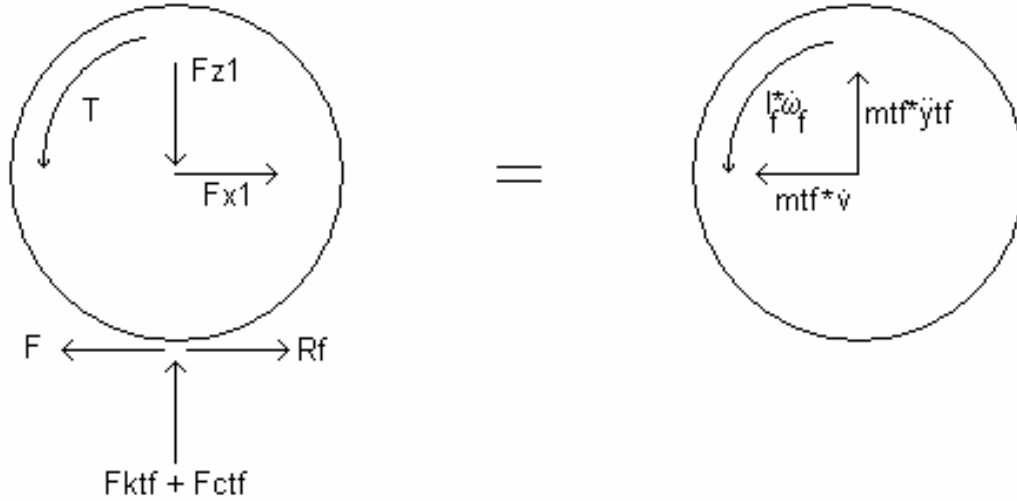
Figure 2.3: Front Unsprung Mass Free Body Diagram

By summing the moments about the center of the axle and solving for the rotational velocity of the axle, we get the second equation of motion for the five DOF model. This equation is shown in Equation (A.13).

$$\dot{\omega}_f = \frac{1}{I}\left(T - Fr - fN_f r\right)$$ (A.13)

I is the rotational inertia of the front drive axle, T is the torque delivered by the motor to the front axle, and r is the outside radius of the tire measured from the center of the wheel.

Using the free body diagram of the front axle, we can also derive the vertical motion equation of the front axle. Summing the forces in the vertical direction will accomplish this and is shown in Equation (A.14).

$$F_{Ktf} + F_{Ctf} - F_{Kf} - F_{Cf} = m_{tf}\,\ddot{y}_{tf}$$ (A.14)

114

m_{tf} is the front sprung mass and y_{tf} is the vertical displacement of the front axle. F_{Ktf} and F_{Ctf} are the forces exerted on the front axle from the spring constant and damping constant of the front tire respectively. F_{Kf} and F_{Cf} are the forces exerted by the front springs and dampers respectively. The forces caused by the spring deflection are calculated by multiplying the appropriate spring constant by the deflection of the appropriate spring, whether it is the front spring or the deflection of the tire. The forces exerted by the dampers is simply the damper constant multiplied by the velocity across the appropriate damper, whether it is the front shocks or the dampening of the tire. Calculating the deflection of the springs and differences in velocity over shocks is a simple task. Substituting the forces into Equation (A.14) gives Equation (A.15), or the third equation of motion for the five DOF front wheel drive drag racing vehicle.

$$\ddot{y}_{tf} = \frac{1}{m_{tf}}\left(K_f\left(y + l_1\theta - y_{tf}\right) + C_f\left(\dot{y} + l_1\dot{\theta} - \dot{y}_{tf}\right) + K_{tf}\left(y_{rf}(t) - y_{tf}\right) + C_{tf}\left(\dot{y}_{rf}(t) - \dot{y}_{tf}\right)\right) \quad \text{(A.15)}$$

K and C, respectively, are the spring constant and damper coefficients of the front suspension, f, and the front tire, tf. The vertical displacements are denoted as y, with subscripts rf being the road at the front tire and tf being the displacement of the front axle.

The vertical dynamics of the rear axle can be derived in the exact same way. The only difference from the front axle is the location of the rear axle, the values of the spring and damper constants, and the fact that there is no drive torque exerted on the rear axle, which does not affect the vertical motion of the axle anyway for this simple model. The equation will be exactly the same as that for the front axle except that all of the constants

will be for the rear axle, and the deflections and velocity differences will be for the rear axle. The equation of motion for the rear axle is shown in Equation (A.16).

$$\ddot{y}_{tr} = \frac{1}{m_{tr}}\left(K_r\left(y - l_2\theta - y_{tr}\right) + C_r\left(\dot{y} - l_2\dot{\theta} - \dot{y}_{tr}\right) + K_{tr}\left(y_r(t) - y_{tr}\right) + C_{tr}\left(\dot{y}_r(t) - \dot{y}_{tr}\right)\right) \quad \text{(A.16)}$$

$y_r(t)$ denotes the vertical displacement of the road at the rear axle.

The final equation of motion for the front wheel drive drag racing vehicle is that of the sprung mass. The free body diagram of the sprung mass is shown below to aid in deriving the equation.
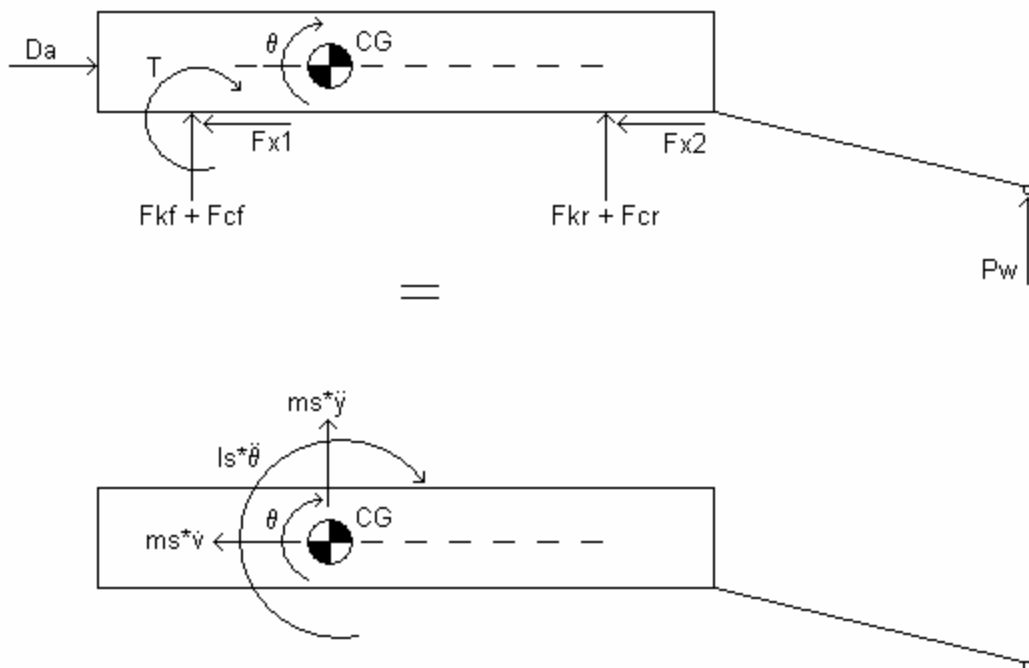
Figure 2.2: Free Body Diagram of Sprung Mass

The first thing that is done to derive this equation of motion is to determine the wheelie bar force. This is done simply by summing the forces in the vertical direction. By performing the summation, substituting, and solving for P_w, we come up with Equation (A.17).

$$
\begin{aligned}
P_w = &\ m_s\left(\left(l_2 + l_w\right)\ddot{\theta} + \ddot{y}_{rw}(t)\right) - K_f\left(y_{tf} - \left(L + l_w\right)\theta - y_{rw}(t)\right) - C_f\left(\dot{y}_{tf} - \left(L + l_w\right)\dot{\theta} - \dot{y}_{rw}(t)\right) \\
&- K_r\left(y_{tr} - l_w\theta - y_{rw}(t)\right) - C_r\left(\dot{y}_{tr} - l_w\dot{\theta} - \dot{y}_{rw}(t)\right)
\end{aligned}
\tag{A.17}
$$

The next step is to sum the moments about the center of gravity of the vehicle. This is done using the diagrams of the sprung mass and the total vehicle, and is shown in Equation (A.18).

$$
\begin{aligned}
T + &\ l_1\left(F_{Kf} + F_{Cf}\right) - D_a\left(h - h_a\right) + \left(F_{x1} + F_{x2}\right)\left(h - r + y\right) - l_2\left(F_{Kr} + F_{Cr}\right) \\
&- \left(l_2 + l_w\right)P_w = I_s\ddot{\theta}
\end{aligned}
\tag{A.18}
$$

F_{x1} and F_{x2} are resistances exerted from the road to the sprung mass through the suspension. These forces were assumed to be trivial and dropped from the equations before inputting the model in Simulink. I_s is the inertia of the sprung mass.

Substituting Equation (A.17) into Equation (A.18) gives the equation of motion of the sprung mass of the front wheel drive drag racing vehicle. This is shown in Equation (A.19).

$$
\begin{aligned}
\ddot{\theta} = &\ \frac{1}{I_s + m_s\left(l_2 + l_w\right)^2}\left(T + \left(L + l_w\right)\left(K_f\left(y_{tf} - \left(L + l_w\right)\theta - y_{rw}(t)\right) + C_f\left(\dot{y}_{tf} - \left(L + l_w\right)\dot{\theta} - \dot{y}_{rw}(t)\right)\right)\right. \\
&+ l_w\left(K_r\left(y_{tr} - l_w\theta - y_{rw}(t)\right) + C_r\left(\dot{y}_{tr} - l_w\dot{\theta} - \dot{y}_{rw}(t)\right)\right) - D_a\left(h - h_a\right) \\
&\left. + \left(F_{x1} + F_{x2}\right)\left(h - r + \left(l_2 + l_w\right)\theta + y_{rw}(t)\right)\right)
\end{aligned}
\tag{A.19}
$$

The five equations of motion for the five degrees of freedom front wheel drive drag racing vehicle are given in Equations A.12, A.13, A.15, A.16, and A.19. These are the

equations modeled in block diagram form in Simulink. The five unknowns represented in these equations are the vehicle pitch and heave, front axle vertical displacement, front axle angular velocity, and the longitudinal motion of the vehicle.

Appendix B

Vehicle Parameters

Table B.1: List of Input Data

Variable	Value	Units	Variable Description
A	20.02	ft^2	Frontal Area
Cd	0.263	N/A	Drag Coefficient
Ctf	7	lb/ft/sec	Front Tire Damping Coefficient per Axle
Ctr	7	lb/ft/sec	Rear Tire Damping Coefficient per Axle
F	0.03	N/A	Tire Coefficient of Rolling Resistance
G	32.2	lb*ft/sec^2	Gravitational Constant
H	0.8583333	Ft	Height of CG
Ha	0.8583333	Ft	Height of Drag Force Action
I	1.568	slugs*ft^2	Per Axle Rotational Inertia
Is	650	Slugs*ft^2	Sprung Mass Pitch Moment of Inertia
Kf	5052	lb/ft	Front Wheel Rate per Axle
Kr	1464	lb/ft	Rear Wheel Rate per Axle
Ktf	12400	lb/ft	Front Tire Stiffness per Axle
Ktr	23300	lb/ft	Rear Tire Stiffness per Axle
ls	9.2408333	Ft	Wheel Base
l1	2.2791667	Ft	Distance from Front Axle to CG
l2	6.9616667	Ft	Distance from Rear Axle to CG
lw	7.42	ft	Distance from Rear Axle to End of Wheelie Bar
Nlaunch	8000	RPM	Launch RPM
R	12.048	in	Tire Radius
Tef	0.95	N/A	Transmission Efficiency
Tpf	6.5	psi	Front Tire Pressure
Tpr	35	psi	Rear Tire Pressure
Twf	11.5	in	Front Tire Width
Twr	4.5	in	Rear Tire Width
W	1808	lbs	Weight of Car
Ws	1512	lbs	Sprung Weight of Car
Wtf	182	lbs	Unsprung Weight of Front Axle
Wtr	114	lbs	Unsprung Weight of Rear Axle
z1st	3.33	N/A	Original 1st Gear Ratio
z2nd	2.33	N/A	Original 2nd Gear Ratio
z3rd	1.93	N/A	Original 3rd Gear Ratio
z4th	1.48	N/A	Original 4th Gear Ratio
z5th	1.33	N/A	Original 5th Gear Ratio
z6th	1.2	N/A	Original 6th Gear Ratio
zf	3.769	N/A	Final Drive Ratio
P	0.00238	lb/ft^3	Density of Air

Appendix C

Simulation Methods

Introduction

The five DOF model of the front wheel drive drag racing car is simulated in MATLAB and Simulink. MATLAB is used first to generate the random road profile. MATLAB is then used to input all of the physical data of the front wheel drive drag racing car and then run the simulation through Simulink.

Simulation Model

Random Road Profile Generator

The sine wave attributes attained from MATLAB, as described in the previous section, are passed to Simulink to create the actual sine waves. The sine waves are generated using the phases, frequencies and amplitudes provided from MATLAB. The sine waves are then multiplied by an identity matrix to effectively sum all of the sine waves to create one random surface. The randomly generated sine waves phases are shifted ninety degrees to create the slope of the randomly generated road surface. This will allow for simple calculations of velocities over the dampers while the vehicle is performing a simulated drag run. The randomly simulated road profile and slope are then combined into a one dimensional array for ease of transfer to the rest of the simulation. The block diagram in Simulink that sums the sine waves and creates the random road profile is shown in Figure C.1.
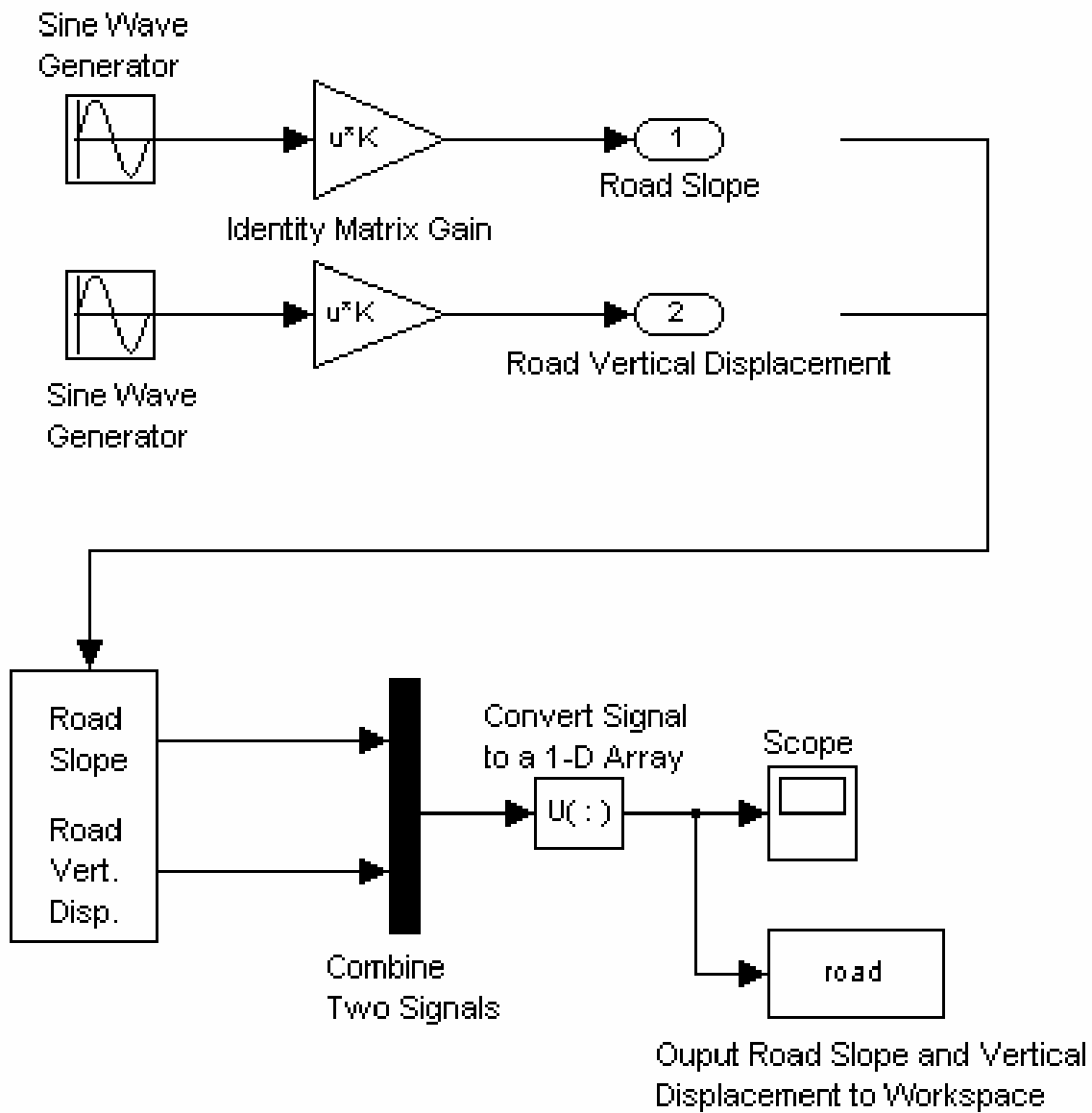
Figure C.1: Random Road Profile Generator

Fixed Footprint Tire Model

The fixed footprint tire model was developed by Captain [2]. This tire model assumes the tire is comprised of evenly distributed stiffness and damping elements that conform to the profile of the road surface. The fixed footprint simulation model uses the longitudinal position of the front axle, rear axle, and wheelie bar pin joint as inputs to the system. The block diagram flows from left to right, with the inputs coming into the simulation on the left and the outputs being given on the right.

The wheelie bar, since it is modeled as a point contact, just uses the instantaneous longitudinal position of the wheelie bar, Xwheelie in the diagram, contact with the road to determine, via look-up tables Road Profile Wheelie Bar and Road Slope Wheelie Bar, the road vertical displacement and slope.

The average vertical displacement of the simulated road is slightly more difficult to determine. Half of the longitudinal lengths of the contact patch of the front, Ltf/2, and rear, Ltr/2, tires are added to and subtracted from the longitudinal position of the respective axle, Xfront and Xrear. These two numbers are subtracted from each other to give the length of the contact patch. This length is then partitioned into ten equally spaced points. These are the points over which the footprint deformation will be averaged. This number is under full control of the user and was found that ten points were enough to get an accurate average vertical displacement of the road. The rear position of the contact patch is then added to this partitioned length to give the absolute position of the tire as it is traveling down the simulated drag strip. These particular

calculations are performed in the subsystem labeled "Contact Patch Location Calculation".

The ten points of the absolute position of each tire are passed to look-up tables which determine the vertical displacement of the simulated road at each point along the contact patch. These vertical deflections are then summed and divided by ten, contained in the "Average" subsystems, to give the average vertical displacement over the front and rear contact patches at any given time in the simulated drag run. The height of the road profile underneath the tire contact patch is then output to the vehicle simulation.

The same operation is performed to find the average road slope under the contact patches, with the exception of the road profile look-up table being replaced with a road slope look-up table. The average road slope is multiplied by the instantaneous velocity, V, of the drag car to calculate the vertical velocity across the tire damping elements. The Simulink block diagram is shown in Figure C.2.
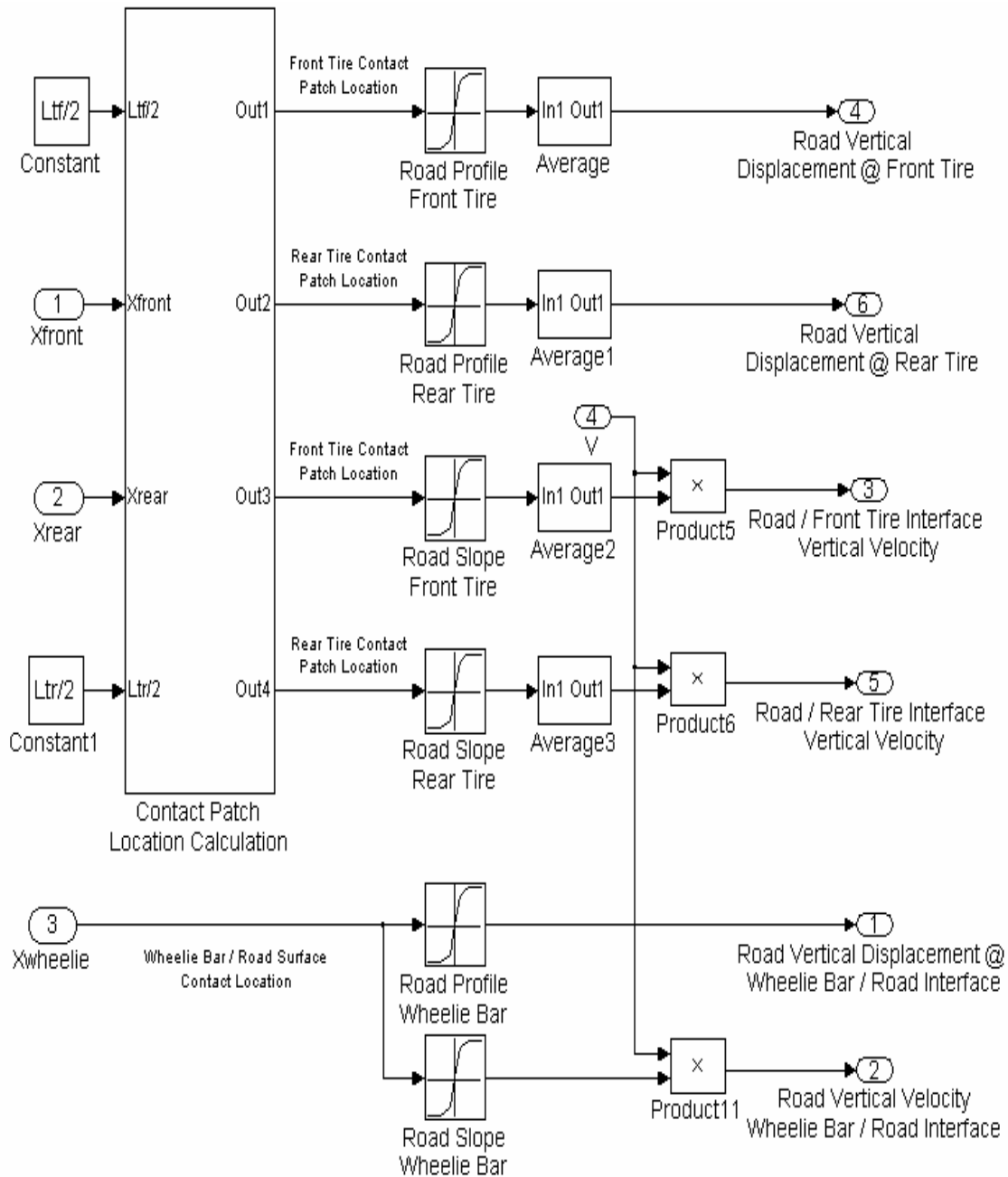
Figure C.2: Simulink Fixed Footprint Tire Model

Sprung Mass Dynamics

This portion of the Simulink model is the block diagram form of the sprung mass equation of motion, given in Equation (20). The model assumes that the sprung mass is free to pivot about the modeled pinned joint of the wheelie bar contact with the road surface. Thus, the vertical acceleration, velocity and displacement of the vehicle center of gravity are functions of the pitch angle and derivatives of the pitch angle of the vehicle.

Inputs to the simulation are shown as oval blocks with arrows exiting them. The inputs on the bottom right of the diagram include the normal force on the front and rear axle, Nf and Nr respectively, and the wheel drive torque, wheel torque. The aerodynamic drag, Da, and the available traction force, F, are also inputs to this portion of the simulation. The inputs on the left of the diagram are forces exerted on the sprung mass by the components of the front and rear suspension. The other two inputs to this portion of the simulation are in the upper right portion and include the vertical displacement of the simulated road at the wheelie bar contact with the road surface, Road Displacement Wheelie Bar, and the vertical velocity of the wheelie bar contact, Road Velocity Wheelie Bar.

The lower portion of this simulation is in effect the recreation of Equation (20). Pitch acceleration, Thetaddot, is calculated and then integrated once to get pitch velocity, Thetadot, and then integrated again to obtain the pitch angle, Theta. The upper half of the simulation is actually calculating vertical acceleration, displacement and velocity, Zddot, Zdot, and Z respectively, of the center of gravity of the front wheel drive drag

racing car. Since the wheelie bar contact with the road is modeled as a pin joint constrained in the vertical direction, the vertical velocity and displacement of the CG can be found by multiplying the longitudinal distance between the wheelie bar contact with the road surface and the CG with the vehicles rotational velocity and pitch angle respectively. This action is performed in the upper portion of this diagram. The vertical acceleration of the CG is found by integrating the CG vertical velocity.

The Simulink block diagram of the sprung mass portion of the simulation is shown in Figure C.3.
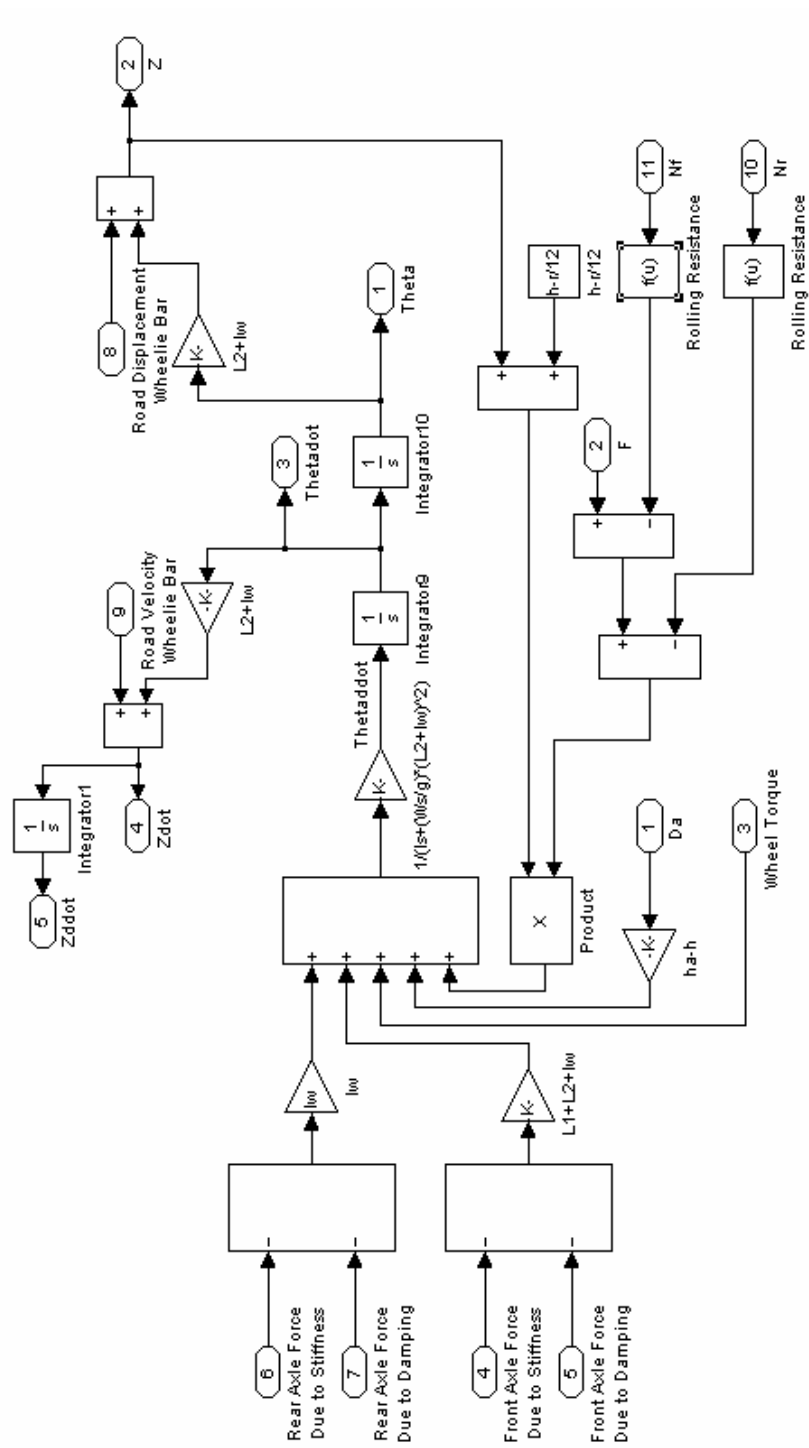
Figure C.3: Simulink Model of Sprung Mass Dynamics

Front and Rear Axle Dynamics

The front and rear axle dynamics are created in block diagram form in Simulink from Equations (18) and (19) respectively. The only differences between the front and rear axle diagrams are the values of the parameters used for each respective axle. Therefore, only the front axle diagram will be discussed.

The inputs to this portion of the simulation are the road vertical displacement and the vertical velocity of the contact with the road, as well as the pitch and heave displacement, Theta and Z, and velocity, Thetadot and Zdot, of the sprung mass. The simulation calculates the difference in motion between the axle, ytf, and road surface, Road Displacement Front Tire, and multiplies this with the stiffness of the tire to calculate the force exerted on the axle via deflection of the tire, Front Tire Force Due to Tire Stiffness. The same calculation is performed to obtain the force exerted on the axle via the damping element, Front Tire Force Due to Tire Damping.

The differences of velocity and displacement between the axle and sprung mass are also calculated to determine the force exerted on the unsprung mass from the spring, Front Axle Force Due to Stiffness, and damper, Front Axle Force Due to Damping, elements. The simulation uses a lookup table to determine the non-linear damping constants. The velocity across the shock is calculated and then used through the lookup table, "Look-Up Table for Cf", to determine the correct damping constant for that particular velocity. The vertical velocity and displacement of the axle, ytfdot and ytf, are derived from the vertical acceleration, ytfdot, of the axle through integration. The tire and spring deflections, ftiredef and faxledef respectively, are output from the simulation

128

to the workspace to give an idea of the vertical motion of the vehicle. The velocity across the shock, fshockvel, is also output to be used in determining the aggressiveness of the simulated drag strip.

The Simulink diagram of the front axle is shown in Figure C.4. The diagram for the rear axle looks exactly the same except that the front axle values and variables are replaced with those of the rear axle.
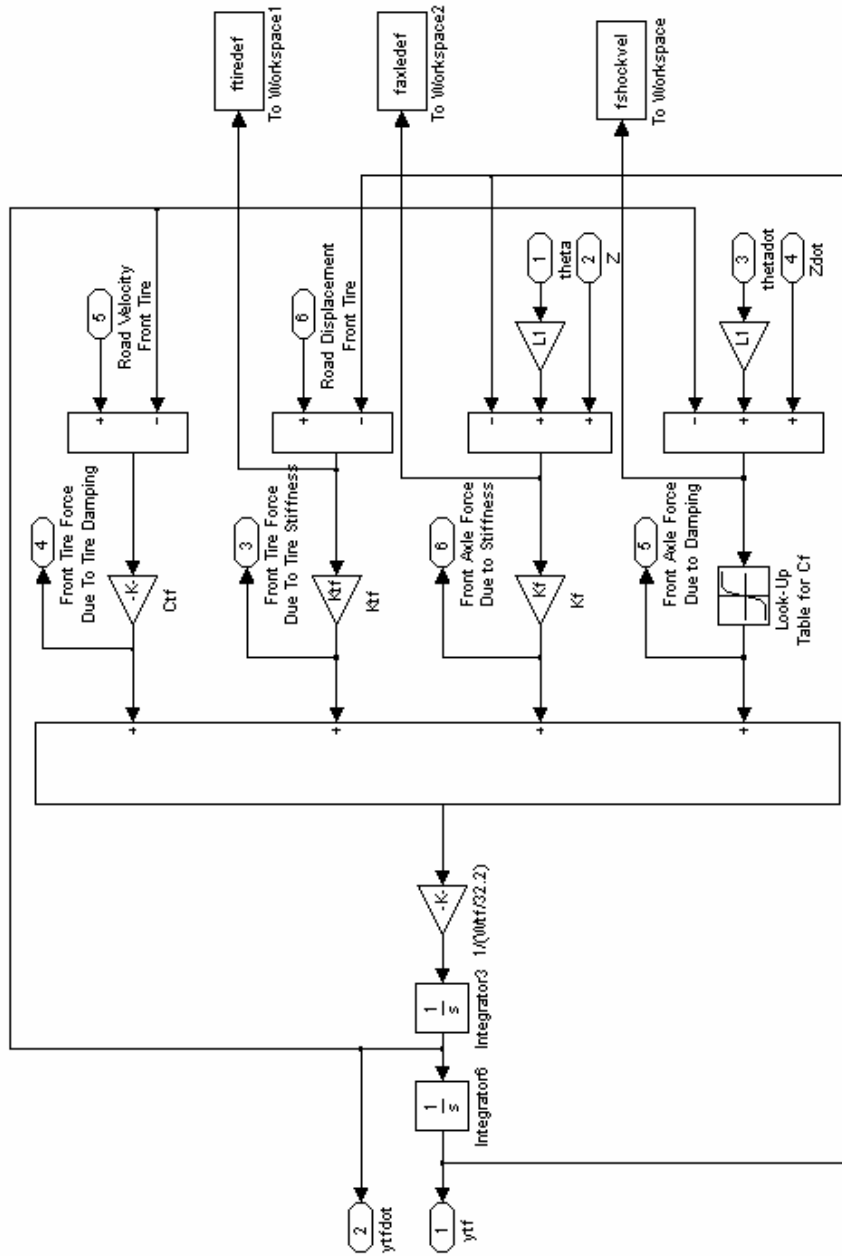
Figure C.4: Simulink Diagram of Front Axle Dynamics (Typical to Rear Axle)

Wheel Slip

This portion of the Simulink model calculates the wheel slip, engine revolutions per minute, wheel rotational velocity, drive torque, and traction force of the drive axle for the front wheel drive drag racing vehicle using Equation (17). The Simulink diagram for this portion of the model is shown in Figure C.5.

The inputs to this diagram are the vehicle longitudinal velocity, Vx, and the front wheel / road interface normal force, Nf. The upper portion of the diagram is Equation (17), in block format, which calculates the rotational acceleration of the drive axle, Wdot. The upper right portion of the diagram calculates the difference between vehicle longitudinal velocity and front axle rotational velocity, Omega, times tire radius, Gain3, to determine the longitudinal slip, Slip, the vehicle is undergoing. This percent slip is then passed to a look-up table, Fx/Fz, to determine the traction force relationship with front tire normal force, which is given as a ratio. This ratio is then multiplied by front normal force to determine the traction force available at the front wheels for the given longitudinal slip at that moment in time.
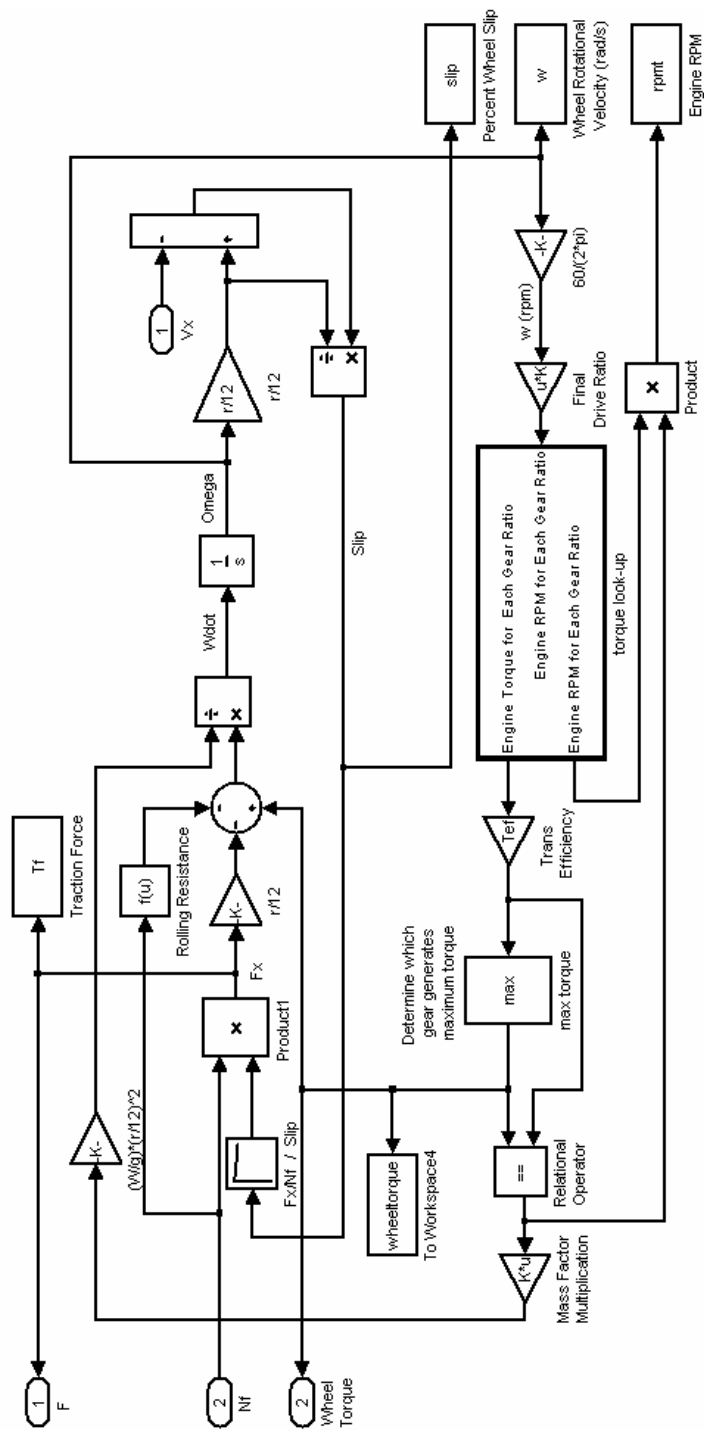
Figure C.5: Simulink Diagram of Wheel Slip

132

The torque driving the front axle is found using the wheel rotational velocity, Omega. Omega is multiplied by a constant to convert it to revolutions per minute. The simulation uses this rotation of the drive axle to determine the rotation of the crankshaft in the engine for each of the gears, first through sixth.

The simulation then uses a look-up table for each gear, torque 1st gear, torque 2nd gear, etc., that contains the engine torque versus engine RPM to find the drive torque for each gear. The torque look-up table portion of the Simulink diagram is shown in Figure C.6. The simulation calculates the engine RPM and torque for every gear ratio which will be used later in the simulation to choose which gear ratio the "driver" should be in to generate the maximum traction force available at the front tire road interface.

The simulation then multiplies this torque by a value for transmission efficiency. For this simulation, a value of 95% was used. The torques are then examined to determine the gear that produces the maximum torque for the given rotational speed of the tires. This particular gear is the gear that the vehicle is in while performing the simulated drag run. As the vehicle gains speed, the torque available in the lower gears decreases and the simulation shifts to the next gear to make use of the maximum torque available from the motor. This gear ratio is then used to determine the rotational inertia of the gear train, derived in Knauff [1], using an empirical equation for the mass factor of the gear train.
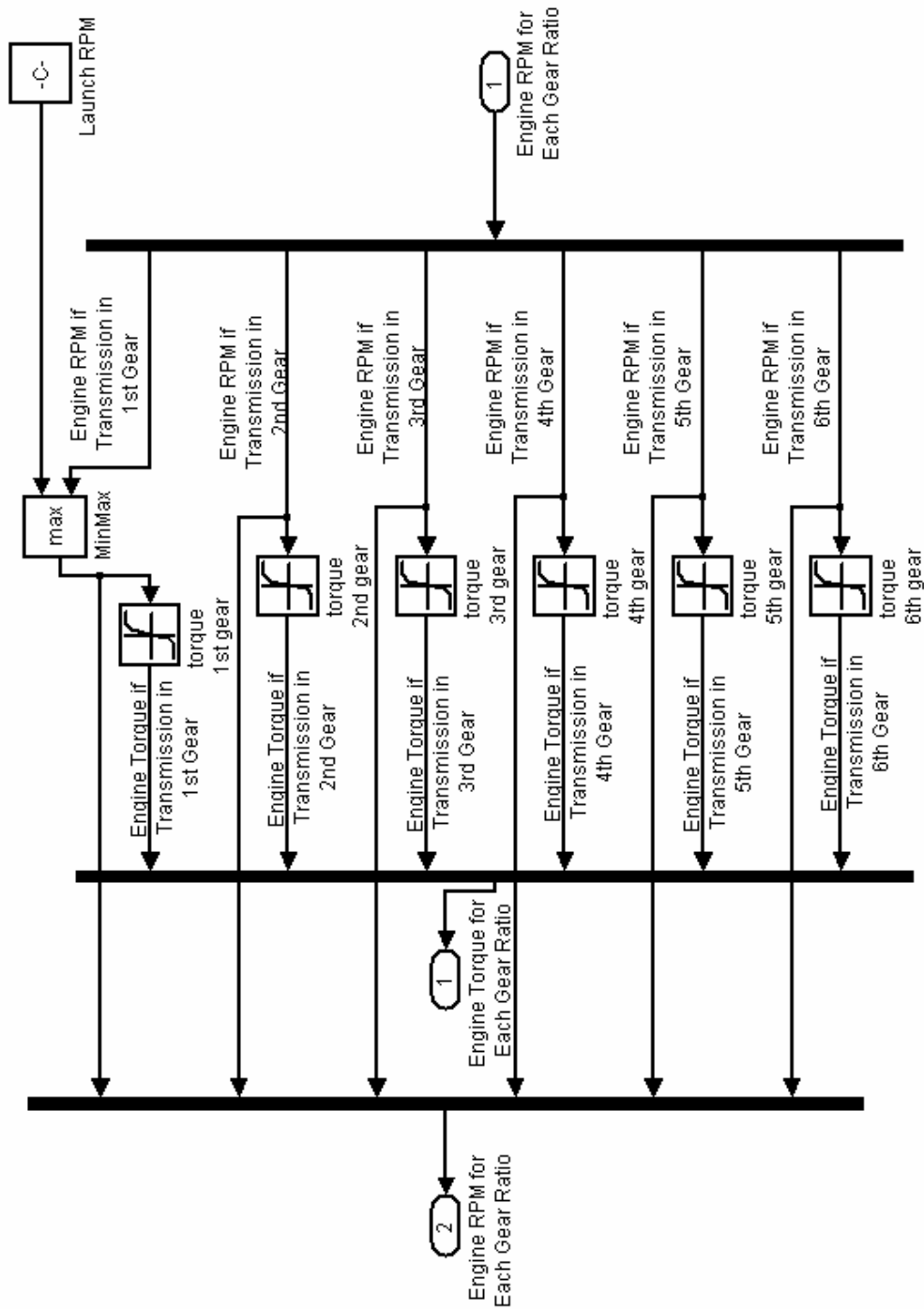
Figure C.6: Simulink Diagram of Torque Look-Up for Each Gear Ratio

Longitudinal Dynamics

The Simulink diagram for the longitudinal dynamics is shown in Figure C.7. The longitudinal dynamics model is in the block diagram form of Equation (16). The simulation uses traction force, F, front and rear normal forces, Nf and Nr, to calculate vehicle longitudinal acceleration, a. The acceleration is then integrated twice to calculate vehicle longitudinal velocity, Vx, and vehicle longitudinal displacement, X. The front and rear normal forces are multiplied by their respective rolling resistances to determine the drag force from roll resistance. This force is then subtracted, along with the aerodynamic drag, from the traction force component of the diagram to calculate the vehicle longitudinal acceleration. The drag force of the vehicle is calculated using Equation (C.1).

$$D_A = 0.5\rho \cdot C_D \cdot A \cdot V^2 \tag{C.1}$$

C_D is the constant drag coefficient, A is the frontal area of the vehicle, ρ is the density of air, V is the vehicle longitudinal velocity, and D_A is the total drag force on the front wheel drive drag racing car. The drag coefficient is affected by many aspects. As pitch angle increases, the drag coefficient normally would increase. Due to the small amount of pitch, less than one degree, we will assume that the drag coefficient is constant.
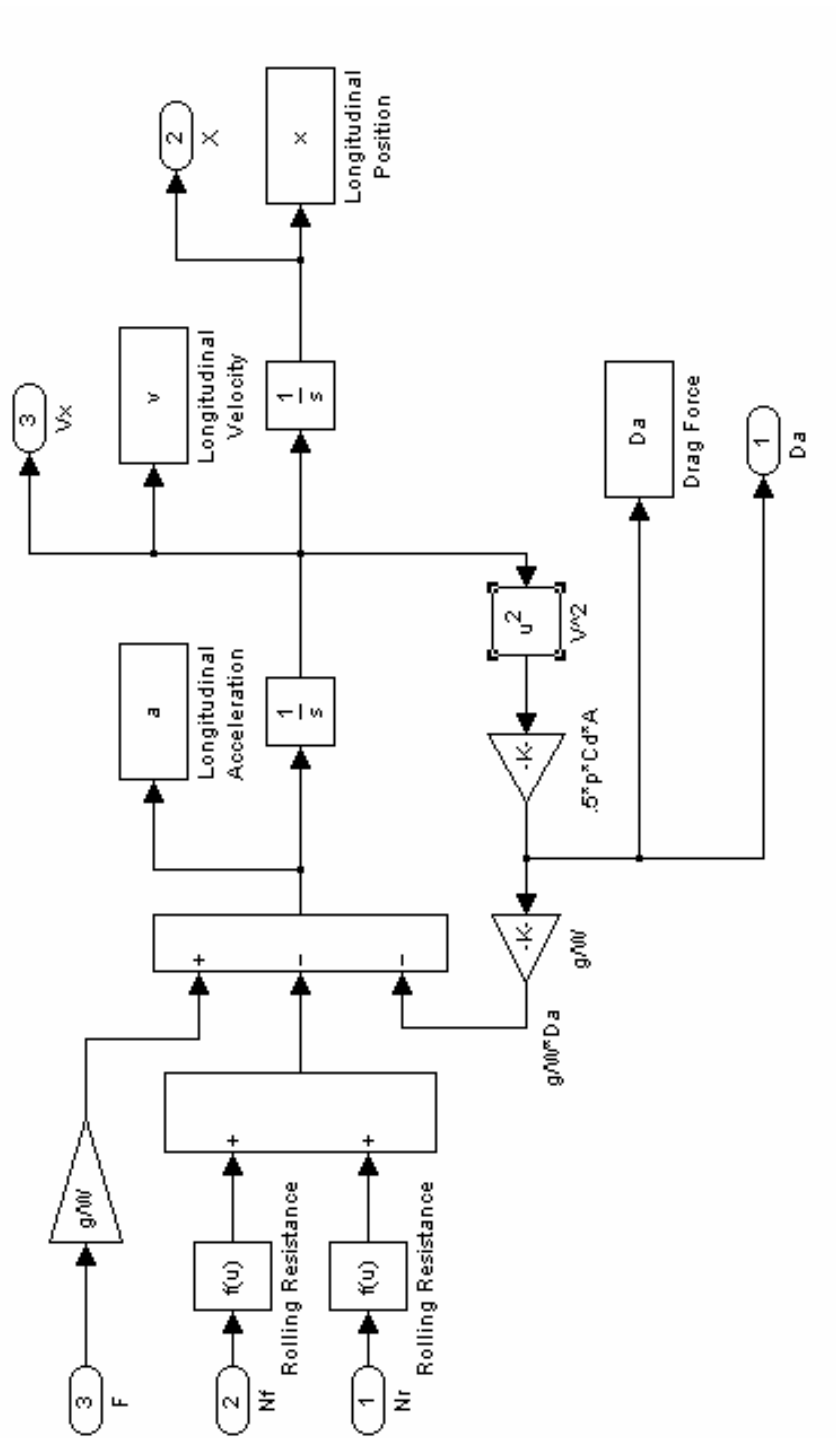
Figure C.7: Simulink Diagram of Longitudinal Dynamics

Simulink Program Description

The parent diagram of the Simulink program divides the dynamics of the front wheel drive drag racing vehicle into three parts. These three parts include the suspension dynamics, longitudinal dynamics, and wheel slip of the race car. This diagram allows the user to easily see which components of the vehicle dynamics are inputs and outputs of each respective system. The output of the entire simulation is shown as susout. This output includes each output of the suspension dynamics diagram. The Parent diagram of the Simulink model is shown in Figure C.8.

The wheel slip and longitudinal dynamics blocks have already been described and are shown in Figures C.5 and C.7 respectively. The "suspension dynamics with wheelie bar in contact" block is split up into four sections. These four sections include front and rear axle dynamics, the sprung mass dynamics, and the fixed footprint tire model. These four sections are shown in Figures C.4, C.3, and C.2 respectively. The block diagram for the suspension dynamics is shown in Figure C.9.
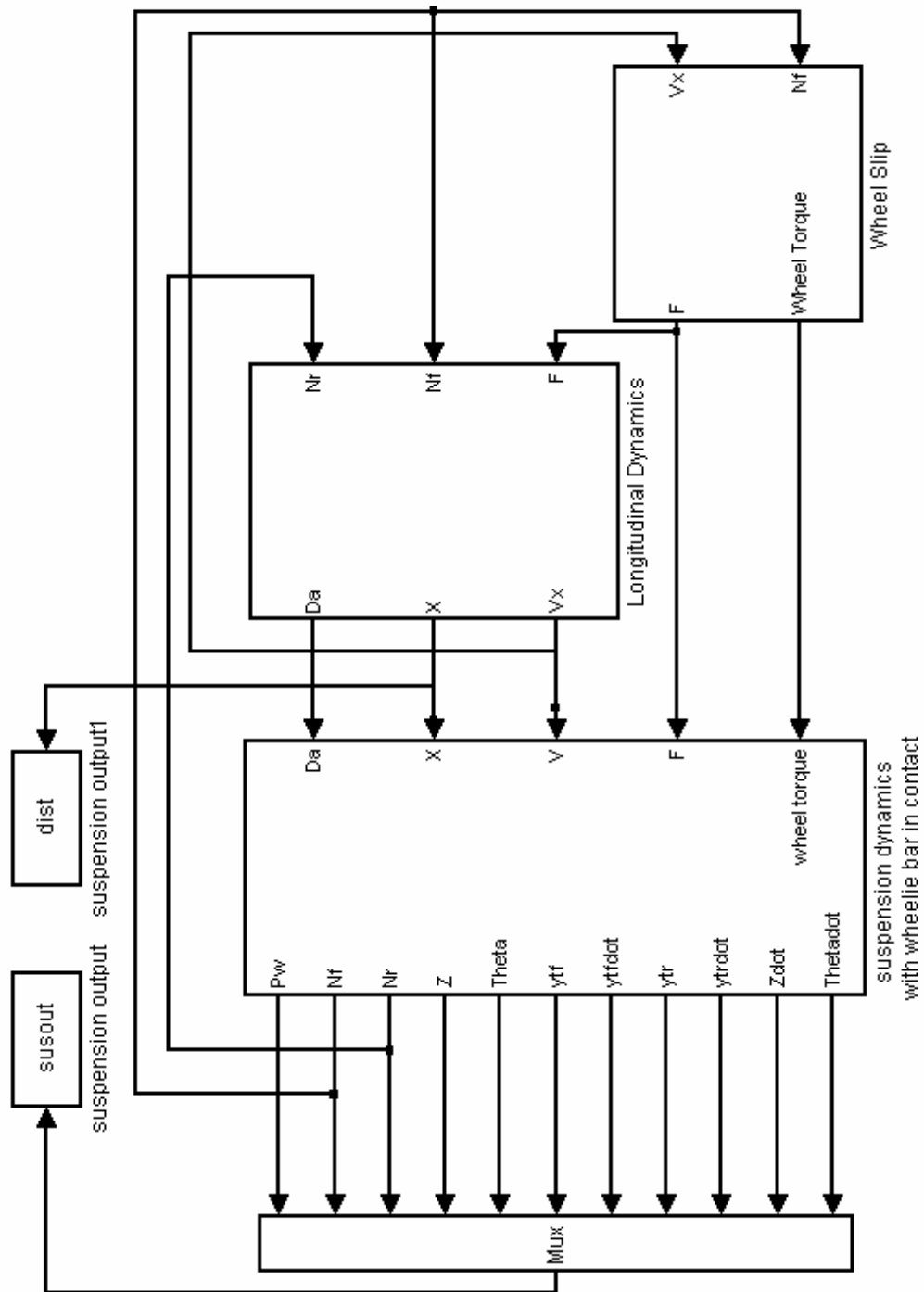
Figure C.8: Parent Diagram of Simulink Model
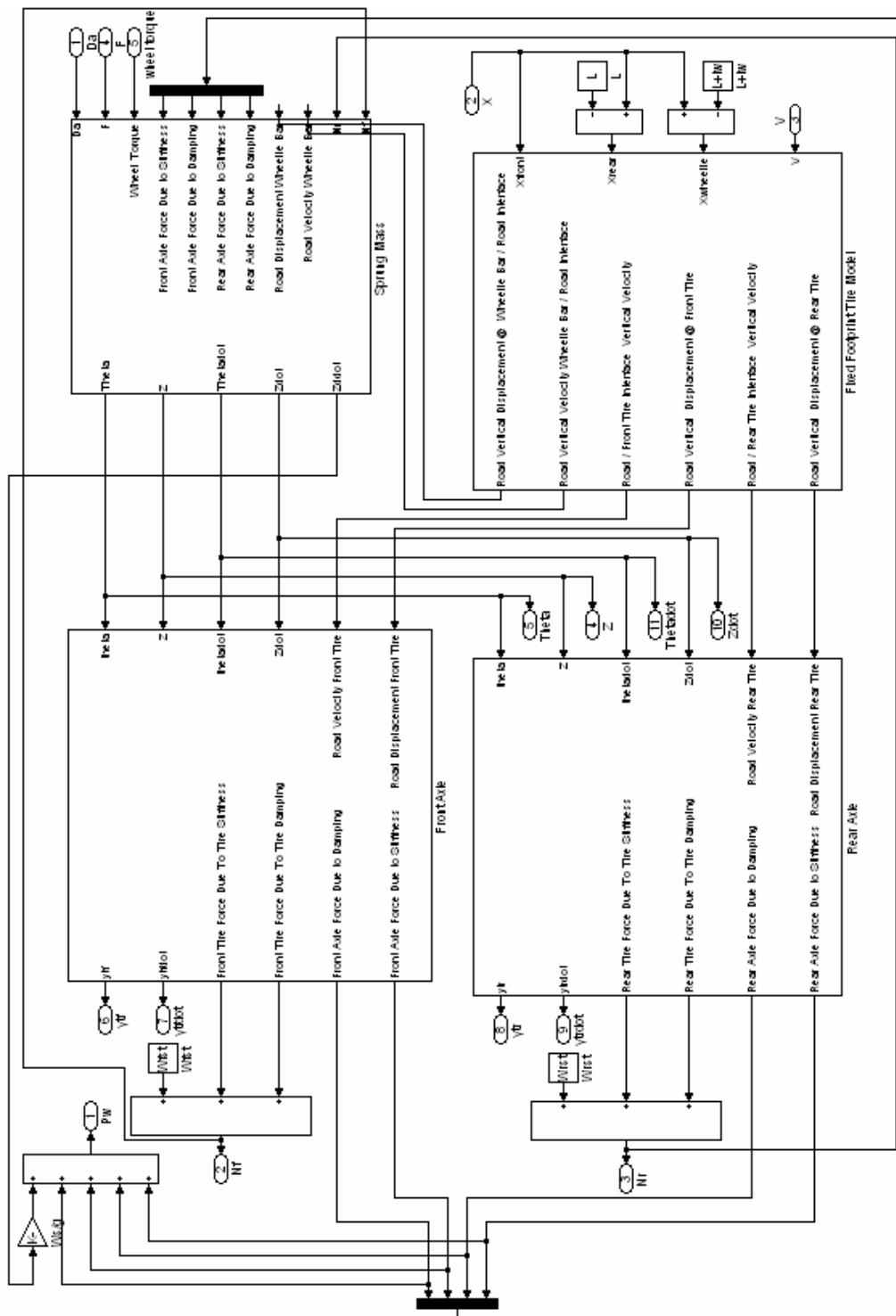
Figure C.9: Simulink Diagram for "Suspension Dynamics with Wheelie Bar in Contact"

139

Inputs used for this portion of the simulation, which is mainly used to simplify the complexity of the overall simulation, include the aerodynamic drag force, Da, the traction force, F, the drive Wheel Torque, and the longitudinal position and velocity of the drag racing vehicle. These variables are input into the Sprung Mass Dynamics diagram and Fixed Footprint Tire Model diagram. The outputs of these diagrams are then passed along to the Front and Rear Axle Dynamics diagrams and are also used as outputs of the simulation. These outputs include vehicle CG vertical position, Z, and pitch angle, θ, and vertical velocity, $\dot{Z}$, and pitch velocity, $\dot{\theta}$. The inputs of the Fixed Footprint Tire Model diagram use the longitudinal position of the front axle to calculate the absolute longitudinal position of the rear axle and wheelie bar point contact with the road by subtracting the distances between said points. The output vertical position of the wheelie bar contact with the road is used as an input to the Sprung Mass Dynamics diagram.

The outputs of the Front and Rear Axle Dynamics are used to calculate the front and rear road to tire normal forces, Nf and Nr respectively, and the vertical force exerted from the road to the point contact of the wheelie bar, Pw. The other outputs of the axle dynamics diagrams are the vertical displacement and velocity of the front axle, ytf and $\dot{y}$tf respectively, and the vertical displacement and velocity of the rear axle, ytr and $\dot{y}$tr respectively. The last of the outputs from the axle dynamics diagrams are used as inputs to the Sprung Mass Dynamics diagram.

Usage of Computer Program

The first thing that must be done to run the computer program is to input the parameters of the front wheel drive drag racing vehicle into the MATLAB m-file named "drag4mp.m". All of the values must be entered in the correct units, which are given as comments in the code. The next operation that must be completed is to create the random road profile. The type of road must be chosen on which you wish to simulate the drag run. Three types of road surfaces can be used. Each road surface has an associated m-file which will create the random road profile with the approximate power spectral density of the desired road surface. The three surfaces are a highway, runway, and an estimated drag strip. The m-files which will create these random roads are roadpsdSH.m, roadpsdSR.m, and roadpsdDS.m respectively. These programs generate the random road profile and the simulation can be continued.

Once the random road profile has been generated, the program "drag4mp.m" must be run. This program generates all of the vehicle parameters and passes them along to the Simulink model. The program then calls for the Simulink model to run with the given parameters and random road profile. The Simulink model then generates the motions and forces present throughout the vehicle. The motions of all of the degrees of freedom are recorded and all of the forces acting on the vehicle body are recorded.

When the simulation is complete, plots can be made to visualize the dynamic behavior of the drag racing vehicle. This can be done by using the program "plots.m" or by physically plotting any of the data through MATLAB. A flowchart of the computer simulation method is shown below in Figure C.10.
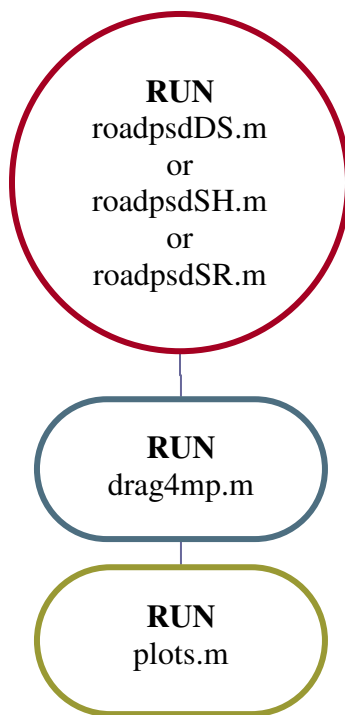
Figure C.10: Computer Simulation Flow Chart

Appendix D

MATLAB and SIMULINK Programs

DRAG4MP.M

```
%   Program that runs Front Wheel Drive Drag Race Car Simulation
%   Mike New
%   9/27/02

global numpoints

%   Constant Parameters

g=32.2;                 % gravitational constant lb ft/s^2
W=1808;                 % weight of car lbs
Ws=1512;                % Sprung weight of car lbs
Wtf=182;                % Unsprung weight of front axle lbs
Wtr=114;                % Unsprung weight of rear axle lbs
Is=650;                 % sprung mass pitch moment of inertia slugs ft^2
h=10.3/12;              % Height to CG ft
ha=10.3/12;             % Height of drag force ft
L1=27.35/12;            % Distance from front axle to CG ft
L2=83.54/12;            % Distance from rear axle to CG ft
L=L1+L2;                % Wheel base ft
I=.784*2;               % Wheel Rotational Inertia slugs ft^2
p=.00238;               % density of air lb/ft^3
Cd=.263;                % coefficient of drag
A=20.02;                % frontal area in ft^2
f=.03;                  % tire coefficient of rolling resistance
r=12.048;               % tire radius in inches
zf=3.769;               % final drive ratio
z1st=3.33;              % 1st gear ratio
z2nd=2.33;              % 2nd gear ratio
z3rd=1.93;              % 3rd gear ratio
z4th=1.48;              % 4th gear ratio
z5th=1.33;              % 5th gear ratio
z6=1.20;                % 6th gear ratio
Kf=5052;                % Front wheel rate per axle lb/ft
Kr=1464;                % Rear wheel rate per axle lb/ft
Cf=673.2;               % Front damping coefficient per axle lb/ft/sec
Cr=394.8;               % Rear damping coefficient per axle lb/ft/sec
Ktf=12400;              % Front tire stiffness per axle lb/ft
Ktr=23300;              % Rear tire stiffness per axle lb/ft
```

```
Ctf=7;                  % Front tire damping coefficient per axle lb/ft/sec
Ctr=7;                  % Rear tire damping coefficient per axle lb/ft/sec
lw=7.42;                % Distance from rear axle to end of wheely bar ft
Nlaunch=8000;           % Launch RPM
Tef=.95;                % Transmission Efficiency
Tpf=6.5;                % Tire Pressure (Front Tire), psi
Tpr=35;                 % Tire Pressure (Rear Tire), psi
Twf=11.5;               % Tire Width (Front Tire), in
Twr=4.5;                % Tire Width (Rear Tire), in
Nsf=(L2/L)*(Ws+Wtr)/2   % Half of Static Normal Force (Front Axle), lb
Nsr=(L1/L)*(Ws+Wtr)/2   % Half of Static Normal Force (Rear Axle), lb
Ltf=(Nsf/(Twf*Tpf))/12; % Fixed Footprint Contact Patch Length (Front Tire), ft
Ltr=(Nsr/(Twr*Tpr))/12; % Fixed Footprint Contact Patch Length (Rear Tire), ft
numpoints=10;           % Number of points for Footprint average calculation


Cfvel=[-1.6308, -.8191, -.4075, -.1625, 0, .16833, .4125, .825, 1.6467];
        % Front Damper Velocity (ft/s)
Cf1=-2*[463.78, 284.24, 179.72, 110.83, 0, -69.69, -131.43, -224.02, -361.73];
        % Front Damper Force (lb) per axle
Crvel=[-1.6358, -.8192, -.4075, -.1608, 0, .1683, .4158, .8300, 1.6500];
        % Rear Damper Velocity (ft/s)
Cr1=-2*[310.45, 234.43, 194.05, 165.55, 0, -45.87, -81.48, -136.1, -219.2];
        % Rear Damper Force (lb) per axle


Wfst=(L2/L)*W;
Wrst=(L1/L)*W;


%   Rolling Resistance Fit
%   Front Tire (28.0/11.5-15)

Fz=linspace(0,1200,100);
FR1=10.22;FR2=22.42;
coeff_front=polyfit([0 500 900],[0 FR1 FR2],2);


%   Rear Tire (25.0/4.5-15)

P1=30.6;FR1=5.51;FR2=11.35;
P2=45.2;FR3=3.49;FR4=7.59;
P3=35;FR5=(P3-P1)*(FR1-FR3)/(P1-P2)+FR1;FR6=(P3-P1)*(FR2-FR4)/(P1-P2)+FR2;
coeff_rear=polyfit([0 500 900],[0 FR5 FR6],2);
```

% Engine Torque vs. RPM

T=[221; 227; 234; 242; 251; 261; 272; 284; 300; 319; 346; 380; 419; 474; 460; 450; 454;
    453; 451; 448; 450; 454; 442; 437; 428; 420; 414; 403];
RPM=[5000; 5166; 5321; 5500; 5711; 5963; 6247; 6554; 6868; 7152; 7389; 7542; 7603;
    7650; 7706; 7829; 7902; 8045; 8142; 8233; 8318; 8403; 8526; 8605; 8710; 8813;
    8906; 9006];

FxFz=[0; 3; 2.85; 2.82; 2.80; 2.79; 2.77; 2.75; 2.73; 2.71; 2.7; 2.69; 2.68; 2.67; 2.66;
    2.65; 2.64; 2.63; 2.62; 2.61; 2.60];
Slip=[0; .05; .1; .15; .20; .25; .30; .35; .40; .45; .50; .55; .60; .65; .70; .75; .80; .85; .90;
    .95; 1.0];

xxf=[-Ltf/2;xx+Ltf/2];
roadfilteredf=[0 0;roadfiltered];

xxr=[-(L+(Ltr/2));xx+Ltr/2];
roadfiltered(1,1)=0;
roadfilteredr=[0 0;roadfiltered];

xxw=[-(L+lw);xx];
roadfilteredw=[0 0;roadfiltered];

T1st=T.*z1st*zf;
sp1st=(RPM./(z1st*zf));

T2nd=T.*z2nd*zf;
sp2nd=(RPM./(z2nd*zf));

T3rd=T.*z3rd*zf;
sp3rd=(RPM./(z3rd*zf));

T4th=T.*z4th*zf;
sp4th=(RPM./(z4th*zf));

T5th=T.*z5th*zf;
sp5th=(RPM./(z5th*zf));

% Gear Optimization Loop

tic
for i=1:length(z6);
  z6th=z6;
  z6th=z6th(i);

```
    T6th=T.*z6th*zf;
    sp6th=(RPM./(z6th*zf));
    sim('drag2')
    l=length(tout);
        while (x(l)>1320)
        l=l-1;
end
    ET(i)=tout(l)
end
toc
geartime=ET;
[min_time,zz]=min(geartime);
min_time=min_time
min_z6=z6(zz)

% Quarter Mile Performance Measurements

pp=length(tout);
        while (x(pp)>1320)
        pp=pp-1;
        end

  ET=tout(pp)
  MPH=v(pp)*3600/5280

  pp=length(tout);
        while (x(pp)>660)
        pp=pp-1;
        end
  eighthmi=tout(pp)
  eighthmph=v(pp)*3600/5280

   pp=length(tout);
        while (x(pp)>330)
        pp=pp-1;
     end
  threethirty=tout(pp)

pp=length(tout);
        while (x(pp)>60)
        pp=pp-1;
        end
            sixtyfoot=tout(pp)
```

FOOTPRINT.M

% This file calculates the length of the footprint with a specified number of equally
% spaced points

```
function out=footprint(x);
global numpoints
out=linspace(x(1),x(2),numpoints)';
```

PLOTS.M

% This file creates all of the dynamics plots for the Front Wheel Drive Drag Race Car

```
figure(1)
subplot(2,2,1),plot(tout,x)
title('Position vs. Time')
ylabel('X (ft)')
xlabel('Time (sec)')
axis([0 10 0 2000])
grid

subplot(2,2,2),plot(tout,v*3600/5280)
title('Velocity vs Time')
ylabel('V (mph)')
xlabel('Time (sec)')
axis([0 10 0 200])
grid

subplot(2,2,3),plot(Slip*100,FxFz)
title(' Tractive Effort Coefficient vs. Slip')
xlabel('% Slip')
ylabel('Fx/Fz')
axis([0 100 0 3])
grid

vel=0:1:200;
Da2=.5*p*Cd*A*(vel*5280/3600).^2;
res=f*W+Da2;

subplot(2,2,4),plot(sp1st*(2*pi*r/12)*60/5280,T1st*12/r,sp2nd*(2*pi*r/12)*60/5280,
        T2nd*12/r,sp3rd*(2*pi*r/12)*60/5280,T3rd*12/r,sp4th*(2*pi*r/12)*60/5280,
        T4th*12/r,sp5th*(2*pi*r/12)*60/5280,T5th*12/r,sp6th*(2*pi*r/12)*60/5280,
        T6th*12/r,vel,res)
title('Available Tractive Force and Total Resistance vs Velocity')
xlabel('Velocity (mph)')
ylabel('Force (lbs)')
axis([0 200 0 6000])
grid

figure(2)
subplot(2,2,1),plot(tout,a/32.2)
title('Acceleration vs. Time')
ylabel('A (g)')
```

```
xlabel('Time (sec)')
grid

subplot(2,2,2),plot(tout,susout(:,2)/Wfst)
title('Front Normal Force Ratio vs. Time')
ylabel('Nf/Wfst  (lbs)')
xlabel('Time (sec)')
grid

subplot(2,2,3),plot(tout,susout(:,3)/Wrst)
title('Rear Normal Force Ratio vs. Time')
ylabel('Nr/Wrst  (lbs)')
xlabel('Time (sec)')
grid

subplot(2,2,4),plot(tout,susout(:,1))
title('Force on Wheelie Bar')
ylabel('Fwb (lbs)')
xlabel('Time (sec)')
grid

figure(3)
subplot(2,2,1),plot(tout,susout(:,4)*12)
title('Heave (Positive Indicates Vertical Displacement Up)')
xlabel('Time (sec)')
ylabel('Z (in)')
axis([0 10 -.2 1.2])
grid


subplot(2,2,2),plot(tout,susout(:,5)*57.3)
title('Pitch Angle (Positive Indicates Lift at Front)')
xlabel('Time (sec) ')
ylabel('Theta (deg) ')
axis([0 10 -.2 0.5])
grid

subplot(2,2,3),plot(tout,sin(susout(:,5))*L1*12+susout(:,4)*12)
title('Front Vertical Displacement. Positive(up)')
xlabel('Time (sec)')
ylabel('Displacement (in)')
axis([0 10 -.2 1.2])
grid
subplot(2,2,4),plot(tout,-sin(susout(:,5))*L2*12+susout(:,4)*12)
```

```matlab
title('Rear Vertical Displacement. Positive(up)')
xlabel('Time (sec)')
ylabel('Displacement (in)')
axis([0 10 -.2 1.2])
grid

figure(4)
subplot(2,2,1),plot(tout,slip*100)
title('Percent Slip vs. Time')
xlabel('Time (sec)')
ylabel('% Slip')
axis([0 10 0 80])
grid

subplot(2,2,2),plot(tout,v,':',tout,w*r/12)
title('Wheel Speed and Velocity vs. Time')
legend('Velocity','Wheel Speed')
xlabel('Velocity (mph)')
axis([0 10 0 300])
grid

subplot(2,2,3),plot(Slip*100,FxFz)
title(' Tractive Effort Coefficient vs. Slip')
xlabel('% Slip')
ylabel('Fx/Fz')
axis([0 100 0 3])
grid


subplot(2,2,4),plot(RPM,T)
title('Torque vs. RPM')
xlabel('RPM')
ylabel('Torque (ft-lbs)')
axis([5000 10000 200 500])
grid

figure(5)
subplot(2,2,1),plot(tout,wheeltorque)
title(' Wheel Torque vs. Time')
xlabel('Time (s)')
ylabel('Wheel Torque (ft*lbs) ')
axis([0 10 0 6000])
grid
subplot(2,2,2),plot(tout,rpmt),axis([0 10 2000 12000])
```

```
title('Engine Rpm vs. Time')
xlabel('Time (sec)')
ylabel('RPM')
axis([0 10 0 2e4])
grid

subplot(2,2,3),plot(tout,Tf)
title('Traction Force vs. Time')
xlabel('Time (sec)')
ylabel('Traction Force (lbs)')
grid

subplot(2,2,4),plot(tout,a/32.2)
title('Acceleration vs. Time')
ylabel('A (g)')
xlabel('Time (sec)')
grid

figure(6)
plot(tout,susout(:,2)/W,tout,susout(:,3)/W,'-.',tout,susout(:,1)/W,':')
title('Weight Normalized Vertical Forces')
ylabel('Vertical Force/Weight')
xlabel('Time (s)')
grid
legend('Front', 'Rear', 'Wheelie Bar')

figure(7)
[ax,h1,h2]=plotyy(tout,v,tout,rpmt);
hold on
h3=plot(tout,w*r/12,':');
legend([h1;h3;h2],'Vehicle Speed','Wheel Speed','Engine RPM',4)
xlabel('Time (s)')
ylabel('Wheel Speed,Vehicle Speed (ft/s)')
axes(ax(2));
ylabel('Engine RPM')
grid
hold off
```

ROADPSDSR.M

% This file randomly generates the smooth runway vertical road profile and
% calculates the statistics and power spectral density of the road
% This file is used to randomly generate the smooth highway and drag strip also.
% A few changes of parameters are made to create the desired PSD.

% Program to create Random Road Profile with desired PSD
% Special Thanks to David Moline
% Mike New
% 9/27/02

```
clear
close all
clc
randn('state',0);          % Resets generator to initial state
minfreq=0.1;               % Minimum Frequency, Hz
maxfreq=100;               % Maximum Frequency, Hz
nfreq=300;                 % Number of Different Frequencies
N=-3.8;                    % Exponent for Approximaste Fitted Curve (S=Csp*Omega^N)
                           % N=-2.1 for Smooth Highway
                           % N=-3 for Simulated Drag Strip
Q=(N/2)+1;                 % Exponent on Magnitude
phases0=randn(1,nfreq)*pi; % Vector of Different Phases
freqs0=linspace(minfreq,maxfreq,nfreq);
                           % Vector of Frequencies, Hz (Flat Velocity PSD)
amp0=.03*freqs0.^Q;        % Amplitude, Either Constant or Fequency Dependent
                           % amp0=0.1*freqs0.^Q for Smooth Highway
                           % amp0=0.16*freqs0.^Q for Simulated Drag Strip
% SIMULINK Simulation

tic,sim('RoadProfile',12,simset('reltol',1e-3,'abstol',1e-3,'refine',1,'solver',...
   'FixedStepDiscrete','fixedstep',5e-4));toc
Vmph=125;
V=Vmph*5280/3600;     % Vehicle Speed,ft/s
xx=tout*V;
road1(:,1)=road(:,1);
road1(:,2)=road(:,2)-road(1,2);
road1=road1*[1/V 0;0 1];
froad=1/(xx(2)-xx(1));
```

% filter the low spatial freq stuff...this creates the "flat" section in
% the road PSD. Do another one at even low wlow to really can the DC stuff.

wlow=0.01; %cyc/ft ; the low frequency cut-off 0.02 is 50 ft/cyc
Wn=2*wlow/froad;
[filtb,filta]=butter(2,Wn,'high'); % "1" is first order filter--kills the hummocks.
roadfiltered=filter(filtb,filta,road1);

% Get the PSD

[pp,ww]=PWELCH(roadfiltered(:,2),[],[],2^13,froad);

% Pick the Range of Interest

jj=find(ww<=(maxfreq/V)&ww>=max(wlow,minfreq/V));
ii=jj;

% Do the PSD fit, Assuming a Power Model

cc=[ones(size(ii(:))) log(ww(ii))]\log(pp(ii));

% Desired PSD (Values from Wong [3])

Omega=linspace(0.005,0.5,300);
N=3.8;
Csp=1.6e-11;
Sg=Csp*Omega.^-N;

% Plot PSD

jjj=find(ww<=(maxfreq/V)&ww>=max(cc));
figure(1)
loglog(Omega*V,Sg*144/V,'r',ww(jjj)*V,pp(jjj)*144/V,'g',ww(ii)*V,exp(cc(1))*(ww(ii).
^cc(2))*144/V)
title(['Power Spectral Density for Smooth Runway (V = ' num2str(Vmph) ' mph)']);
xlabel('Frequency, Hz');ylabel('PSD, in^2/Hz');
legend('Desired PSD','Actual PSD','Actual PSD (Fit)');
axis([10^-1 10^3 10^-14 10^1])
grid;

figure(2)
subplot(2,1,1)
plot(xx,roadfiltered(:,2));
title(['Road Profile for Smooth Runway (V = ' num2str(Vmph) ' mph)']);

```
xlabel('Distance Along Track, ft');ylabel('Vertical Displacement, ft');grid
axis([0 5280/4 -0.05 0.05])
subplot(2,1,2)
plot(xx,roadfiltered(:,1));
title(['Road Slope for Smooth Runway (V = ' num2str(Vmph) ' mph)']);
xlabel('Distance Along Track, ft');ylabel('Road Slope, ft/ft');grid
axis([0 5280/4 -0.02 0.02])

% Statistics

StanDev=std(roadfiltered(:,2))
Avg=mean(roadfiltered(:,2))
RMS=sqrt(mean(roadfiltered(:,2).^2))
x=sort(roadfiltered(:,2));
I=find(x<(StanDev+Avg)&x>Avg);
disp('Percent Within +1 Standard Deviations from Mean (34.1% for Normal
        Distribution)')
Sig1=100*length(I)/length(xx)
I=find(x<(2*StanDev+Avg)&x>Avg);
disp('Percent Within +2 Standard Deviations from Mean (47.7% for Normal
        Distribution)')
Sig2=100*length(I)/length(xx)
I=find(x<(3*StanDev+Avg)&x>Avg);
disp('Percent Within +3 Standard Deviations from Mean (49.865% for Normal
        Distribution)')
Sig3=100*length(I)/length(xx)
I=find(x>(-StanDev+Avg)&x<Avg);
disp('Percent Within -1 Standard Deviations from Mean (34.1% for Normal
        Distribution)')
Sig_1=100*length(I)/length(xx)
I=find(x>(-2*StanDev+Avg)&x<Avg);
disp('Percent Within -2 Standard Deviations from Mean (47.7% for Normal
        Distribution)')
Sig_2=100*length(I)/length(xx)
I=find(x>(-3*StanDev+Avg)&x<Avg);
disp('Percent Within -3 Standard Deviations from Mean (49.865% for Normal
        Distribution)')
Sig_3=100*length(I)/length(xx)

% Calculate Histogram Plot of Statistics

Y=(x-Avg)/StanDev;
for i=1:15;
   z(i)=-4+0.5*i;
```

```
end
N=histc(Y,z);
N=N(1:i-1);
for j=1:14;
    X(j)=-3.75+.5*j;
end

% Statistics Plots

figure(3)
bar(X',N/length(x))
hold
y=(1/sqrt(2*pi*StanDev^2))*exp((-((x-Avg).^2))/(2*StanDev^2));
plot(Y,29*y/length(x))
xlabel('Standard Deviations from Mean');
ylabel('Probability');
Title('Probability Density Function for Smooth Runway');
legend('Gaussian Distribution Function');
hold
```

REFERENCES

1. Knauff, Mike, "Dynamic Modeling and Simulation of Front Wheel Drive Drag Cars", Thesis, Dept. of Mechanical Engineering, Clemson University, Clemson, SC, 2004.

2. Captain, K. M., Boghani, A. B. and Wormley, D. N., "Analytical Tire Models for Vehicle Dynamic Simulation", Vehicle System Dynamics, Vol 8, 1979, pp. 1-32.

3. Wong, J. Y., *Theory of Ground Vehicles*, John Wiley & Sons, New York, 1993.

4. Ramji, K., Gupta, A., Saran, V. H., Goel, V. K. and Kumar, V., "Road Roughness Measurements using PSD Approach", Journal of the Institution of Engineers, India, Civil Engineering Division, Vol 85, 2004, pp. 193-201.

5. Moline, David, "Random Road Profile Generator", MATLAB and Simulink Program, Dept. of Mechanical Engineering, Clemson University, Clemson, SC, 2001.

6. Andrén, P., "Power Spectral Density Approximations of Longitudinal Road Profiles", International Journal of Vehicle Design, Vol 40, 2006, Nos. 1/2/3, pp. 2-14.

7. Xia, X., "A Nonlinear Analysis of Closed Loop Driver/Vehicle Performance with Four Wheel Steering Control." Ph.D. Dissertation, Dept. of Mechanical Engineering, Clemson University, Clemson, SC, 1990.